

VFP

CONFIDENTIAL

Copy
RM E54E253

NACA RM E54E25



RESEARCH MEMORANDUM

(NACA-RM-E54E25) COOLING CHARACTERISTICS
OF A TRANSPIRATION-COOLED AFTERBURNER WITH
A POROUS WALL OF BRAZED AND ROLLED WIRE
CLOTH (NASA) 69 p

N73-74689

Unclas

00/99 20998

COOLING CHARACTERISTICS OF A TRANSPIRATION-COOLED
AFTERBURNER WITH A POROUS WALL OF BRAZED
AND ROLLED WIRE CLOTH

By William K. Koffel

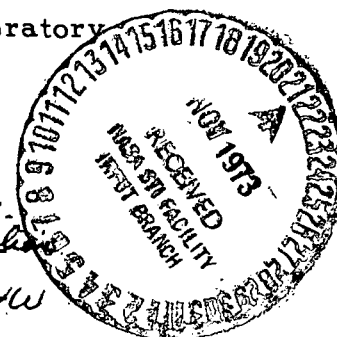
Lewis Flight Propulsion Laboratory
Cleveland, Ohio

CLASSIFICATION CHANGED

To Unclassified

By authority of NACA Reclassification

Notice #127 Date 6/5/58 /W



CLASSIFIED DOCUMENT

This material contains information affecting the National Defense of the United States within the meaning of the espionage laws, Title 18, U.S.C., Secs. 793 and 794, the transmission or revelation of which in any manner to an unauthorized person is prohibited by law.

NATIONAL ADVISORY COMMITTEE FOR AERONAUTICS

WASHINGTON

August 19, 1954

CONFIDENTIAL

NATIONAL ADVISORY COMMITTEE FOR AERONAUTICS

RESEARCH MEMORANDUMCOOLING CHARACTERISTICS OF A TRANSPIRATION-COOLED AFTERBURNER WITH A
POROUS WALL OF BRAZED AND ROLLED WIRE CLOTH

By William K. Koffel

SUMMARY

Cooling data were obtained for a transpiration-cooled afterburner having a porous combustion-chamber wall of brazed and rolled wire cloth for a range of exhaust-gas temperatures from 1200° to 3340° R, total flow ratio of cooling air to combustion gas of 0.025 to 0.106, and pressure altitudes of 15,000 to 45,000 feet. The data are successfully correlated over a range of Reynolds number from 75,000 to 1,500,000, based on the distance downstream of the leading edge of the porous wall.

Maximum wall temperatures based on the cooling correlation were determined for a porous wall of uniform permeability at sea-level take-off and for flight Mach numbers of 0.8, 1.5, and 2.0 at an altitude of 35,000 feet. The cooling-air requirements were nearly independent of the flight conditions. A total flow ratio of cooling air to combustion gas of about 0.032 can maintain a maximum wall temperature of 1210° R with an exhaust-gas temperature of 3700° R. The total flow ratios with a uniform permeability distribution and air flows sufficient to limit the maximum wall temperatures to 1210° R are about 15 percent higher than the minimum total flow ratios corresponding to a variable-permeability wall with a constant wall temperature of 1210° R. The total flow ratios for a maximum wall temperature of 1210° R with a wire-cloth afterburner are about 16 percent of the total flow ratios required to cool a stainless-steel afterburner wall convectively to a maximum wall temperature of 1760° R with exhaust-gas temperatures of 3200° and 3700° R. The analysis of cooling-air requirements for the previously mentioned flight conditions indicated that cooling-air static pressures must be closely controlled, especially at a flight Mach number of 2.0.

INTRODUCTION

The satisfactory cooling of high-thrust-augmentation afterburners for supersonic aircraft requires large amounts of cooling air. These large quantities of cooling air, whether supplied from the ambient-air

stream or from compressor bleed, involve large losses in net thrust. These losses, however, can be minimized through the use of more effective cooling methods. Transpiration cooling has been shown theoretically (ref. 1) to be more effective than film cooling or the conventional method of afterburner cooling by forced convection. The high effectiveness of transpiration cooling was experimentally verified in a preliminary investigation of a transpiration-cooled afterburner having a wall of sintered porous stainless steel (ref. 2). The commercial sintered porous stainless steel used in the preliminary investigation of transpiration cooling for afterburners was unsuitable for use in flight afterburners because of low strength-to-weight ratio, poor control over the uniformity of permeability, and fabrication difficulties.

In the search for more suitable porous materials, wire cloth was investigated (ref. 3) because of its high strength-to-weight ratio, availability in large sheets, ease of fabrication, and low cost compared with sintered porous metals. The NACA Lewis laboratory designed and built a transpiration-cooled afterburner with a porous wall of the brazed and rolled wire cloth, described in reference 3. This burner was operated on a turbojet engine to determine the feasibility of a wire-cloth transpiration-cooled afterburner and to evaluate its cooling performance.

The cooling data from the wire-cloth afterburner are reported herein for pressure altitudes of 15,000 to 45,000 feet, exhaust-gas temperatures from 1200° to 3340° R, and total flow ratios of cooling air to combustion gas of 0.025 to 0.106. A cooling correlation is derived from these data. This correlation is then used to predict the cooling-air requirements of this afterburner with exhaust-gas temperatures of 3200° and 3700° R for several typical flight conditions of a supersonic airplane. A comparison is also made between the cooling-air requirements of this afterburner with transpiration cooling and with conventional forced-convection cooling. The experimental cooling correlation is briefly compared with the approximate theory of Rannie and Friedman (refs. 4 and 5) for transpiration cooling with turbulent boundary-layer flow.

APPARATUS AND INSTRUMENTATION

Test Installation

The wire-cloth afterburner was mounted on a conventional axial-flow turbojet engine installed in an altitude test chamber. The test installation aft of the turbine flange is shown in figure 1. The engine and afterburner assembly were mounted on a bed plate suspended in the altitude chamber in such a manner as to permit the measurement of jet thrust. A sectional view of the afterburner is shown in figure 2 together with details of the flame holder and fuel-spray bars. The configuration between

the turbine flange and the beginning of the porous wall, including the fuel-spray bars and flame holder, was identical with the high-performance afterburner configuration of reference 6, which was evolved from configuration C of reference 7.

Cooling air from an independent source was filtered through 100 square feet of 1-inch-thick Fiberglas filter media that retained particles greater than 1 micron. The flow was measured by means of an A.S.M.E. standard thin-plate orifice. The plenum chamber and the high-temperature impermeable wall upstream of the porous-wall section were Inconel, and the cooling-air side of the mild steel shroud was painted with zinc chromate primer in order to eliminate the possibility of clogging the wire cloth with fine scale.

The engine fuel was clear unleaded gasoline of 62-octane rating, and the afterburner fuel was MIL-F-5624A, grade JP-4.

Wire-Cloth Porous Wall

The porous combustion-chamber wall was made from wire cloth that was brazed and rolled, for permeability reasons, as described in reference 3. The particular cloth used was monel 21x70 twilled Dutch weave (designated cloth B in ref. 3) sprayed with three coats of silver solder per side and brazed and rolled to a 35-percent reduction in original thickness. The average final thickness was 0.0274 inch, and the average permeability coefficient K was about 1×10^{-8} square inch. The tapered combustion chamber was lined with a porous wall made from 20 pieces of wire cloth formed into shallow channels. Each channel was 1/2 inch deep by about 41 inches long and tapered in width from about 4 inches at the upstream end to about 3.5 inches at the downstream end. The channels were spot-welded to angles (fig. 3) that were fastened to the structural shroud by blind rivets. The permeability of each channel differed slightly from the average permeability for all the channels. It was expected that the cooling-air static pressure would vary somewhat circumferentially because of the tangential inlet to the plenum chamber. Therefore, the channels were arranged in an order that would tend to produce a circumferentially uniform distribution of cooling air.

The newly fabricated porous combustion-chamber wall is shown in figure 4(a). The channels of wire cloth were permanently bulged toward the center line of the combustion chamber after the initial operation of the engine. Figure 4(b) shows the bulged channels at the end of the cooling investigation with cooling passage heights of about 3/4 to 7/8 inch in midchannel. The method of suspending the wire cloth caused a minimum of disturbance to the cooling-air film on the gas side of the porous wall, and the bulging of the channels reduced tensile stresses in the wire cloth caused by pressure forces. The impermeable wall

upstream of the porous wall was forced-convection cooled by the cooling air before it flowed into the 20 dead-ended cooling-air passages.

Instrumentation

The research instrumentation for measurement of temperatures and pressures at several stations through the turbojet engine was the same as in reference 6. The location of each temperature and pressure measurement on the afterburner is shown in figure 5. The five principal stations of instrumentation on the porous wall were 24, 32.6, 41, 49.6, and 57.5 inches downstream of the quick-disconnect flange at the combustion-chamber inlet (see fig. 2).

Details of a typical group of instrumentation are shown in figure 6. The cooling-air temperature probes had butt-welded iron-constantan thermocouple junctions shaved smooth to 0.010-inch diameter. The thermocouples on the wire cloth were 28-gage (0.013-in.) chromel-alumel wire individually wrapped with silicone-treated asbestos insulation and overbraided with Fiberglas insulation. The orientation and application of the spot-welded junctions on both sides of the wire cloth can be seen in figure 6. There were only four thermocouples on the gas side of the wire cloth because of difficulties in installation. The shroud temperatures were measured with 22-gage (0.025-in.) iron-constantan thermocouples (not shown in fig. 6) spot-welded to the outside of the shroud. The longitudinal profile of static pressure in the combustion chamber was determined by means of 0.080-inch outside diameter by 0.010-inch wall stainless-steel tubes sweat-brazed into the wire cloth and ground flush. The flexibility of these tubes and the method of leading them out of the passage permitted the wire cloth to assume a natural curve with minimum distortion of the cloth at the point of pressure measurement.

Strain-gage pressure pickups were mounted on the cooling-air plenum chamber and on the combustion-chamber wall at the flame-holder station to obtain the static-pressure pulsations in the cooling air and combustion chamber during ignition and normal afterburning. The pressure pulsations were recorded on a two-channel oscillograph.

TEST PROCEDURE

Air-flow calibrations were obtained for each piece of wire cloth before fabrication into the porous wall. These calibrations were taken at points where temperature instrumentation was later applied. Additional cold-air-flow calibrations were made of the assembled porous wall, as a whole, at several ambient pressure levels before and during the cooling investigation to detect any over-all change in the air-flow calibrations from plugging by fuel or combustion residues or from oxidation of the

brazing alloy. Nonafterburning check points were also made during the cooling investigation as a check on instrumentation and changes in the wire cloth.

The data are presented in tables I to V, and the approximate range of some of the variables are given in the following table for an inlet cooling-air temperature of 535° R:

Pressure altitude, ft	Compressor air flow, lb/sec	Cooling-air flow, W_a , lb/sec	Exhaust-gas total temperature, $T_{g,2}$, °R	Type of test
Sea level	0	0.970-5.810	^a 535	Check on air-flow calibration and plugging of wire cloth
15,000	0	1.255-4.344	^a 535	
35,000	0	.903-2.849	^a 535	
45,000	0	1.49-1.79	^a 535	
15,000	45.8	1.2-3.8	1200	Cooling, non-afterburning
35,000	25.5	.83-2.7	1250	
15,000	45.8	1.37-3.25	2580-3010	Cooling, afterburning
35,000	25.5	1.26-3.16	1800-3340	
45,000	15.6	1.49-1.79	3185	

^aApproximate ambient-air temperature.

The cooling-air flow was varied at a given pressure altitude and fuel-air ratio between the following limits:

- (1) Minimum static-pressure difference Δp across upstream edge of wire cloth of 0.5 lb/sq in. to prevent reverse flow of combustion gas through wire cloth
- (2) Maximum Δp across downstream edge of wire cloth of 6 lb/sq in. to avoid bursting channels of wire cloth
- (3) Maximum wire-cloth temperature of 1460° R to avoid excessive rate of plugging from oxidation of silver solder
- (4) Maximum turbine-outlet gas temperature of 1625° R to protect turbine from over-temperature

METHODS OF CALCULATION AND ANALYSIS

Cooling-Air Flow

Local values of the cooling-air flow normal to a unit of wire-cloth surface area $(\rho V)_a$ were computed for two channels, channel 1 having the hottest and channel 9 having the coldest porous-wall temperatures. This computation was based on the air-flow calibrations of figure 7, the thickness of each channel, the respective longitudinal profiles of cooling-air static pressure, and the assumption that the longitudinal profile of combustion-gas static pressure was circumferentially uniform.

(Symbols are defined in appendix A.) The ordinate $\frac{\Delta(p^2)}{\tau} \left(\frac{\mu_o}{\mu}\right)^2 \frac{T_o}{T}$ of figure 7 is in effect a measure of the pressure drop per unit thickness across the porous wall, and the abscissa $(\rho V)_a \frac{\mu_o}{\mu}$ is the reduced weight flow of cooling air per unit of wire-cloth surface area. The viscosity and temperature ratios, μ_o/μ and $(\mu_o/\mu)^2 T_o/T$, reduce the air-flow data to NACA standard temperature. A theoretical analysis in reference 8 indicates that the profile of air temperature across a porous wall should practically coincide with profile of metal temperature except for a very short distance on the side the air enters the wall. Consequently, the viscosity- and temperature-ratio factors should be evaluated at the average local wall temperature. Measured wall temperatures on either side of the wire cloth in this afterburner were within 20° R of each other, so for convenience the factors were evaluated at the temperature measured by the air-side thermocouples, which were installed at each station of channels 1 and 9.

The calculated total cooling-air flows in a later section, Cooling-Air Requirements Calculated from Cooling Correlation, were obtained from the step-by-step summation of $\pi D(\rho V)_a \Delta x$.

Exhaust-Gas Temperature

The total temperature of the exhaust gas was calculated from the exhaust-nozzle total pressure P_{68} , measured jet thrust, velocity coefficient, and gas flow by the following equation (ref. 7):

$$T_{g,2} = \left(\frac{F_{j,m}}{C_v}\right)^2 \left(\frac{g}{2R}\right) \left(\frac{\gamma_g - 1}{\gamma_g}\right) \left\{ \frac{1}{W_{g,68}^2 \left[1 - \left(\frac{P_o}{P_{68}}\right)^{\frac{\gamma_g - 1}{\gamma_g}} \right]} \right\} \quad (1)$$

The values of R were computed according to the method of reference 9, and the jet velocity coefficient was determined to be 0.97 from data presented in reference 10.

Local Combustion-Gas Temperatures

Local values of the combustion-gas total temperature $T_{g,x}$ with afterburning were computed from the empirical equation (ref. 11)

$$\frac{T_{g,x} - T_{g,1}}{T_{g,2} - T_{g,1}} = \sin \frac{\pi x'}{L} \quad (2)$$

where $T_{g,1}$ is assumed equal to the turbine-discharge gas temperature, and $T_{g,2}$ is the exhaust-gas total temperature. Equation (2) makes no allowance for possible hot streaks and implies a uniform transverse profile of combustion-gas temperature. Hot streaks undoubtedly were present, although observation of the combustion color and pattern by means of a periscope directed up the burner axis showed good circumferential uniformity. The transverse temperature profile was made as uniform as possible in a previous investigation of the radial fuel-air distribution when this same configuration had a convection-cooled impermeable wall.

For nonafterburning cooling data, local values of bulk total temperature $T_{g,x}$ were assumed equal to the turbine-discharge gas temperature $T_{g,1}$.

Correlation of Cooling Data

Cooling data from five stations along the two typical channels of wire cloth were correlated by plotting the temperature-difference ratio $(T_w - T_a)/(T_g - T_a)$ against the coolant-flow ratio $(\rho V)_a/(\rho U)_g$ for constant values of bulk Reynolds number. The flow over the porous wall was believed to be similar to the boundary-layer flow over a flat plate, so that the length used in the Reynolds number was taken as the distance from the leading edge of the porous wall. Consequently, the temperature-difference ratios and the coolant-flow ratios are local values corresponding to the local Reynolds numbers. The viscosity of the combustion gas was assumed to be the same as for air given in table 2 of reference 12 and was evaluated at the film temperature T_f . The quantity $(\rho U)_g$ was assumed identical to the local one-dimensional value of total weight flow per unit of combustion-chamber flow area.

The wall temperature T_w in the temperature-difference ratio $(T_w - T_a)/(T_g - T_a)$ was measured on the cooling-air side of the wire cloth but can be considered practically to represent the wall temperature on the hot-gas side because of the small difference in measured temperatures across the wire cloth in this afterburner.

Cooling-Air Requirements Calculated from Cooling Correlation

The experimental cooling correlation of this investigation was used to calculate the longitudinal profile of porous-wall temperature in this afterburner. The conditions analyzed are given in the following table:

Flight condition	Flight Mach number	Altitude, ft	Exhaust-gas total temperature, $T_{g,2}$, °R
A	0	Sea level	3700
B	.8	35,000	3700
B	.8	35,000	3200
C	1.5	35,000	3700
D	2.0	35,000	3700

The turbine-discharge temperature was 1710° R for all conditions. The cooling-air static pressure and the permeability of the porous wall were assumed to be absolutely uniform, and the air-flow calibration of the porous wall was assumed to be identical with the mean calibration curve of figure 7. With a uniform permeability, most of the porous wall will be overcooled except for some peak temperature region, which must not exceed the maximum allowable operating temperature of the porous material. The calculated maximum wall temperatures were plotted against total flow ratio for each flight condition. It should be kept in mind that wall temperatures calculated from the cooling correlation are assumed to be uniform around the circumference at each station. Usually, a safety factor must be allowed for random hot spots in the porous wall caused by hot streaks in the combustion gas or by local areas that have less than the mean permeability.

Minimum cooling-air flow. - The minimum cooling-air flow for a given temperature limit results when the wall temperature is maintained constant at the maximum allowable operating temperature of the porous material by use of an infinitely variable permeability distribution along the porous wall. The assumption of a constant wall temperature makes it possible to compute the minimum cooling-air distribution and the minimum total flow ratio directly from the cooling correlation without considering the distributions of permeability that would be

required to provide the minimum cooling-air distribution. Although it is not practical to vary the permeability distribution for each flight and operating condition in an actual afterburner, the minimum flow ratios are useful for reference and for examination of trends. Minimum total flow ratios were therefore also computed for flight conditions A to D with a constant porous-wall temperature of 1210° R.

Longitudinal profile of combustion-gas static pressure. - The static-pressure profile along the length of the combustion chamber was calculated step-by-step from well-known one-dimensional flow relations for momentum pressure drop in a constant-area duct and the isentropic variation of Mach number with area ratio. The friction pressure drop, which was assumed to be small relative to the momentum pressure loss, was neglected.

Cooling-air pressure and temperature. - The cooling air was assumed to have been bled from an interstage of the compressor (at a compressor efficiency of 0.85) at a pressure high enough to allow for a pressure drop of 1 pound per square inch through valves and ducting to the upstream edge of the porous wall. The pressure drop across the porous wall was limited to a minimum of 1 pound per square inch for practical control, and to a maximum of 6 pounds per square inch to prevent bursting the channels of wire cloth. The cooling-air pressure and temperature were presumed to be uniform in all cooling-air passages. Convective heat transfer to the cooling air by the impermeable wall upstream of the porous wall was assumed to raise the air temperature 50° above that corresponding to the compressor bleed temperature.

Cooling-Air Requirements with Forced-Convection Cooling

Cooling-air requirements for forced-convection cooling of this afterburner with ram air were calculated for exhaust-gas temperatures of 3200° and 3700° R for flight condition B from data in reference 13 and the cooling correlation of reference 11.

RESULTS AND DISCUSSION

Typical Data

Figure 8 shows typical measured circumferential profiles of the cooling-air static pressure and wire-cloth temperature. The static-pressure profiles shown result from the tangential inlet on the plenum chamber and the previously mentioned order of assembling the channels of wire cloth. As would be expected, the temperature profiles are the reverse of the pressure profiles. Figure 8 shows that channel 1 was generally the hottest and channel 9 the coldest, with or without afterburning.

Typical longitudinal profiles for the wire-cloth afterburner are shown in figure 9. The importance of eliminating circumferential gradients in cooling-air static pressure and in permeability is obvious from the 530° R variation in wall temperature at station 62 in figure 9(a). Part of the circumferential temperature spread in this afterburner would have been averted if there had been no circumferential pressure gradient in the cooling air. The pressure gradient could have been reduced by a better plenum-chamber inlet or by cross-flow holes in the angles that supported the channels of wire cloth. Wire cloth more closely meeting the specified permeability could have practically eliminated circumferential variations in wall temperature, except for those caused by any hot streaks in the combustion gas. The slight drop in cooling-air temperature (figs. 9(a) and (c)) along the length of the cooling-air passage is due to heat losses through the uninsulated shroud.

The longitudinal profiles of static pressures on both sides of the porous wall are shown at the top of figures 9(b) and (d). For the relatively high flow ratios shown (W_a/W_g of 0.0716 to 0.0951), the continuous bleeding of air through the porous wall caused a deceleration of the cooling-air flow and a corresponding rise in static pressure of the cooling air in the flow direction. With the low flow ratios of practical interest, the static pressure of the cooling air was almost independent of passage length.

The variation of pressure drop across the porous wall with distance along the wall is represented by the vertical distance between the static pressures of the cooling air and of the combustion gas. The resulting longitudinal profiles of coolant-flow ratio $(\rho V)_a/(\rho U)_g$ are shown in figures 9(b) and (d). The coolant-flow ratios for channel 9 were considerably higher than for channel 1. The differences in coolant-flow ratios are caused by the differences in permeability and the absolute pressure level in each channel. It is recalled that the air-flow calibrations of figure 7 indicate $(\rho V)_a$ is a function of the difference of the squares of the absolute static pressure on both sides of the porous wall instead of the pressure drop alone. The curves of the fraction of total cooling-air flow in each channel are almost linear and nearly identical for channels 1 and 9 (figs. 9(b) and (d)). It can be inferred, therefore, that the longitudinal addition of cooling air was almost linear through all the channels of wire cloth.

Before discussing the cooling correlation, it is of interest to determine whether there was any progressive change in the air-flow calibration of the wire cloth during the cooling investigation. A dull greasy smudge formed on the combustion-gas side of the wire cloth in spite of the cooling-air film flowing away from the wire cloth during all periods of engine operation. The smudge is visible in figure 10 to the left of the white lines. The areas to the right of the white lines have

been wiped clean with cleansing tissue to show the condition of the wire cloth after 4 hours 10 minutes of afterburning. The smudge caused no discernible effect on air-flow calibration.

Figure 11 shows the circumferential average static-pressure drop across the porous wall against orifice cooling-air flow for several levels of combustion-chamber pressure at stations 24 and 57.5. The agreement between data taken before and during the cooling investigation was excellent at all stations. On the basis of figure 11 and the close agreement between temperature-difference ratios for nonafterburning check points, it is concluded that there was no significant change in the air-flow calibration of the wire cloth during the cooling investigation.

Cooling Correlation

The experimental cooling data with afterburning are correlated over a range of Reynolds numbers in figures 12(a) to (f). Cooling data obtained from channels 1 (hottest) and 9 (coldest) met, or overlapped, to define a single curve when the Reynolds number was held approximately constant. The mean curves drawn through groups of data points having approximately the same Reynolds number are summarized in figure 12(g). Within the ranges investigated, neither Reynolds number nor radiation had any marked effect on the correlation of afterburning cooling data for coolant-flow ratios less than about 0.007. Above a coolant-flow ratio of 0.007, the temperature-difference ratio, and hence the porous-wall temperature for fixed cooling-air and gas temperatures, decreased as Reynolds number increased from about 75,000 to 800,000. The curves for Reynolds numbers of 1,000,000 and 1,500,000 lie, respectively, above and below the curve for 800,000. It is probable that in this Reynolds number range, corresponding to stations 49.6 and 57.5, increases in radiant heat transfer tend to counterbalance increases in the Reynolds number (see ref. 1), although the radiant heat transfer was calculated to be less than one-tenth of the convective heat transfer.

A direct comparison between the curves of the experimental cooling correlation and those predicted by the approximate theory of references 4 and 5 is not entirely realistic because of the different assumptions used with these data and those used for developing the approximate theory. However, a partial comparison is made in appendix B.

Although nonafterburning conditions were not of primary importance to the present investigation, the nonafterburning conditions are of somewhat general interest in connection with the heat-transfer process of transpiration cooling. The combustion-gas temperature was almost constant along the length of the combustion chamber during nonafterburning, and radiation from the gas was negligible because of the low

gas temperature and pressures. The nonafterburning cooling data are presented in tables I to IV. Nonafterburning cooling data are shown in figure 13 by plotting $(T_w - T_a)/(T_g - T_a)$ against Reynolds number for constant values of $(\rho V)_a/(\rho U)_g$. Cooling correlation curves for Reynolds numbers of 10^5 and 10^6 (fig. 14) were obtained from a cross plot of figure 13. The curves of figure 14 are similar in shape and magnitude to the afterburning data for comparable Reynolds numbers, as can be seen in figure 15. Although somewhat better cooling is indicated by the nonafterburning than by the afterburning data at coolant-flow ratios less than about 0.007, the agreement between afterburning and nonafterburning data is considered satisfactory. The agreement probably would have been closer if measured values had been available of the local combustion-gas temperatures and of $(\rho U)_g$ near the wall, instead of assuming $(\rho U)_g = W_g/A_g$. The profiles of $(\rho U)_g$ are known to differ between nonafterburning and afterburning conditions.

Transpiration-Cooling Performance

Figure 16 is a plot of the calculated maximum wall temperature against total flow ratio W_a/W_g for the assumed flight conditions A to D when operating with an exhaust-gas temperature of 3700°R . It should be emphasized that the air flow through the porous wall is a function of the difference of the squares of the absolute pressures on either side of the wall (see fig. 7). Hence the magnitude and the longitudinal position of the maximum wall temperature are functions of the profiles of the absolute static pressures and of the combustion-gas temperature. The profiles of absolute static pressure are dependent on the flight condition and the pumping characteristics of the engine used, in addition to pressure losses in the afterburner. For the flight conditions investigated, the maximum wall temperature occurred at the leading edge of the porous wall, except when the cooling-air static pressure was reduced to 10.85 pounds per square inch absolute. At this pressure, the maximum wall temperature moved to about station 49.6.

~~Separate curves of maximum wall temperature against total flow ratio~~ were obtained for each flight condition (fig. 16). The curves closely overlap so that the cooling-air requirements were nearly independent of flight conditions; however, the curves would be separated more if the gas temperature had been widely varied. The operable range of total flow ratio varied with flight condition because of the related minimum and maximum pressure drops across the porous wall. The upper symbol on each curve corresponds to the assumed minimum pressure drop across the porous wall of 1 pound per square inch at the leading edge. The lower symbol corresponds to the assumed maximum pressure drop of 6 pounds per square inch at the trailing edge. The resulting minimum and maximum cooling-air pressures are given in figure 16. With a uniform distribution of cooling-air pressure,

the range in static pressure for control of cooling-air flow at a given flight condition is then 5 pounds per square inch minus the drop in combustion-chamber static pressure along the porous wall. Consequently, large drops in combustion-chamber pressure along the porous wall tend to decrease the range of cooling-air static pressure for control of cooling-air flow. The control range for cooling-air static pressure varied from 3.70 to 0.66 pounds per square inch, respectively, for flight conditions B and D. Cooling-air pressure must be accurately controlled within this range. For example, at flight condition D, a decrease in cooling-air static pressure of 0.66 pound per square inch (only 1.85 percent of the absolute cooling-air pressure) causes a 256° R increase in maximum wall temperature.

Greater range could be obtained in cooling-air static pressure by using several layers of wire cloth. This type of construction would permit higher pressure drops across the porous wall and would make possible the control of low flows corresponding to high maximum wall temperatures without danger of reverse flow through the wall. The peak temperature limit for the porous wall was about 1410° R because of oxidation of the brazing alloy on the wire cloth in this afterburner. Therefore, a temperature of 1210° R is assumed to be safe for the maximum wall temperatures computed from the cooling correlation. This temperature provides a 200° safety factor for local peak temperatures caused by hot streaks in the combustion gas and from small random areas of the cloth that have less than the mean permeability. A total flow ratio W_a/W_g of about 0.032 can maintain a maximum wall temperature of 1210° R with an exhaust-gas temperature of 3700° R at conditions A to C. Calculations indicated that a maximum wall temperature of 1210° R could also be maintained at condition D by increasing the assumed maximum allowable pressure drop across the wire cloth by about 20 percent (point indicated by the end of the dotted extension). A visual extrapolation of the curves of figure 16 (disregarding pressure limits) to a wire-cloth temperature of 1760° R, which is a representative temperature for a wall of stainless steel, results in a total flow ratio of about 0.018. This value compares favorably with the total flow ratio of 0.016 computed in reference 2 for the same maximum wall temperature with a porous wall of sintered stainless steel and an exhaust-gas temperature of about 3800° R. The somewhat more effective cooling indicated for a porous wall of sintered stainless steel in reference 2 may be caused by a more uniform film of cooling air on the sintered wall than that produced by the fewer number of larger pores in the surface of the wire cloth.

A total flow ratio of 0.032 for flight conditions A to D when using a uniform permeability distribution is about 15 percent higher than the minimum total flow ratio for a constant wall temperature of 1210° R which would generally require a different permeability distribution for each flight condition. Therefore, the practicability of

using wire cloth having a nonuniform longitudinal distribution of permeability, compromising the variable permeability distributions required to maintain a constant wall temperature for each of the flight conditions investigated, is questionable.

Some reductions should be expected in the total flow ratios of transpiration-cooled afterburners if, through quality control, the tolerance on the uniformity of permeability can be decreased from that of the brazed and rolled wire cloth used. The use of porous materials having sufficient strength and resistance to oxidation at higher operating temperatures will also permit a reduction in cooling-air flow. For example, the minimum total flow ratio would decrease about 49 percent if the maximum wall temperature could be increased from 1210° to 1760° R, which may be possible for cloth woven from stainless steel or Inconel wires. It is expected that problems due to oxidation of a braze alloy can be solved by the use of high-temperature brazing alloys under development, or by the substitution of sintering for brazing.

Comparison of Transpiration and Forced-Convection Cooling

The cooling-air requirements for transpiration and forced-convection cooling of this afterburner are compared in figure 17 for exhaust-gas temperatures of 3200° and 3700° R at flight condition B. A typical maximum wall temperature for a forced-convection-cooled wall of stainless steel is 1760° R. With a maximum wall temperature of 1210° R, or limited by minimum practical pressure drop, for a transpiration-cooled wall of brazed and rolled wire cloth, the total flow ratios with transpiration cooling are about 16 percent of the convective requirements for exhaust-gas temperatures of 3200° and 3700° R. The corresponding inlet cooling-air temperatures are shown at the top of the figure to be about 635° and 444° R, respectively, for transpiration and forced-convection cooling. The higher temperature with transpiration cooling results from compressor bleed and from heat absorbed in convectively cooling the impermeable wall upstream of the porous wall.

Pressure Environment of Wire Cloth

The wire cloth successfully withstood the pressure surges of six afterburner starts and the usual pulsations in pressure during normal steady-state afterburning. Ignition of the afterburner usually caused surges in combustion-chamber static pressure to peak values of 2 to 5 inches of mercury. The surges damped out in less than 1 second to the steady-state values. The surge in combustion-chamber static pressure caused similar surges in cooling-air static pressure that varied anywhere from 0.2 to 1.0 or 1.5 inches of mercury. These surges dissipated to steady-state values in several seconds. During steady-state operation

both the cooling-air and combustion-chamber pressure traces showed background pressure pulsations of 100 cps with a total amplitude of about 0.10 to 0.15 inch of mercury superimposed with peaks up to about 1 or 2 inches of mercury total amplitude at roughly 3 cps. The duration of these peaks was about 0.01 second. In one or two instances beats were observed in the trace of combustion-chamber static pressure at a beat frequency of 7 cps with a total amplitude of about 1 to 2 inches of mercury.

CONCLUDING REMARKS

Cooling data were obtained for a transpiration-cooled afterburner having a porous combustion-chamber wall of brazed and rolled wire cloth. The data cover a range of exhaust-gas temperature from 1200° to 3340° R, total flow ratio of cooling air to combustion gas of 0.025 to 0.106, and pressure altitudes of 15,000 to 45,000 feet. The data are successfully correlated over a range of Reynolds numbers from 75,000 to 1,500,000 based on the distance downstream of the leading edge of the porous wall.

Maximum wall temperatures, based on the cooling correlation, were determined for a porous wall of uniform permeability at sea-level take-off and for flight Mach numbers of 0.8, 1.5, and 2.0 at an altitude of 35,000 feet. The cooling-air requirements were nearly independent of the flight conditions. A total flow ratio of cooling air to combustion gas of about 0.032 can maintain a maximum wall temperature of 1210° R with an exhaust-gas temperature of 3700° R. Savings in cooling air would, of course, be possible with porous material having a higher allowable maximum wall temperature.

The total flow ratios with a uniform permeability distribution and air flows sufficient to limit the maximum wall temperature to 1210° R are about 15 percent higher than the minimum total flow ratios corresponding to a variable-permeability wall with a constant wall temperature of 1210° R.

The total flow ratios of cooling air to combustion gas for a maximum wall temperature of 1210° R with the wire-cloth afterburner are about 16 percent of the total flow ratios required to convectively cool a stainless-steel afterburner wall to a maximum temperature of 1760° R with exhaust-gas temperatures of 3200° and 3700° R.

The analysis of cooling-air requirements for the previously mentioned flight conditions indicated that cooling-air static pressure must be closely controlled, especially at a flight Mach number of 2.0.

Lewis Flight Propulsion Laboratory
National Advisory Committee for Aeronautics
Cleveland, Ohio, June 11, 1954

APPENDIX A

SYMBOLS

The following symbols are used in this report:

A_g	combustion-chamber flow area, sq in.
C_v	jet velocity coefficient, measured jet thrust divided by isentropic jet thrust for measured mass flow
c_p	specific heat at constant pressure
D	inside diameter of combustion chamber, in.
$F_{j,m}$	measured jet thrust, lb
g	acceleration due to gravity, ft/sec ²
$H_{g,c}$	convective heat-transfer coefficient that would apply to a solid surface under identical outside flow conditions, Btu/(sec)(sq in.)(°R)
$H_{g,r}$	coefficient of nonluminous heat transfer, Btu/(sec)(sq in.)(°R)
K	permeability coefficient, sq in. (defined in eq. (6) of ref. 3)
L	distance from flame holder to exhaust-nozzle exit, 66 in.
Nu	Nusselt number
P	total pressure, lb/sq in. abs
Pr	Prandtl number
p	static pressure, lb/sq in. abs
$\Delta(p^2)$	difference between squares of absolute static pressures on both sides of porous wall, $p_a^2 - p_g^2$, lb ² /in. ⁴
$\log_{10} \left[\frac{\Delta(p^2)}{\tau} \left(\frac{\mu_o}{\mu} \right)^2 \frac{T_o}{T} \right]$	pressure-drop parameter, lb ² /in. ⁵

R	gas constant, ft-lb/(lb)(°R)
Re	Reynolds number, $(\rho U)_g(x - 21)/\mu_f$
T	total temperature of a gas or surface temperature of a solid, °R
T_f	film temperature, $\frac{T_g + T_w}{2}$, °R
$T_{g,1}$	total temperature at combustion-chamber inlet, °R
$T_{g,2}$	total temperature of exhaust gas at nozzle exit, °R
T_o	NACA standard sea-level temperature, 518.4° R
$\frac{T_w - T_a}{T_g - T_a}$	temperature-difference ratio
U	velocity in axial-flow direction, in./sec
V	velocity normal to porous-wall surface, in./sec
W	weight flow, lb/sec
W_a/W_g	total flow ratio
x	distance downstream of quick-disconnect coupling at combustion-chamber inlet, in.
x'	distance downstream of flame holder, x - 2, in.
Δx	incremental length of combustion chamber, in.
α_g	absorptivity of combustion gas
γ_g	ratio of specific heats of exhaust gas
ϵ	emissivity
μ	absolute viscosity, lb/(in.)(sec)
ρ	weight density, lb/cu in.
$(\rho U)_{g,x}$	total weight flow per unit of combustion-chamber flow area, $\left(W_g + \sum_0^x W_a \right) / A_{g,x}, \text{ lb/((sec)(sq in.))}$

$(\rho V)_a \mu_o / \mu$ reduced weight flow per unit area, lb/(sec)(sq in.)

$(\rho V)_a / (\rho U)_g$ coolant-flow ratio

τ thickness of wire cloth, in.

Subscripts:

a cooling air

f refers to property evaluated at film temperature T_f

g combustion gas

w wall

x at distance x

O free-stream conditions

Numbers greater than 2 represent stations along combustion chamber in inches downstream of quick-disconnect coupling.

3295

APPENDIX B

COMPARISON OF EXPERIMENTAL COOLING CORRELATION WITH THEORY

A brief comparison is made between the experimental cooling correlation and the approximate theory of Rannie and Friedman (refs. 4 and 5) for turbulent boundary-layer flow. The comparison is made between the temperature-difference ratio for individual data points and the theoretical temperature-difference ratio corresponding to the same experimental conditions.

The theoretical equation is given by Friedman (ref. 5) as

$$\frac{T_w - T_a}{T_g - T_a} = \frac{r}{e^{r\phi} + r - 1} \quad (B1)$$

where r is the ratio of the velocity parallel to the surface at the border between the laminar sublayer and the turbulent part of the boundary layer to the stream velocity outside the boundary layer. Eckert (ref. 14) gives

$$r = \frac{2.11}{(Re)_g^{0.1}} \quad (B2)$$

$$\phi = \frac{(\rho V)_a c_{p,a}}{H_{g,c}} \quad (B3)$$

For turbulent boundary-layer flow over a flat plate, Colburn gives

$$Nu = 0.0296(Re)^{0.8}(Pr)^{1/3} \quad (B4)$$

where Re is based on the distance from the leading edge. Rearranging equation (B4) gives

$$\frac{Nu}{RePr} = \frac{H_{g,c}}{(\rho U)_g c_{p,g}} = \frac{0.0296}{(Re)^{0.2}(Pr)^{2/3}} \quad (B5)$$

from which the local value of convective heat-transfer coefficient at any station x is

$$H_{g,c,x} = \frac{0.0296(\rho U c_p)_{g,x}}{(Re)_{g,x}^{0.2} (Pr)_{g,x}^{2/3}} \quad (B6)$$

The effect of temperature level on the Prandtl number is so small that a mean value was used for all cases.

The effects of nonluminous radiation were accounted for by substituting the sum of the equations (B6) and (B7) for $H_{g,c}$ in equation (B3). From the data of reference 15,

$$H_{g,r,x} = \frac{0.173 \epsilon'_s}{(144)(3600)(T_{g,x} - T_{w,x})} \left[\epsilon_{g,x} \left(\frac{T_{g,x}}{100} \right)^4 - \alpha_{g,x} \left(\frac{T_{w,x}}{100} \right)^4 \right] \quad (B7)$$

where $H_{g,r,x}$ is the heat-transfer coefficient for nonluminous radiation at station x . A value of 0.52 was used for the pseudoemissivity ϵ'_s . The local values of combustion-gas emissivity $\epsilon_{g,x}$ and absorptivity $\alpha_{g,x}$ were based on the total fuel-air ratio and local one-dimensional values of temperature and static pressure. No distinction was made between total and static combustion-gas temperature, because the Mach numbers in the combustion chamber were low.

The density and viscosity in the Reynolds number in equation (B6) are usually based on the gas temperature just outside the boundary layer. However, in order to obtain a better correlation of heat-transfer data over a large range of T_w/T_g , the combination of equations (B3) and (B6) (ignoring radiation) was modified in reference 16 to

$$\phi = \frac{(Re)^{0.2} (Pr)^{2/3} (\rho V)_a T_w}{0.0296 (\rho U)_g T_g} \quad (B8)$$

The temperature ratio T_w/T_g has the effect of evaluating the density and viscosity in the Reynolds number at the wall temperature.

In view of equation (B8), the following equation was derived for ϕ_x :

$$\phi_x = \frac{T_{w,x}}{T_{g,x}} \frac{(\rho V c_p)_{a,x}}{\frac{0.0296(\rho U c_p)_{g,x}}{(Re)_{g,x}^{0.2} (Pr)_{g,x}^{2/3}} + \frac{0.173 \epsilon'_s}{(144)(3600)(T_{g,x} - T_{w,x})} \left[\epsilon_{g,x} \left(\frac{T_{g,x}}{100} \right)^4 - \alpha_{g,x} \left(\frac{T_{w,x}}{100} \right)^4 \right]} \quad (B9)$$

Equation (B9) was used in equation (B1) and found to overcorrect the theoretical temperature-difference ratio, so that the intermediate temperature ratio $T_{w,x}/T_{f,x}$ was used in the comparison figures 18 and 19. With afterburning, the inclusion of $T_{w,x}/T_{f,x}$ in equation (B9) results in theoretical wall temperatures generally higher (fig. 18(a)) than those measured. When a value of 1 is assumed for $T_{w,x}/T_{f,x}$, the theoretical wall temperatures are lower than those measured and the scatter is less (fig. 18(b)).

For the nonafterburning data, the inclusion of $T_{w,x}/T_{f,x}$ in equation (B9) results in theoretical wall temperatures that are equal to or slightly lower than those measured (fig. 19(a)). The assumption of $T_{w,x}/T_{f,x}$ of 1 results in a slight lowering of the theoretical wall temperatures over the entire range of temperature-difference ratio (fig. 19(b)).

The determination of an empirical coefficient or exponent for $T_{w,x}/T_{f,x}$ to produce a better agreement does not appear warranted because of differences in the assumptions made in the theory and conditions in the afterburner. Therefore, no conclusion is made as to the validity of including the temperature ratios $T_{w,x}/T_{f,x}$ or $T_{w,x}/T_{g,x}$ in the equation for ϕ .

REFERENCES

1. Eckert, E. R. G., and Livingood, John N. B.: Comparison of Effectiveness of Convection-, Transpiration-, and Film-Cooling Methods with Air as Coolant. NACA TN 3010, 1953.
2. Koffel, William K.: Preliminary Experimental Investigation of Transpiration Cooling for an Afterburner with a Sintered, Porous Stainless-Steel Combustion-Chamber Wall. NACA RM E53D08, 1953.
3. Koffel, William K.: Air-Flow Characteristics of Brazed and Rolled Wire Filter Cloth for Transpiration-Cooled Afterburners. NACA RM E53H24, 1953.
4. Rannie, W. D.: A Simplified Theory of Porous Wall Cooling. Prog. Rep. 4-50, Power Plant Lab. Proj. No. MX801, Jet Prop. Lab., C.I.T. Nov. 24, 1947. (AMC Contract No. W-535-ac-20260, Ord. Dept. Contract No. W-04-200-ORD-455.)
5. Friedman, Joseph: A Theoretical and Experimental Investigation of Rocket-Motor Sweat Cooling. Jour. Am. Rocket Soc., no. 79, Dec. 1949, pp. 147-154.

6. Huntley, S. C., Auble, Carmon M., and Useller, James W.: Altitude Performance Investigation of a High-Temperature Afterburner. NACA RM E53D22, 1953.
7. Conrad, E. William, and Campbell, Carl E.: Altitude Wind Tunnel Investigation of High-Temperature Afterburners. NACA RM E51L07, 1952.
8. Weinbaum, S., and Wheeler, H. L., Jr.: Heat Transfer in Sweat-Cooled Porous Metals. Prog. Rep. 1-58, Air Lab. Proj. No. MX121, Jet Prop. Lab., C.I.T., Apr. 8, 1947. (AMC Contract No. W-535-ac-20260, Ord. Dept. Contract No. W-04-200-ORD-455.)
9. Pinkel, Benjamin, and Turner, L. Richard: Thermodynamic Data for the Computation of the Performance of Exhaust-Gas Turbines. NACA WR E-23, 1944. (Supersedes NACA ARR 4B25.)
10. Wallner, Lewis E., and Wintler, John T.: Experimental Investigation of Typical Constant- and Variable-Area Exhaust Nozzles and Effects on Axial-Flow Turbojet-Engine Performance. NACA RM E51D19, 1951.
11. Koffel, William K., and Kaufman, Harold R.: Empirical Cooling Correlation for an Experimental Afterburner with an Annular Cooling Passage. NACA RM E52C13, 1952.
12. Keenan, Joseph H., and Kaye, Joseph: Gas Tables. John Wiley & Sons, Inc., 1948.
13. Koffel, William K., and Kaufman, Harold R.: Cooling Characteristics of an Experimental Tail-Pipe Burner with an Annular Cooling-Air Passage. NACA RM E51K23, 1952.
14. Eckert, E. R. G.: Introduction to the Transfer of Heat and Mass. McGraw-Hill Book Co., Inc., 1950.
15. McAdams, William H.: Heat Transmission. Second ed., McGraw-Hill Book Co., Inc., 1942, pp. 64-69.
16. Esgar, Jack B.: An Analytical Method for Evaluating Factors Affecting Application of Transpiration Cooling to Gas Turbine Blades. NACA RM E52G01, 1952.

TABLE I. - FLIGHT AND OPERATING CONDITIONS

Series and run	Altitude, ft	Altitude pressure, lb/sq ft abs	Flight Mach number	Engine speed, rpm	Afterburner fuel-air ratio at exhaust nozzle	Engine inlet air temperature, °R	Engine inlet total pressure, lb/sq ft abs	Engine inlet flow, lb/sec	Engine fuel flow, lb/hr	Afterburner fuel flow, lb/hr	Cooling air flow, W _a	Total flow, W _a /g	Cooling air inlet temperature, °R	Turbine gas outlet temperature, °R	Turbine total pressure, lb/sq ft abs	Exhaust gas total temperature, °R
Nonafterburning																
127-27	15,000	1193	0.7	12,478	-----	536	1639	45.77	1590	0	1.201	0.0553	536	1203	2040	-----
127-28		1200	0.7	12,486	-----	535	1700	45.94	1601	0	2.172	0.0299	536	1203	2044	-----
127-29		1193	0.7	12,486	-----	535	1700	45.94	1601	0	2.172	0.0299	535	1203	2044	-----
127-23		1193	0.7	12,480	-----	535	1701	45.99	1601	0	3.827	0.0761	535	1204	2029	-----
127-28		1192	0.7	12,489	-----	535	1700	45.81	1601	0	3.846	0.0768	535	1201	2028	-----
127-21	35,000	500	1.0	12,502	-----	535	946	25.57	1050	0	0.828	0.0310	535	1241	1159	-----
127-20		498	1.0	12,505	-----	535	947	25.52	1057	0	1.082	0.0406	535	1247	1154	-----
130-17		512	1.0	12,464	-----	536	1021	25.53	1056	0	1.29	0.0426	535	1251	1160	-----
127-17		500	1.0	12,496	-----	532	942	25.53	1056	0	1.317	0.0485	532	1251	1158	-----
127-22		489	1.0	12,496	-----	537	1003	25.52	1045	0	1.334	0.0482	533	1254	1156	-----
130-24		499	1.0	12,508	-----	537	1003	25.52	1045	0	1.334	0.0482	533	1254	1156	-----
128-4		501	1.0	12,499	-----	535	949	25.46	1070	0	1.35	0.0504	528	1249	1158	-----
129-18		500	1.0	12,505	-----	535	940	25.37	1055	0	1.392	0.0515	535	1256	1155	-----
129-7		508	1.0	12,519	-----	537	940	25.84	1073	0	1.412	0.0513	531	1204	1171	-----
129-32		520	1.0	12,492	-----	537	957	25.54	1050	0	1.446	0.0530	537	1249	1156	-----
127-18		497	1.0	12,502	-----	533	947	25.57	1060	0	2.141	0.0764	533	1249	1162	-----
127-19		494	1.0	12,515	-----	534	942	25.42	1050	0	2.704	0.0951	534	1249	1153	-----
Afterburning																
129-25	15,000	1202	0.7	12,508	0.036	540	1710	45.71	1929	5170	2.570	0.0511	539	1384	2470	2583
129-26		1195	0.7	12,499	0.036	540	1710	45.71	1918	5170	2.433	0.0500	539	1379	2454	2767
129-24		1195	0.7	12,503	0.037	540	1715	45.94	1929	5170	2.861	0.0564	537	1377	2475	2594
129-23		1175	0.7	12,487	0.037	540	1700	45.46	1940	5192	1.3660	0.0280	537	1391	2482	2784
130-37		1206	0.7	12,531	0.0365	456	1705	51.51	2218	5950	3.10	0.0602	537	1331	2725	1886
130-32		1200	0.7	12,492	0.0386	460	1710	51.35	2287	6175	2.68	0.0475	537	1364	2794	2896
130-33		1211	0.7	12,503	0.033	459	1707	51.35	2310	6175	3.13	0.0531	537	1371	2813	2714
130-30		1197	0.7	12,495	0.033	459	1703	50.77	2211	6448	2.71	0.0483	537	1329	2703	2627
130-29		1204	0.7	12,489	0.0407	465	1700	50.77	2246	6488	2.96	0.0527	537	1350	2743	2626
130-34		1207	0.7	12,471	0.0409	458	1707	50.85	2246	6488	3.01	0.0535	537	1362	2752	2477
130-35		1204	0.7	12,484	0.0421	457	1707	51.37	2440	6535	3.09	0.0602	537	1417	2916	2958
130-36		1207	0.7	12,521	0.0432	456	1707	51.41	2502	6715	3.08	0.0599	537	1433	2857	3013
129-21	16,500	1108	0.63	12,499	0.033	538	1445	38.94	1612	4150	3.015	0.0692	536	1347	2332	2384
129-22		1112	0.63	12,502	0.037	539	1445	38.70	1612	4665	3.503	0.0796	536	1470	2232	2831
129-20	23,500	835	0.74	12,511	0.037	537	1200	32.28	1582	3807	3.168	0.0857	535	1487	1867	2793
128-5	35,000	512	1.0	12,528	0.03205	534	948	25.60	1102	2770	3.16	0.1059	529	1280	1218	1801
128-6		492	1.0	12,541	0.03364	534	941	25.48	1091	2865	2.87	0.0975	529	1284	1213	1832
130-20		504	1.0	12,508	0.0353	540	953	25.28	1197	3050	1.67	0.0895	540	1436	1398	1932
130-21		508	1.0	12,514	0.0359	537	953	25.26	1236	3055	2.21	0.0456	537	1436	1436	2719
130-18		509	1.0	12,486	0.0347	537	951	25.31	1236	3055	2.21	0.0456	537	1436	1430	2820
130-19		508	1.0	12,508	0.0349	539	953	25.30	1213	3055	1.95	0.0888	539	1453	1415	2744
129-19		510	1.0	12,496	0.040	536	970	25.41	1329	3230	2.601	0.0888	535	1534	1517	3042
129-11		500	1.0	12,546	0.041	531	937	25.55	1320	3260	2.068	0.0716	533	1521	1495	2954
129-10		500	1.0	12,515	0.041	530	938	25.52	1320	3260	2.332	0.0801	532	1535	1500	2963
129-8		500	1.0	12,558	0.040	529	945	25.70	1321	3260	2.623	0.0886	533	1525	1513	2930
129-9		508	1.0	12,509	0.040	530	938	25.57	1345	3260	2.896	0.0973	532	1551	1522	2913
129-27		504	1.0	12,505	0.0431	536	955	25.31	1322	3260	2.32	0.0792	532	1557	1523	3104
130-28		504	1.0	12,496	0.0438	536	953	25.38	1322	3265	2.06	0.0716	538	1550	1524	3120
130-26		504	1.0	12,515	0.0487	536	950	25.31	1360	3305	2.23	0.0761	536	1592	1554	3216
130-25		508	1.0	12,499	0.0541	536	943	25.15	1413	4186	2.29	0.0789	536	1627	1581	3340
130-22	45,000	318	1.0	12,521	0.0464	540	601	15.71	957	2230	1.79	0.1007	540	1663	967	3176
130-23		321	1.0	12,489	0.0477	540	591	15.50	930	2230	1.49	0.0864	540	1653	941	3198

TABLE II. - COMBUSTION-CHAMBER WALL TEMPERATURES, °F

Series and run	Channel	Solid metal wall		Wire-cloth porous wall				
		T _{w,10}	T _{w,19}	T _{w,24}	T _{w,32.6}	T _{w,41}	T _{w,49.6}	T _{w,57.5}
127-27	1	558	553	429	459	443	419	400
	9	588	530	459	422	366	323	358
127-26	1	543	533	412	422	410	389	370
	9	570	512	420	382	331	293	330
127-25	1	499	489	348	338	326	310	300
	9	524	464	338	292	254	231	265
127-24	1	468	449	302	282	270	260	250
	9	490	429	283	239	210	193	220
127-23	1	429	411	268	240	228	213	212
	9	452	392	240	198	183	160	181
127-28	1	428	409	269	240	229	219	213
	9	451	393	240	198	186	160	182
127-21	1	600	549	437	462	460	434	422
	9	610	534	422	388	346	312	339
127-20	1	567	518	394	407	406	379	362
	9	583	499	372	331	293	263	287
130-17	1	557	514	372	355	347	321	322
	9	568	489	338	302	287	252	273
127-17	1	538	503	367	372	368	339	333
	9	568	482	338	295	261	236	256
127-22	1	544	500	367	373	365	343	332
	9	568	481	337	294	260	219	265
130-24	1	569	518	376	364	354	330	330
	9	576	493	347	310	289	262	282
128-4	1	839	815	810	725	780	745	850
	9	686	802	719	677	762	885	823
129-18	1	542	509	371	360	348	329	324
	9	370	482	338	298	279	242	267
129-7	1	532	496	366	353	342	325	322
	9	558	473	326	288	259	237	259
129-32	1	539	510	372	359	346	327	324
	9	566	483	338	296	280	244	270
127-18	1	484	433	297	288	272	251	243
	9	502	413	255	213	192	176	192

TABLE II. - Continued. COMBUSTION-CHAMBER WALL TEMPERATURES, °F

Series and run	Channel	Solid metal wall		Wire-cloth porous wall				
		$T_{w,10}$	$T_{w,19}$	$T_{w,24}$	$T_{w,32.6}$	$T_{w,41}$	$T_{w,49.6}$	$T_{w,57.5}$
127-19	1	454	401	264	249	232	219	207
	9	470	388	220	182	172	151	163
129-25	1	648	662	596	649	680	703	768
	9	669	625	519	478	456	384	458
129-26	1	649	669	608	669	699	728	790
	9	672	632	540	499	488	397	476
129-24	1	628	640	560	599	622	648	700
	9	648	600	481	433	420	359	429
129-23	1	618	630	552	581	611	642	686
	9	640	599	451	403	391	334	401
130-37	1	598	605	506	552	582	577	602
	9	605	577	467	425	396	359	419
130-32	1	648	665	658	684	729	752	798
	9	662	649	556	506	452	403	467
130-33	1	628	643	606	622	662	691	733
	9	640	622	498	448	408	368	428
130-31	1	622	632	586	608	631	638	665
	9	633	602	515	473	437	792	453
130-30	1	622	636	600	611	642	658	702
	9	688	608	500	454	418	375	437
130-29	1	622	632	593	606	648	672	701
	9	638	608	492	448	410	370	430
130-34	1	664	681	692	751	823	877	890
	9	674	682	538	478	427	378	432
130-35	1	676	695	718	806	891	930	948
	9	682	707	551	488	436	382	438
130-36	1	685	703	735	845	930	955	978
	9	687	725	545	482	430	380	430
129-21	1	379	577	457	468	478	478	505
	9	592	541	390	351	348	298	356
129-22	1	625	640	580	619	665	709	760
	9	653	650	417	362	352	299	355
129-20	1	620	631	541	574	617	652	707
	9	650	629	397	347	339	290	340

TABLE II. - Concluded. COMBUSTION-CHAMBER WALL TEMPERATURES, °F

Series and run	Channel	Solid metal wall		Wire-cloth porous wall				
		T _{w,10}	T _{w,19}	T _{w,24}	T _{w,32.6}	T _{w,41}	T _{w,49.6}	T _{w,57.5}
128-5	1	475	435	300	285	281	269	264
	9	489	422	262	220	215	187	214
128-6	1	493	456	321	308	302	293	287
	9	508	441	284	240	235	203	232
130-20	1	690	678	564	629	666	689	759
	9	669	648	505	470	457	401	472
130-21	1	726	710	617	701	744	760	842
	9	721	676	588	572	527	490	558
130-18	1	652	649	537	569	603	629	703
	9	669	626	431	388	380	334	388
130-19	1	670	662	544	589	627	654	727
	9	682	634	465	422	415	364	428
129-19	1	650	672	589	647	692	718	830
	9	696	690	425	368	352	302	354
129-11	1	685	712	647	752	828	870	933
	9	732	748	492	433	418	354	412
129-10	1	662	689	600	680	738	713	857
	9	707	718	449	392	379	322	378
129-8	1	637	660	570	623	675	712	802
	9	678	677	408	353	344	297	340
129-9	1	634	652	546	589	628	650	727
	9	679	678	390	338	330	282	330
130-27	1	709	720	611	682	751	778	842
	9	735	752	484	426	400	361	420
130-28	1	730	741	647	732	820	846	905
	9	751	774	519	464	432	393	449
130-26	1	741	758	662	761	847	880	943
	9	768	808	518	458	430	391	457
130-25	1	753	787	679	803	900	926	986
	9	787	813	532	472	948	408	478
130-22	1	723	741	530	577	602	616	680
	9	769	798	472	420	392	362	426
130-23	1	749	777	560	630	663	681	749
	9	690	845	522	478	447	416	490

TABLE III. - COOLING-AIR AND SHROUD TEMPERATURES, °F

Series and run	Channel	Cooling air						Shroud wall		
		T _{a,19} (a)	T _{a,24}	T _{a,32.6}	T _{a,41}	T _{a,49.6}	T _{a,57.5}	T _{s,24}	T _{s,41}	T _{s,57.5}
127-27	1	112	214	204	195	185	178	169	188	194
	9	121	186	179	---	167	165	---	---	---
127-26	1	107	200	182	184	175	166	160	175	179
	9	117	175	114	---	157	154	---	---	---
127-25	1	101	170	157	157	150	145	138	147	150
	9	108	152	108	---	140	135	---	---	---
127-24	1	97	152	143	142	137	131	126	133	133
	9	103	140	108	---	130	125	---	---	---
127-23	1	94	137	130	131	127	120	116	124	121
	9	98	128	107	---	122	117	---	---	---
127-28	1	94	136	130	130	127	123	116	125	123
	9	98	128	123	---	122	118	---	---	---
127-21	1	115	213	199	196	182	174	168	180	190
	9	125	179	173	---	166	162	---	---	---
127-20	1	105	190	178	175	161	146	150	157	155
	9	117	160	101	---	145	138	---	---	---
130-17	1	104	171	162	159	153	132	139	144	141
	9	113	153	151	---	140	132	---	---	---
127-17	1	101	177	167	164	153	138	140	148	147
	9	110	152	104	---	138	132	---	---	---
127-22	1	106	184	172	170	162	160	147	157	168
	9	115	158	105	---	150	149	---	---	---
130-24	1	107	175	166	165	156	144	144	151	154
	9	117	159	154	---	144	141	---	---	---
128-4	1	97	175	165	163	152	137	142	148	148
	9	107	151	149	---	139	132	---	---	---
129-18	1	101	170	161	160	133	148	138	144	138
	9	112	151	155	---	135	126	---	---	---
129-7	1	99	169	160	158	135	145	136	142	140
	9	109	149	143	---	136	131	---	---	---
129-32	1	104	171	164	163	144	150	141	148	146
	9	115	154	155	---	140	136	---	---	---
127-18	1	95	149	193	142	136	131	123	130	131
	9	101	185	101	---	127	123	---	---	---

^aValues read from circumferential temperature profiles.

TABLE III. - Continued. COOLING-AIR AND SHROUD TEMPERATURES, °F

Series and run	Channel	Cooling air						Shroud wall		
		T _{a,19} (a)	T _{a,24}	T _{a,32.6}	T _{a,41}	T _{a,49.6}	T _{a,57.5}	T _{s,24}	T _{s,41}	T _{s,57.5}
127-19	1	92	137	133	131	127	121	115	121	120
	9	97	127	122	---	120	115	---	---	---
129-25	1	126	255	222	229	242	224	195	224	257
	9	130	200	213	---	181	186	---	---	---
129-26	1	129	264	228	236	254	232	200	232	273
	9	134	207	219	---	185	192	---	---	---
129-24	1	122	235	208	214	224	209	181	208	239
	9	127	190	200	---	173	177	---	---	---
129-23	1	117	223	200	205	210	198	171	195	216
	9	122	182	207	---	165	169	---	---	---
130-37	1	112	219	193	198	195	204	167	191	209
	9	120	190	181	---	163	171	---	---	---
130-32	1	124	265	228	236	231	238	194	227	256
	9	125	213	149	---	177	185	---	---	---
130-33	1	119	240	210	217	216	231	179	210	244
	9	121	196	141	---	168	176	---	---	---
130-31	1	117	241	209	215	210	214	180	206	226
	9	122	201	---	---	171	180	---	---	---
130-30	1	117	138	208	214	208	211	177	205	222
	9	122	197	196	---	168	174	---	---	---
130-29	1	115	235	207	213	210	217	176	206	230
	9	121	194	131	---	166	171	---	---	---
130-34	1	125	264	228	239	239	256	192	230	275
	9	124	208	139	---	174	179	---	---	---
130-35	1	127	273	235	248	249	176	196	239	198
	9	128	212	137	---	177	183	---	---	---
130-36	1	128	274	236	250	256	290	198	246	315
	9	128	210	140	---	177	183	---	---	---
129-21	1	107	190	175	176	178	156	150	165	184
	9	117	167	166	---	154	156	---	---	---
129-22	1	116	219	211	204	210	199	169	191	218
	9	121	174	170	---	160	161	---	---	---
129-20	1	114	210	193	197	203	192	164	183	205
	9	119	170	165	---	156	157	---	---	---

^aValues read from circumferential temperature profiles.

TABLE III. - Concluded. COOLING-AIR AND SHROUD TEMPERATURES, °F

Series and run	Channel	Cooling air						Shroud wall		
		T _{a,19} (a)	T _{a,24}	T _{a,32.6}	T _{a,41}	T _{a,49.6}	T _{a,57.5}	T _{s,24}	T _{s,41}	T _{s,57.5}
128-5	1	89	140	135	134	130	121	117	125	123
	9	96	131	130	---	122	117	---	---	---
128-6	1	90	146	140	139	134	124	121	129	128
	9	98	136	136	---	127	123	---	---	---
130-20	1	129	243	253	179	224	239	191	219	256
	9	132	197	253	---	179	190	---	---	---
130-21	1	137	273	248	259	254	274	217	256	303
	9	142	218	334	---	199	214	---	---	---
130-18	1	117	215	199	203	194	186	169	186	199
	9	122	177	170	---	158	156	---	---	---
130-19	1	124	229	211	216	211	244	180	203	234
	9	127	187	182	---	170	177	---	---	---
129-19	1	118	224	220	213	212	206	173	197	220
	9	123	177	175	---	160	158	---	---	---
129-11	1	124	249	247	238	240	236	191	224	275
	9	128	191	187	---	175	172	---	---	---
129-10	1	118	233	214	220	228	214	179	204	238
	9	125	182	197	---	164	155	---	---	---
129-8	1	114	217	200	205	191	185	166	186	199
	9	119	171	170	---	154	150	---	---	---
129-9	1	118	213	195	200	210	197	164	184	215
	9	120	170	165	---	156	157	---	---	---
130-27	1	127	246	226	236	241	275	192	225	293
	9	133	198	144	---	179	190	---	---	---
130-28	1	129	258	236	247	250	279	200	236	302
	9	137	204	130	---	179	184	---	---	---
130-26	1	129	260	239	251	257	296	201	241	325
	9	137	205	197	---	185	198	---	---	---
130-25	1	126	256	236	247	245	255	199	235	283
	9	137	206	191	---	180	186	---	---	---
130-22	1	127	227	212	216	209	219	181	196	229
	9	139	198	185	---	173	171	---	---	---
130-23	1	132	247	229	235	233	258	195	219	178
	9	149	211	201	---	198	218	---	---	---

^aValues read from circumferential temperature profiles.

TABLE IV. - COMBUSTION-GAS AND COOLING-AIR PRESSURES

Series and run	Channel	Combustion-chamber static pressures, lb/sq in. abs									Cooling-air pressures, lb/sq in. abs						
		P _{g,10}	P _{g,19}	P _{g,24}	P _{g,32.6}	P _{g,41}	P _{g,49.6}	P _{g,57.5}	P _{g,63.8}	P _{g,67.8}	P _{a,15}	P _{a,24}	P _{a,24}	P _{a,32.6}	P _{a,41}	P _{a,49.6}	P _{a,57.5}
127-27	1 9	9.507	9.778	9.840	9.688	9.556	9.243	9.188	8.715	8.354	10.4	10.29 10.42	10.16 10.20	10.21 10.30	10.21 10.31	10.22 10.30	10.22 10.29
127-26	1 9	9.493	9.757	9.813	9.660	9.521	9.194	9.132	8.625	8.326	10.62	10.49 10.66	10.29 10.37	10.37 10.51	10.38 10.52	10.39 10.51	10.38 10.50
127-25	1 9	9.604	9.882	9.910	9.764	9.583	9.257	9.146	8.653	8.319	11.71	11.43 11.79	11.03 11.27	11.19 11.49	11.22 11.53	11.23 11.52	11.23 11.51
127-24	1 9	9.701	9.979	9.993	9.833	9.625	9.285	9.139	8.646	8.319	13.05	12.49 13.11	11.86 12.33	12.14 12.65	12.19 12.71	12.20 12.70	12.21 12.69
127-23	1 9	9.785	10.06	10.07	9.903	9.660	9.292	9.097	8.681	8.326	14.81	13.95 14.87	13.00 13.80	13.43 14.25	13.51 14.34	13.53 14.33	13.54 14.33
127-28	1 9	9.785	10.06	10.08	9.903	9.646	9.299	9.104	8.646	8.340	14.70	13.84 14.75	12.88 13.67	13.31 14.13	13.39 14.22	13.42 14.22	13.42 14.21
127-21	1 9	4.500	4.708	4.757	4.667	4.576	4.326	4.257	3.854	3.500	5.563	5.48 5.57	5.35 5.38	5.39 5.48	5.39 5.49	5.40 5.48	5.39 5.46
127-20	1 9	4.542	4.750	4.778	4.694	4.590	4.340	4.250	3.833	3.479	6.055	5.912 6.077	5.700 5.790	5.780 5.928	5.790 5.939	5.795 5.93	5.790 5.918
130-17	1 9	4.625	4.84	4.889	4.785	4.646	4.444	4.194	3.931	3.556	6.605	6.397 6.647	6.083 6.386	6.195 6.471	6.216 6.482	6.227 6.498	6.216 6.492
127-17	1 9	4.569	4.778	4.819	4.715	4.597	4.354	4.250	3.875	3.500	6.493	6.301 6.536	6.025 6.163	6.121 6.322	6.142 6.344	6.153 6.33	6.147 6.323
127-22	1 9	4.563	4.764	4.806	4.708	4.583	4.326	4.222	3.826	3.479	6.514	6.312 6.551	6.030 6.179	6.136 6.349	6.152 6.365	6.158 6.35	6.158 6.338
130-24	1 9	4.569	4.785	4.826	4.736	4.590	4.389	4.146	3.854	3.465	6.470	6.281 6.509	5.973 6.260	6.079 6.345	6.100 6.355	6.106 6.366	6.100 6.366
128-4	1 9	4.56	4.78	4.76	4.69	4.58	4.33	4.22	3.82	3.48	6.425	6.191 6.414	5.914 6.159	6.031 6.239	6.042 6.265	6.053 -----	6.053 6.265
129-18	1 9	4.576	4.792	4.813	4.750	4.611	4.431	-----	3.910	3.514	6.61	6.39 6.65	6.08 6.40	6.21 6.47	6.22 6.48	6.23 6.48	6.23 6.49
129-7	1 9	4.715	4.931	4.938	4.840	4.729	4.493	4.354	3.958	3.632	6.82	6.59 6.87	6.27 6.60	6.39 6.68	6.41 6.69	6.41 6.69	6.41 6.70
129-32	1 9	4.625	4.833	4.854	4.785	4.646	4.465	6.438	3.922	3.611	6.748	6.499 6.791	6.175 6.515	6.313 6.600	6.329 6.610	6.334 6.175	6.334 6.621
127-18	1 9	4.701	4.903	4.931	4.806	4.646	4.382	4.208	3.847	3.498	8.326	7.847 8.390	7.326 7.746	7.549 8.017	7.592 8.060	7.613 8.045	7.613 8.028
127-19	1 9	4.806	5.000	5.000	4.889	4.701	4.417	4.208	3.847	3.431	9.722	9.06 9.80	8.34 8.99	8.66 9.33	8.72 9.39	8.74 9.38	8.74 9.37
129-25	1 9	14.63	14.55	14.39	13.93	13.25	12.65	-----	10.38	8.382	15.81	15.43 15.88	15.02 15.47	15.17 15.58	15.20 15.60	15.23 15.60	15.23 15.61
129-26	1 9	14.58	14.51	14.36	13.90	13.23	12.63	-----	10.36	8.431	15.59	15.25 15.66	14.87 15.28	15.02 15.38	15.04 15.39	15.06 15.40	15.06 15.41
129-24	1 9	14.65	14.60	14.42	13.97	13.26	12.65	-----	10.38	8.375	16.23	15.52 16.37	14.81 15.61	15.08 15.82	15.14 15.86	15.16 15.87	15.18 15.89
129-23	1 9	14.74	14.65	14.49	14.01	13.28	12.64	-----	10.40	8.306	16.76	15.89 16.92	15.05 16.04	15.41 16.28	15.48 16.34	15.51 16.36	15.52 16.38
130-37	1 9	16.04	16.00	15.97	15.47	14.49	13.73	12.76	-----	8.374	17.46	17.00 17.54	16.48 17.03	16.67 17.18	16.72 17.21	16.74 17.24	16.74 17.24
130-32	1 9	16.59	16.47	16.42	15.85	14.84	14.09	12.86	11.43	8.333	17.33	16.98 17.39	16.59 16.99	16.70 17.10	16.74 17.12	16.76 17.14	16.76 16.79
130-33	1 9	16.69	16.55	16.49	15.91	14.88	14.12	12.90	11.50	8.409	18.01	17.53 18.08	17.01 17.56	17.19 17.71	17.23 17.74	17.26 17.77	17.25 17.77

TABLE IV. - Concluded. COMBUSTION-GAS AND COOLING-AIR PRESSURES

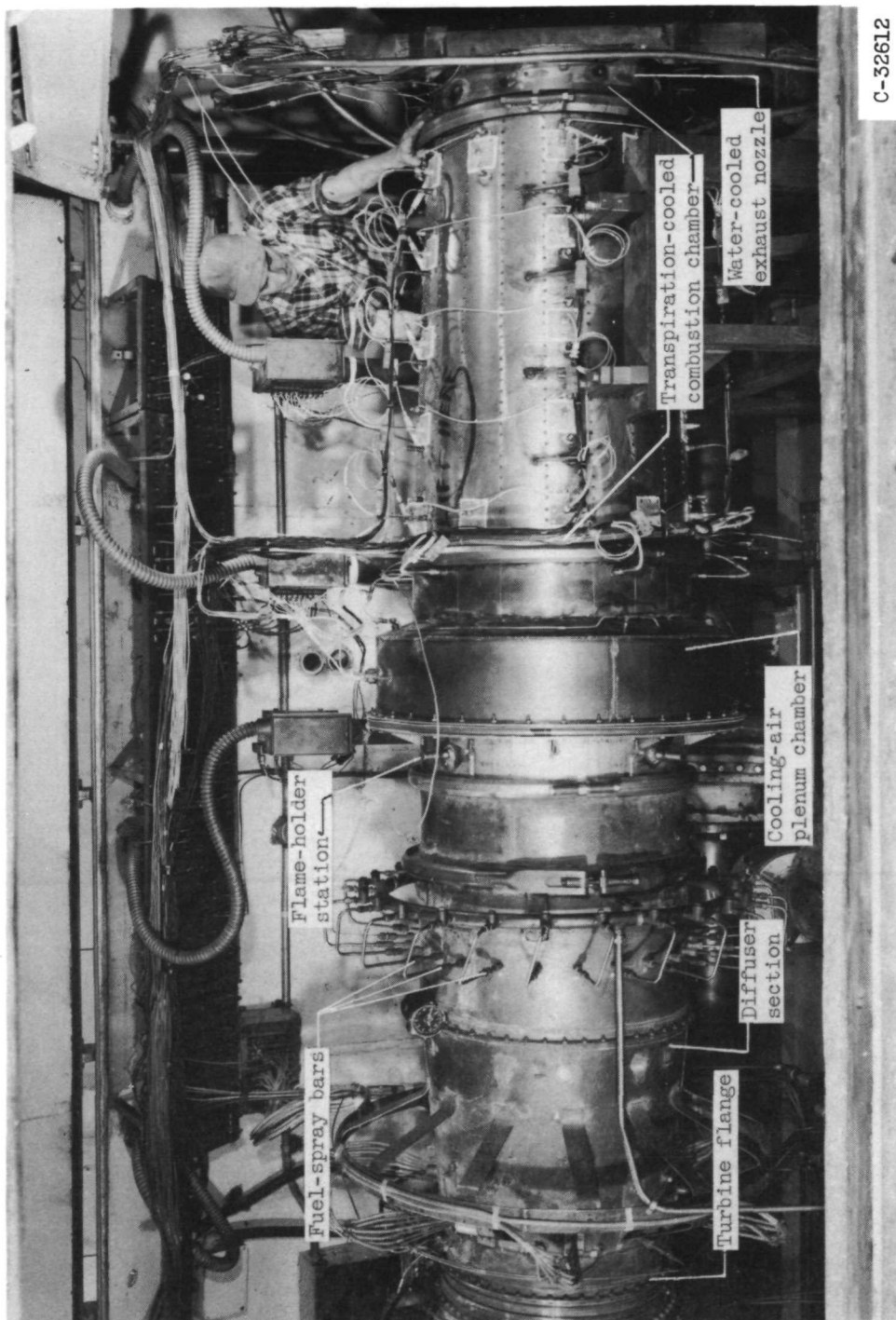
Series and run	Channel	Combustion-chamber static pressures, lb/sq in. abs									Cooling-air pressures, lb/sq in. abs						
		P _{g,10}	P _{g,19}	P _{g,24}	P _{g,32.6}	P _{g,41}	P _{g,49.6}	P _{g,57.5}	P _{g,63.8}	P _{g,67.8}	P _{a,15}	P _{a,24}	P _{a,24}	P _{a,32.6}	P _{a,41}	P _{a,49.6}	P _{a,57.5}
130-31	1 9	15.94	15.88	15.85	15.36	14.42	13.69	12.47	11.15	8.340	16.86	16.50 16.93	16.08 16.52	16.22 16.64	16.25 16.65	16.27 16.67	16.28 16.68
130-30	1 9	16.20	16.11	16.06	15.53	14.55	13.81	12.59	11.27	8.312	17.40	16.95 17.46	16.48 17.00	16.65 17.13	16.68 17.16	16.70 17.18	16.71 17.18
130-29	1 9	16.26	16.16	16.10	15.56	14.58	13.83	12.61	12.17	8.361	17.52	17.07 17.59	16.57 16.98	16.74 17.25	16.79 17.28	16.81 17.30	16.82 17.31
130-34	1 9	17.43	17.21	17.11	16.43	15.29	14.53	13.34	11.80	8.381	18.48	18.10 18.63	17.60 18.11	17.77 18.26	17.81 18.28	17.83 18.31	17.84 18.32
130-35	1 9	17.70	17.45	17.33	16.59	15.42	14.67	13.58	11.94	8.361	18.75	18.29 18.82	17.80 18.30	17.96 18.44	18.01 18.47	18.03 18.50	18.03 18.50
130-36	1 9	17.94	17.67	17.53	16.76	15.53	14.83	13.81	12.10	8.381	19.18	18.70 19.25	18.16 18.70	18.35 18.85	18.39 18.88	18.41 18.91	18.41 18.91
129-21	1 9	11.87	11.88	11.77	11.43	10.90	10.36	-----	8.576	7.153	14.42	13.64 14.67	12.75 13.79	13.15 14.06	13.22 14.11	13.25 14.13	13.26 14.15
129-22	1 9	13.35	13.20	13.00	12.48	11.78	11.21	-----	9.153	7.056	16.42	15.33 16.60	14.26 15.51	14.72 15.83	14.80 15.89	14.85 15.92	14.87 15.94
129-20	1 9	11.18	11.06	10.90	10.45	9.868	9.368	-----	7.604	5.840	14.54	13.84 14.65	13.14 13.96	13.45 14.16	13.50 14.21	13.52 14.22	13.53 14.23
128-5	1 9	6.72	6.80	6.72	6.54	6.22	5.78	5.44	4.74	3.60	11.33	10.52 11.32	9.70 10.56	10.08 10.82	10.14 10.90	10.17 10.91	10.17 10.93
128-6	1 9	6.67	6.74	6.65	6.47	6.17	5.74	5.40	4.71	3.51	10.67	9.95 10.66	9.24 9.98	10.17 10.21	9.62 10.28	9.64 10.29	9.64 10.30
130-20	1 9	8.174	8.132	8.076	7.778	7.382	6.993	6.354	5.590	3.500	9.854	9.321 9.619	9.013 9.342	9.119 9.417	9.140 9.433	9.151 9.449	9.151 9.496
130-21	1 9	8.056	8.021	7.972	7.681	7.319	6.958	6.292	5.549	3.528	8.798	8.650 8.826	8.464 8.661	8.523 8.703	8.533 8.703	8.544 8.714	8.544 8.714
130-18	1 9	8.451	8.396	8.319	7.986	7.549	7.146	6.472	5.715	3.535	10.75	10.36 10.82	9.868 10.39	10.05 10.52	10.08 10.55	10.10 10.57	10.10 10.57
130-19	1 9	8.347	8.300	8.236	7.924	7.500	7.104	6.451	5.660	3.528	10.22	9.896 10.28	9.492 9.928	9.641 10.02	9.662 10.04	9.678 10.07	9.678 10.07
129-19	1 9	9.049	8.931	8.764	8.382	7.910	7.528	-----	6.014	3.646	12.15	11.51 12.11	10.94 11.56	11.18 11.71	11.21 11.74	11.23 11.75	11.23 11.77
129-11	1 9	8.951	8.840	8.681	8.299	7.854	7.514	-----	6.007	3.542	10.98	10.66 11.05	10.23 10.66	10.40 10.77	10.42 10.79	10.43 10.80	10.43 10.80
129-10	1 9	8.972	8.854	8.694	8.299	7.861	7.514	6.875	6.000	3.563	11.50	11.08 11.57	10.58 11.11	10.77 11.23	10.80 11.27	10.82 11.27	10.82 11.28
129-8	1 9	9.090	8.979	8.806	8.396	7.958	7.583	6.924	6.056	3.438	12.08	11.60 12.22	11.01 11.65	11.25 11.81	11.29 11.84	11.31 11.86	11.31 11.87
129-9	1 9	9.097	8.986	8.806	8.396	7.944	7.556	6.903	6.083	3.590	12.70	12.11 12.81	11.42 12.17	11.70 12.37	11.75 12.40	11.77 12.41	11.77 12.42
130-27	1 9	9.153	9.042	8.944	8.542	7.986	7.576	6.896	6.083	3.500	11.51	11.11 11.56	10.64 11.13	10.82 11.26	10.85 11.28	10.86 11.30	10.87 11.30
130-28	1 9	9.132	9.000	8.917	8.528	7.965	7.569	6.944	6.090	3.500	11.04	10.70 11.10	10.33 10.36	10.48 10.83	10.49 10.85	10.51 10.87	10.51 10.86
130-26	1 9	9.361	9.229	9.118	8.319	8.118	7.729	7.090	6.250	3.500	11.61	11.20 11.66	10.79 11.23	10.96 11.36	10.98 11.38	11.00 11.40	11.00 11.40
130-25	1 9	9.549	9.389	9.264	8.792	8.264	7.868	7.118	6.313	3.528	11.87	11.46 11.28	11.05 11.49	11.21 11.61	11.24 11.64	11.25 11.66	11.26 11.66
130-22	1 9	5.750	5.681	5.611	5.340	5.028	4.757	4.340	3.799	2.208	8.430	8.107 8.474	7.687 8.128	7.841 8.229	7.868 8.250	7.879 8.261	7.879 8.266
130-23	1 9	5.604	5.542	5.472	5.208	4.903	4.660	4.250	3.722	2.229	7.048	7.483 7.780	7.175 7.515	7.291 7.589	7.307 7.600	7.323 7.610	7.323 7.610

TABLE V. - AIR-FLOW CALIBRATION DATA OF AFTERBURNER AT AMBIENT TEMPERATURE

Series end run	Ambient tank pres- sure, lb/sq ft abs	Measured cooling- air flow, lb/sec	Cooling- air tem- pera- ture, °F	Combustion-chamber static pressures, lb/sq in. abs								Channel	Cooling-air pressures, lb/sq in. abs							
				P _{g,10}	P _{g,19}	P _{g,24}	P _{g,32.6}	P _{g,41}	P _{g,49.6}	P _{g,57.5}	P _{g,63.8}		P _{g,15}	P _{g,24}	P _{g,32.6}	P _{g,41}	P _{g,49.6}	P _{g,57.5}		
127-14	2028	0.9695	534	14.10	14.10	14.10	14.10	14.10	14.10	14.10	14.10	14.08	1	14.42	14.39	14.31	14.34	14.35	14.35	14.34
127-2	2028	1.005	527	14.10	14.10	14.10	14.10	14.10	14.10	14.10	14.10	14.11	9	14.42	14.39	14.31	14.33	14.34	14.35	14.39
127-3	2028	1.596	530	14.10	14.10	14.10	14.10	14.10	14.10	14.10	14.10	14.08	1	14.42	14.39	14.31	14.33	14.34	14.35	14.33
127-4	2028	1.955	531	14.09	14.09	14.08	14.10	14.10	14.10	14.10	14.10	14.08	9	14.43	14.39	14.36	14.38	14.39	14.39	14.35
127-5	2028	2.296	532	14.09	14.09	14.09	14.09	14.09	14.09	14.09	14.09	14.08	1	14.82	14.73	14.54	14.60	14.62	14.63	14.62
127-6	2028	2.850	534	14.08	14.08	14.08	14.10	14.08	14.08	14.08	14.08	14.08	9	14.83	14.73	14.54	14.62	14.63	14.63	14.62
127-7	2028	3.310	535	14.11	14.11	14.11	14.11	14.11	14.11	14.11	14.11	14.10	1	15.11	14.98	14.70	14.78	14.81	14.82	14.81
127-8	2028	3.914	534	14.07	14.07	14.07	14.07	14.07	14.07	14.07	14.07	14.08	9	15.45	15.28	14.88	15.00	15.05	15.06	15.05
127-9	2028	4.315	535	14.08	14.08	14.08	14.08	14.08	14.08	14.08	14.08	14.08	1	15.50	15.11	15.25	15.25	15.29	15.29	15.25
127-10	2028	4.678	534	14.08	14.08	14.08	14.08	14.08	14.08	14.08	14.08	14.08	9	16.08	15.83	15.23	15.41	15.47	15.49	15.49
127-11	2028	5.083	535	14.10	14.10	14.10	14.10	14.10	14.10	14.10	14.10	14.11	1	16.22	15.60	15.83	15.83	15.86	15.86	15.86
127-12	2028	5.441	535	14.07	14.07	14.07	14.07	14.07	14.07	14.07	14.07	14.08	9	16.67	16.32	15.56	15.81	15.88	15.90	15.90
127-13	2028	5.810	535	14.08	14.08	14.08	14.08	14.08	14.08	14.08	14.08	14.08	1	16.85	15.95	16.31	16.38	16.39	16.39	16.39
127-35	1195	1.255	533	8.285	8.285	8.285	8.285	8.285	8.285	8.285	8.285	8.340	9	17.46	15.48	14.52	14.85	14.96	14.98	14.99
127-36	1195	1.710	532	8.368	8.368	8.361	8.361	8.361	8.361	8.361	8.361	8.410	1	18.11	17.39	16.38	16.80	16.92	16.94	16.94
127-37	1192	2.799	532	8.250	8.250	8.243	8.236	8.243	8.243	8.229	8.264	8.361	9	18.34	17.19	17.59	17.72	17.72	17.72	17.72
127-38	1196	3.200	532	8.368	8.368	8.361	8.361	8.361	8.361	8.354	8.375	8.361	1	18.70	17.85	16.73	17.22	17.34	17.36	17.37
127-39	1200	3.805	532	8.369	8.369	8.375	8.375	8.375	8.375	8.368	8.424	8.361	9	18.93	17.69	16.15	16.26	16.26	16.26	16.27
127-40	1192	4.344	532	8.340	8.340	8.340	8.333	8.333	8.333	8.336	8.347	8.340	1	19.36	18.40	17.16	17.70	17.84	17.86	17.87
127-34	497	9.033	532	-----	-----	-----	-----	-----	-----	-----	3.472	3.493	9	19.60	18.24	16.75	16.89	16.89	16.89	16.90
127-33	493	1.313	532	3.472	3.472	3.472	3.472	3.472	3.472	3.465	3.479	3.479	1	20.04	18.94	17.58	18.18	18.34	18.37	18.37
													9	20.29	18.79	16.94	17.92	18.52	19.53	19.53
													1	20.68	19.47	17.96	18.63	18.81	18.83	18.85
													9	20.93	19.35	19.95	20.11	20.11	20.12	20.12
													1	9.05	8.948	8.778	8.842	8.852	8.852	8.852
													9	9.086	8.889	8.964	8.980	8.980	8.980	8.989
													1	9.63	9.451	9.143	9.260	9.286	9.286	9.286
													9	9.685	9.350	9.483	9.504	9.504	9.504	9.494
													1	11.15	10.67	9.990	10.27	10.33	10.34	10.34
													9	11.26	10.53	10.81	10.87	10.87	10.86	10.86
													1	11.83	11.34	10.52	10.86	10.94	10.95	10.95
													9	12.07	11.19	11.52	11.60	11.60	11.60	11.60
													1	13.03	12.31	11.26	11.70	11.82	11.83	11.83
													9	13.26	12.16	12.59	12.69	12.69	12.69	12.69
													1	14.15	13.19	11.95	12.46	12.60	12.62	12.62
													9	14.33	13.05	13.55	13.68	13.68	13.69	13.69
													1	5.52	3.415	3.234	3.308	3.319	3.319	3.319
													9	5.564	3.551	3.441	3.457	3.457	3.456	3.456
													1	5.212	5.013	4.672	4.811	4.832	4.843	4.837
													9	5.279	4.917	4.587	4.661	4.661	4.661	4.661

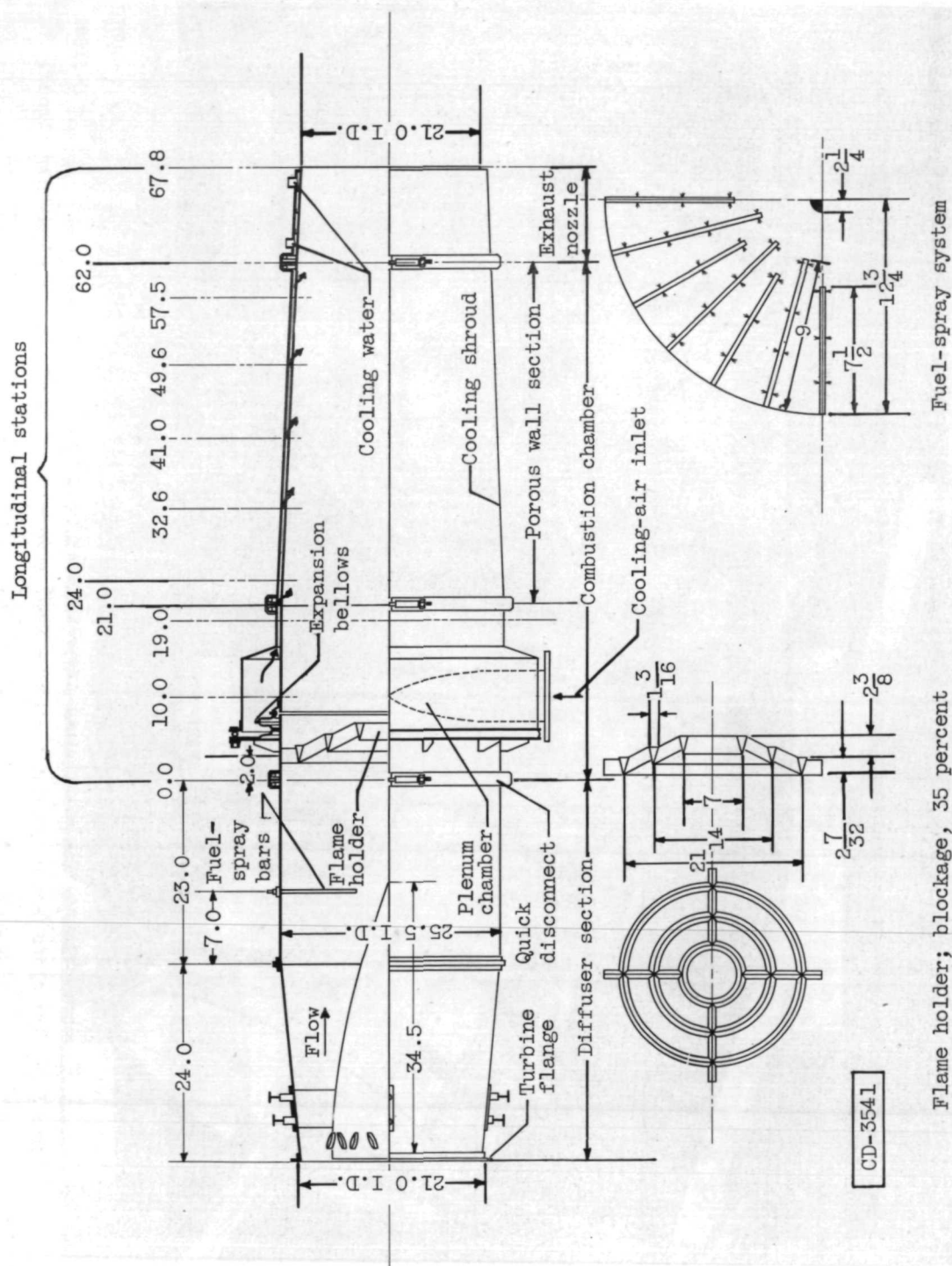
TABLE V. - Continued. AIR-FLOW CALIBRATION DATA OF AFTERBURNER AT AMBIENT TEMPERATURE

Series end run	Ambient tank pres- sure, lb/sq ft abs	Measured cooling- air flow, lb/sec or	Combustion-chamber static pressures, lb/sq in. abs						Channel	Cooling-air pressures, lb/sq in. abs					
			P _{g,10}	P _{g,19}	P _{g,24}	P _{g,32.6}	P _{g,41}	P _{g,49.6}		P _{a,15}	P _{a,24}	P _{a,32.6}	P _{a,41}	P _{a,49.6}	P _{a,57.5}
127-32	495	1.822	3.493	3.493	3.486	3.486	3.486	3.486	1	6.660	6.282	5.702	5.905	5.963	5.968
127-29	491	1.895	3.444	3.444	3.444	3.444	3.444	3.438	9	6.766	6.160	6.394	6.442	6.426	6.426
127-31	498	2.380	3.528	3.528	3.528	3.528	3.528	3.514	1	6.483	6.135	5.571	5.768	5.816	5.826
127-30	492	2.849	3.465	3.465	3.465	3.465	3.465	3.444	9	6.592	6.00	6.231	6.273	6.263	6.263
129-12	1230	1.733	3.493	3.493	3.486	3.486	3.486	3.486	1	7.705	7.197	6.474	6.740	6.814	6.825
129-13	1208	2.202	3.465	3.465	3.465	3.465	3.465	3.444	9	7.830	7.086	6.378	6.742	6.825	7.431
129-14	1218	2.633	3.493	3.493	3.486	3.486	3.486	3.486	1	8.91	8.25	7.357	7.687	7.782	7.793
129-15	1229	3.011	3.444	3.444	3.444	3.444	3.444	3.438	9	9.038	8.144	8.495	8.590	8.570	8.570
129-16	1208	3.763	3.493	3.493	3.486	3.486	3.486	3.486	1	9.847	9.630	9.340	9.470	9.495	9.495
129-17	1201	4.230	3.465	3.465	3.465	3.465	3.465	3.444	9	9.920	9.655	9.730	9.740	9.760	9.760
129-27	1205	1.757	3.493	3.493	3.486	3.486	3.486	3.486	1	10.40	10.06	9.620	9.800	9.850	9.860
129-28	1199	2.241	3.444	3.444	3.444	3.444	3.444	3.438	9	11.11	10.65	10.005	10.32	10.38	10.40
129-29	1216	2.657	3.493	3.493	3.486	3.486	3.486	3.486	1	11.29	10.715	10.93	10.95	10.95	10.95
129-30	1206	3.194	3.444	3.444	3.444	3.444	3.444	3.438	9	11.82	11.245	10.52	10.84	10.91	10.92
129-31	1200	3.751	3.493	3.493	3.486	3.486	3.486	3.486	1	13.20	12.38	11.36	11.68	11.90	11.92
129-2	503	1.126	3.493	3.493	3.486	3.486	3.486	3.486	9	14.11	13.11	12.38	12.53	12.55	12.56
129-3	492	1.554	3.444	3.444	3.444	3.444	3.444	3.438	1	13.52	12.52	12.82	12.91	12.91	12.91
129-4	495	2.023	3.493	3.493	3.486	3.486	3.486	3.486	9	14.48	13.32	13.665	13.78	13.81	13.81
129-5	502	2.459	3.444	3.444	3.444	3.444	3.444	3.438	1	9.722	9.490	9.190	9.335	9.350	9.350
129-6	502	2.862	3.493	3.493	3.486	3.486	3.486	3.486	9	9.868	9.530	9.600	9.62	9.630	9.630
			3.444	3.444	3.444	3.444	3.444	3.438	1	10.38	10.02	9.580	9.760	9.800	9.820
			3.493	3.493	3.486	3.486	3.486	3.486	9	10.52	10.065	10.09	10.12	10.12	10.25
			3.444	3.444	3.444	3.444	3.444	3.438	1	11.13	10.63	10.04	10.31	10.365	10.38
			3.493	3.493	3.486	3.486	3.486	3.486	9	11.28	10.695	10.88	10.92	10.92	10.95
			3.444	3.444	3.444	3.444	3.444	3.438	1	12.04	11.40	10.60	10.95	11.014	11.06
			3.493	3.493	3.486	3.486	3.486	3.486	9	12.26	11.57	11.746	11.815	11.815	11.845
			3.444	3.444	3.444	3.444	3.444	3.438	1	13.10	12.26	11.70	11.805	11.82	11.82
			3.493	3.493	3.486	3.486	3.486	3.486	9	13.41	12.415	12.71	12.80	12.805	12.835
			3.444	3.444	3.444	3.444	3.444	3.438	1	4.930	4.77	4.491	4.605	4.608	4.630
			3.493	3.493	3.486	3.486	3.486	3.486	9	4.985	4.761	4.831	4.857	4.860	4.86
			3.444	3.444	3.444	3.444	3.444	3.438	1	5.770	5.575	5.122	5.305	5.340	5.353
			3.493	3.493	3.486	3.486	3.486	3.486	9	5.938	5.580	5.695	5.720	5.735	5.735
			3.444	3.444	3.444	3.444	3.444	3.438	1	6.993	6.575	5.958	6.22	6.268	6.275
			3.493	3.493	3.486	3.486	3.486	3.486	9	7.118	6.630	6.778	6.820	6.832	6.840
			3.444	3.444	3.444	3.444	3.444	3.438	1	8.138	7.610	6.825	7.150	7.220	7.236
			3.493	3.493	3.486	3.486	3.486	3.486	9	8.305	7.691	7.880	7.940	7.960	7.960
			3.444	3.444	3.444	3.444	3.444	3.438	1	9.263	8.945	7.680	8.020	8.118	8.130
			3.493	3.493	3.486	3.486	3.486	3.486	9	9.46	8.705	8.950	9.020	9.040	9.045



C-32612

Figure 1. - Afterburner installation in altitude test chamber.



Flame holder; blockage, 35 percent

Figure 2. - Sectional view of afterburner. (All dimensions in inches.)

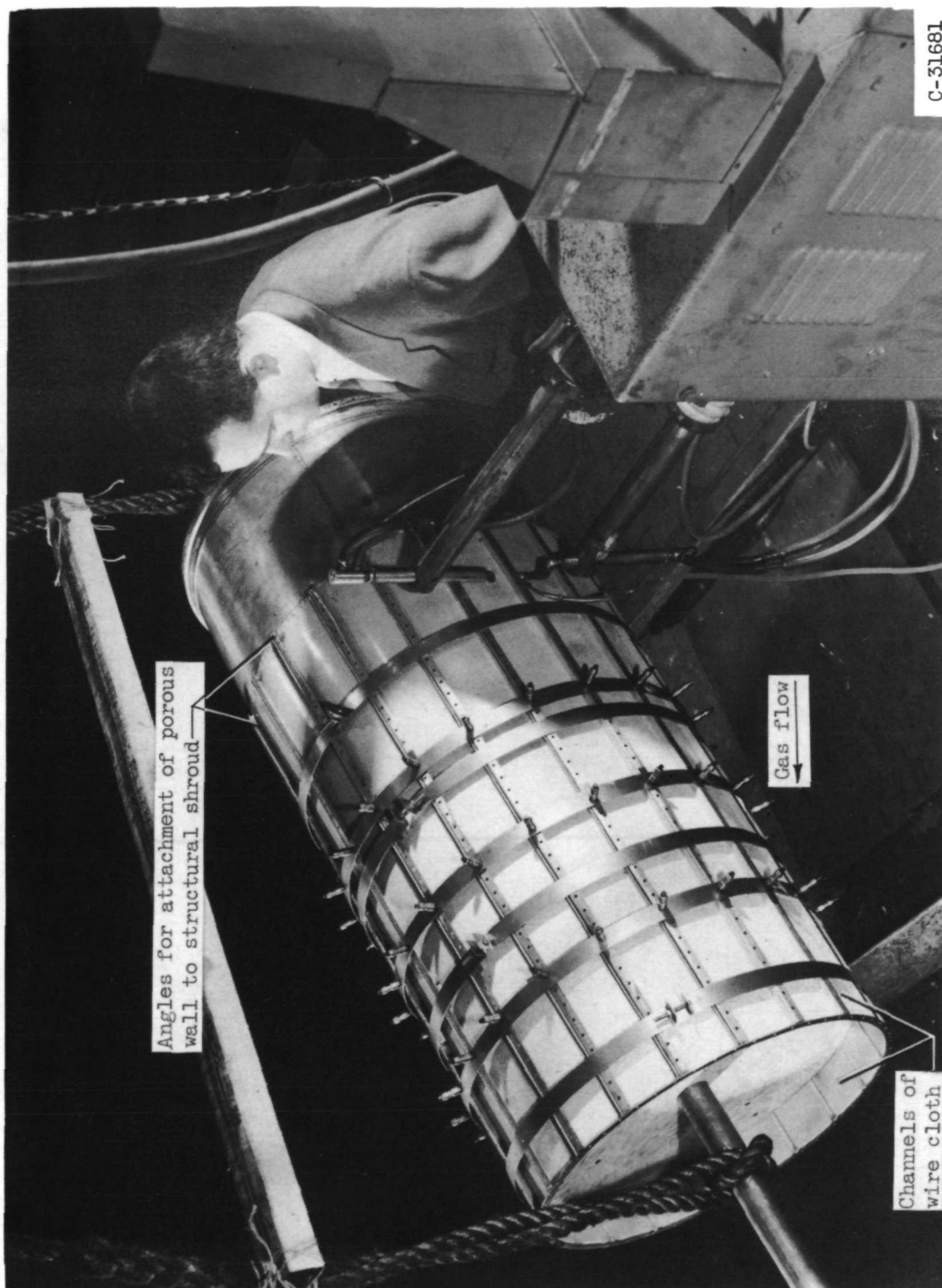
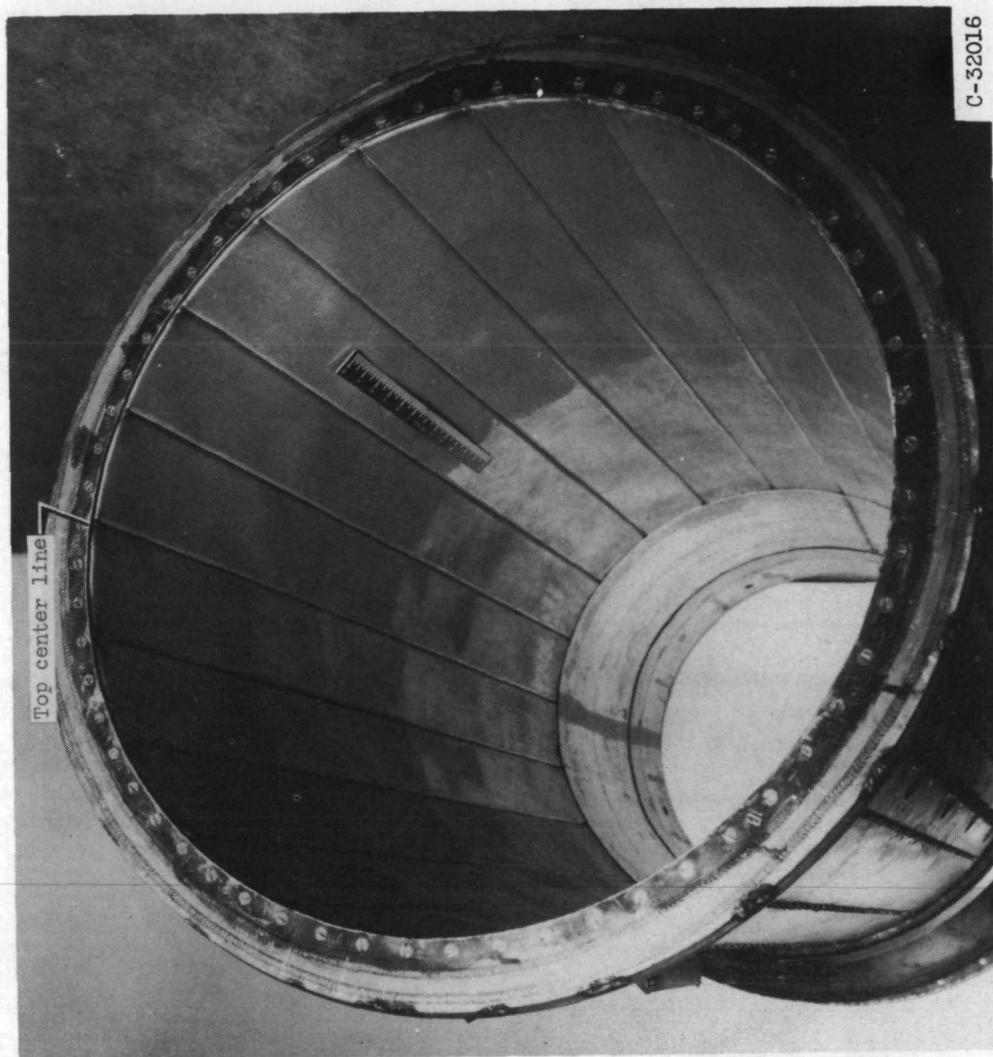


Figure 3. - Wire-cloth porous combustion-chamber wall before assembly of structural cooling shroud.



(a) Before cooling investigation.

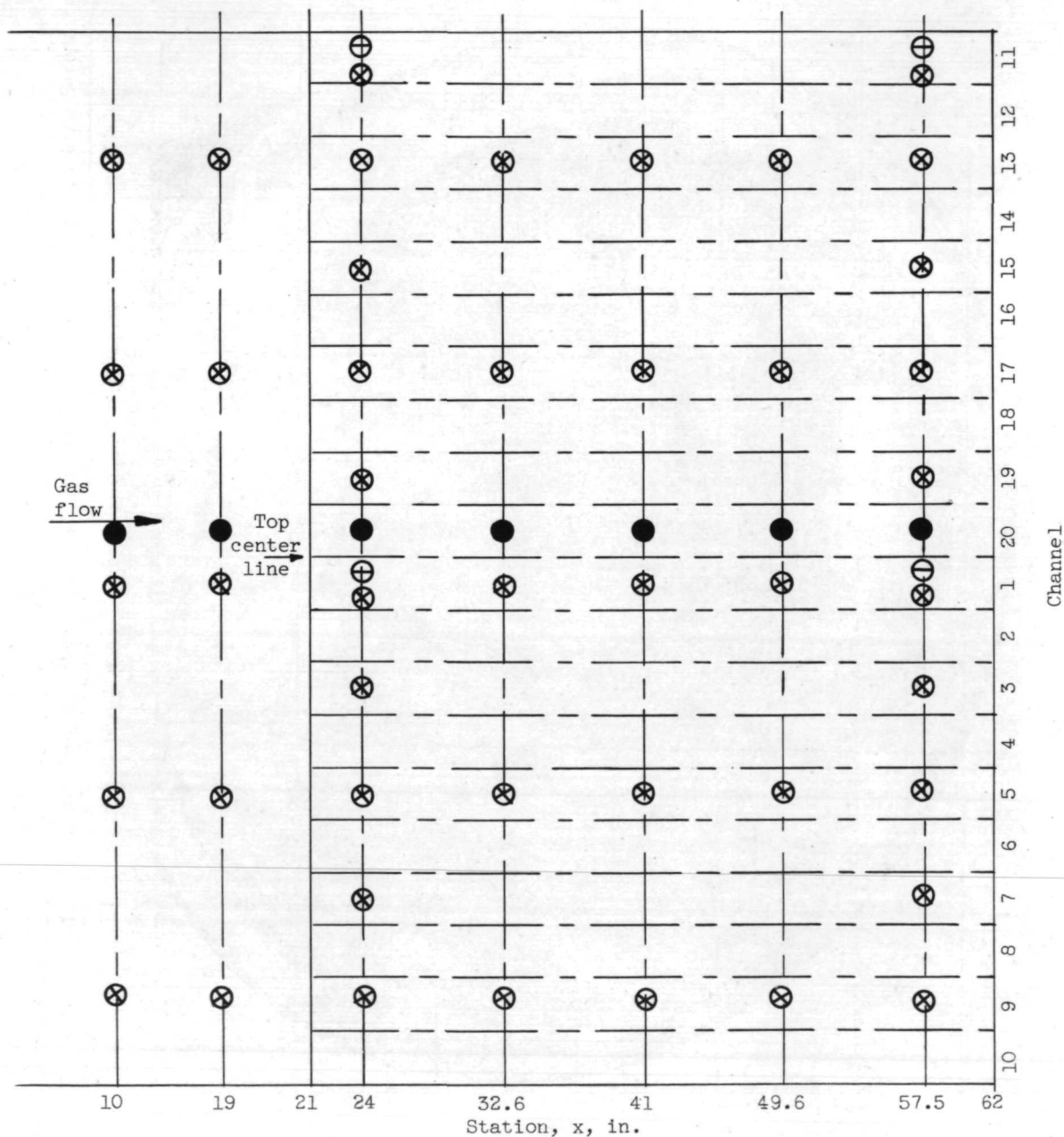
Figure 4. - Interior view of experimental transpiration-cooled afterburner with porous combustion-chamber wall fabricated from brazed and rolled wire cloth. Exhaust nozzle removed.



(b) After 4 hours 10 minutes of afterburning.

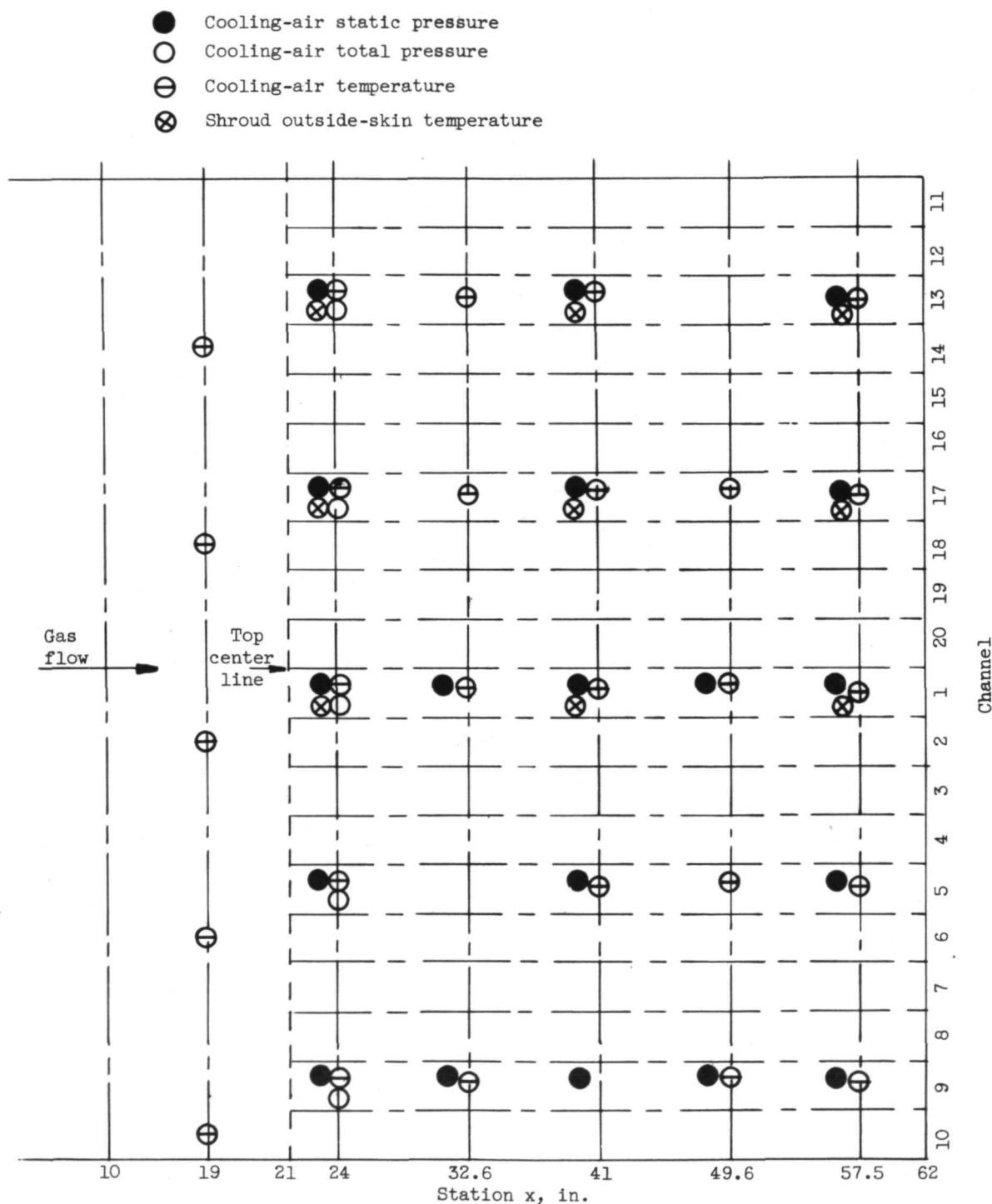
Figure 4. - Concluded. Interior view of experimental transpiration-cooled afterburner with porous combustion-chamber wall fabricated from brazed and rolled wire cloth. Exhaust nozzle removed.

- Combustion-gas static pressure
- ⊗ Wire-cloth or solid metal wall air-side temperature
- ⊖ Wire-cloth gas-side temperature



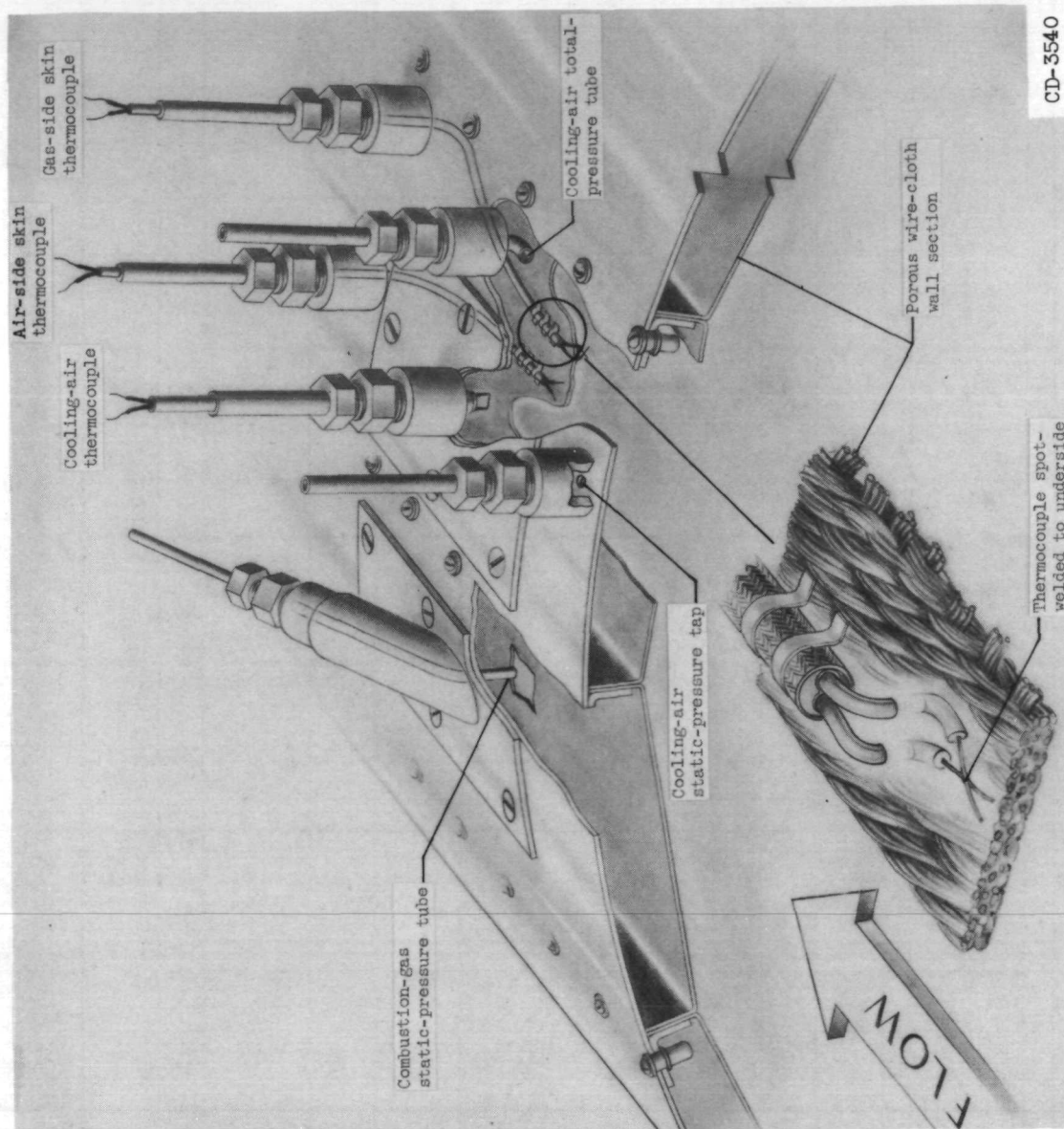
(a) Wire-cloth and combustion-gas instrumentation.

Figure 5. - Schematic development showing locations of temperature and pressure instrumentation on wire-cloth porous-wall afterburner.



(b) Shroud and cooling-air instrumentation.

Figure 5. - Concluded. Schematic development showing locations of temperature and pressure instrumentation on wire-cloth porous-wall afterburner.



CD-3540

Figure 6. - Typical group of instruments on porous-wall section of wire-cloth afterburner.

5295

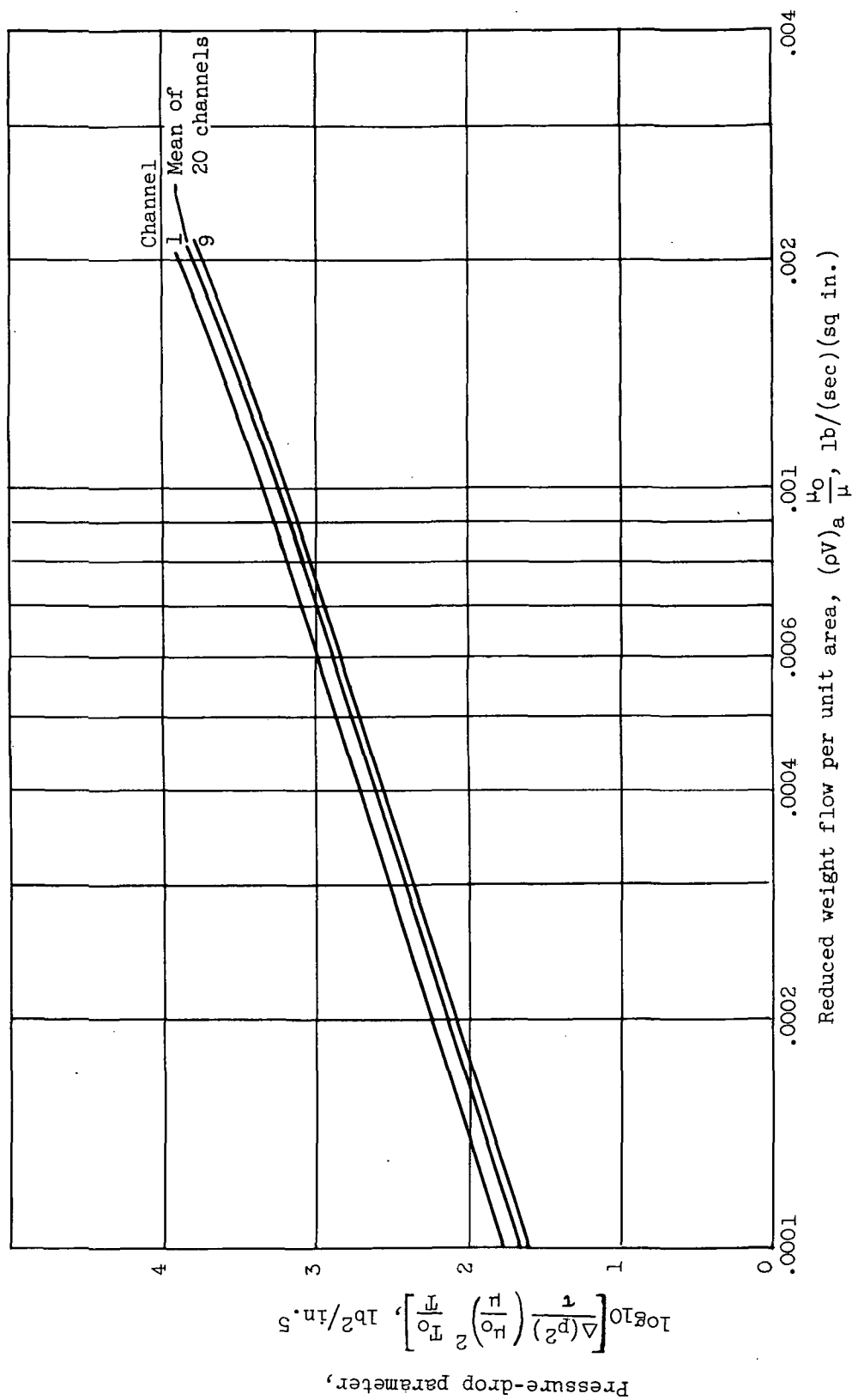
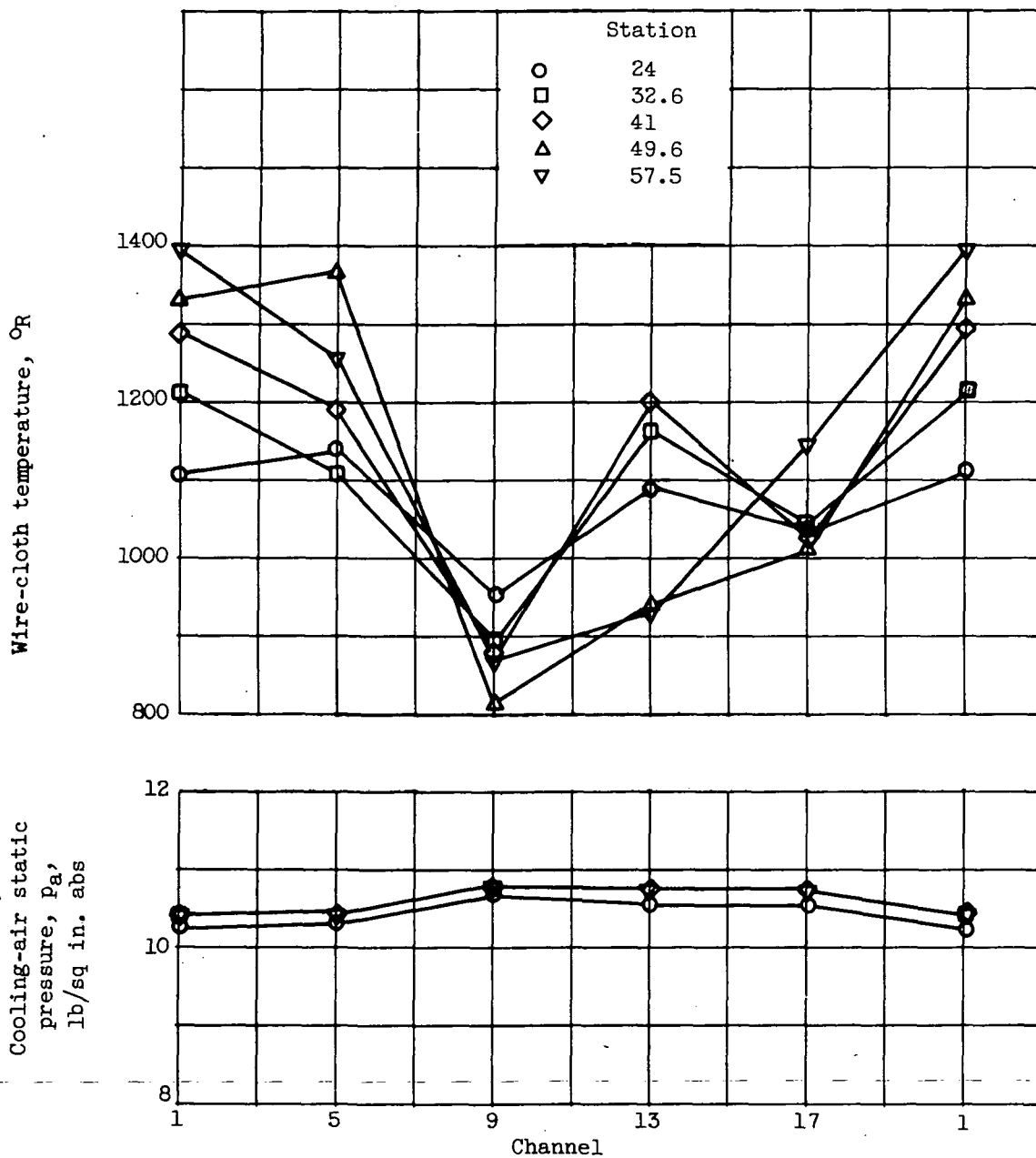
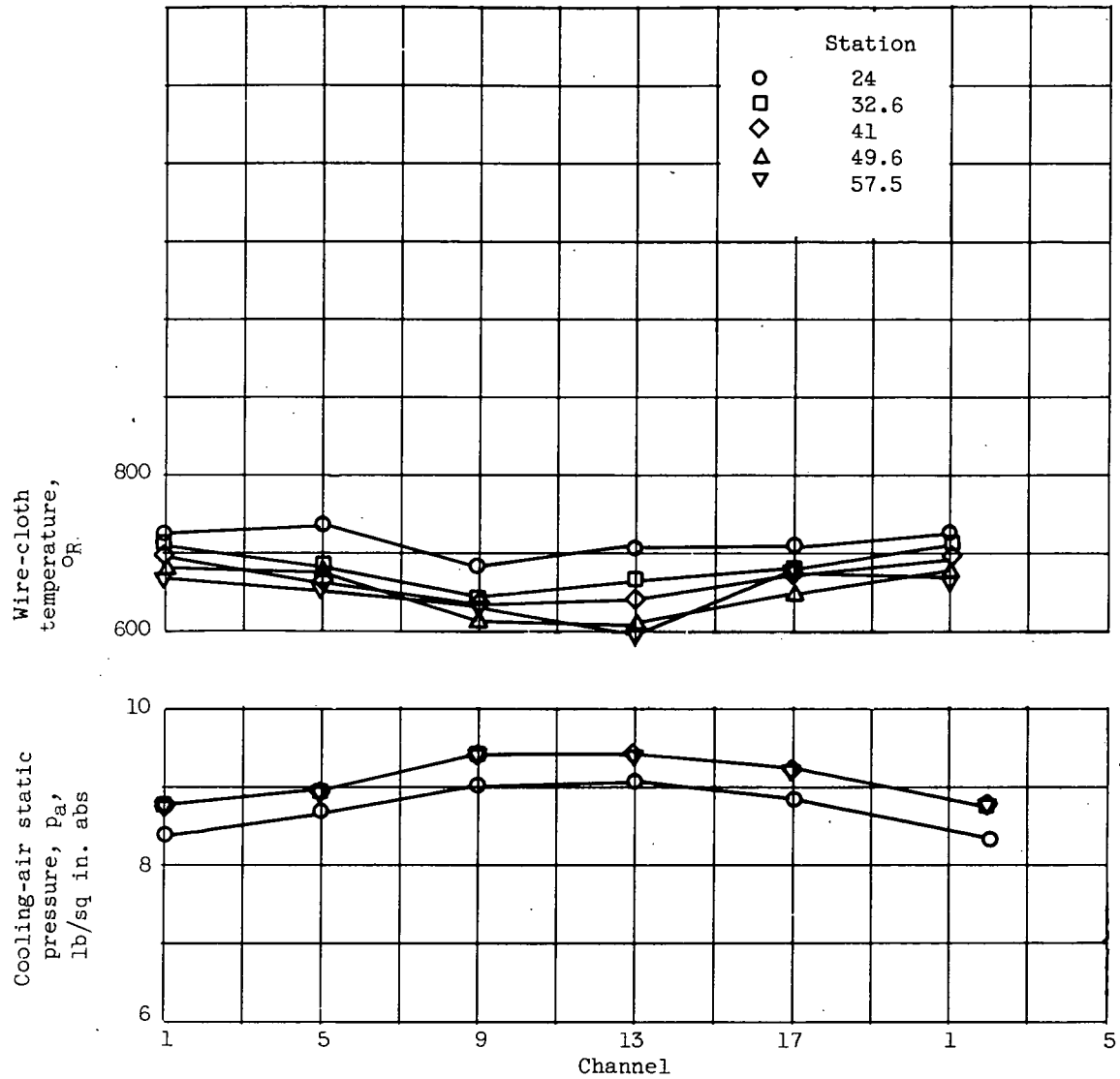


Figure 7. - Air-flow - pressure-drop calibration of wire cloth used in porous-wall section of afterburner.



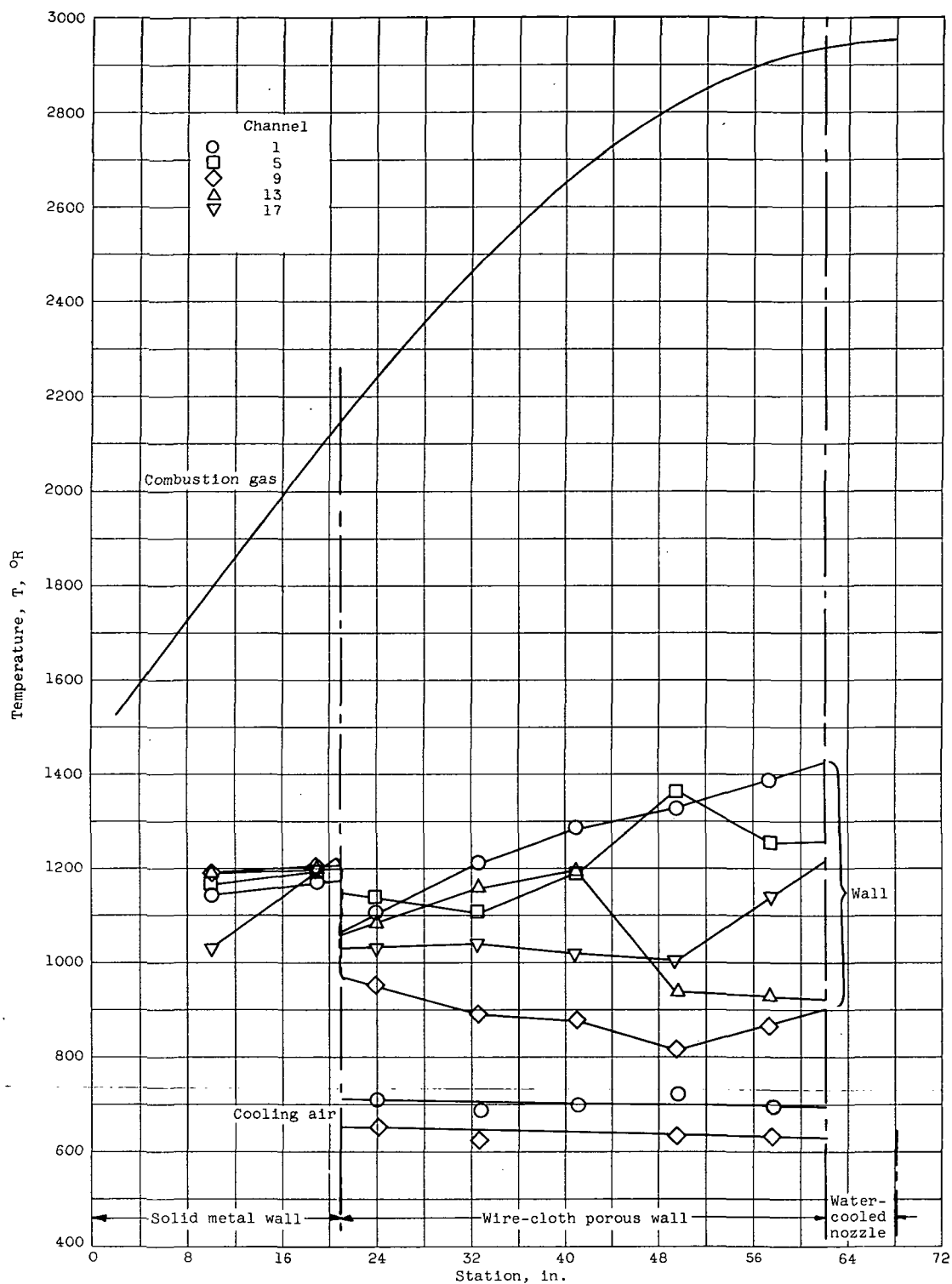
(a) Afterburning. Exhaust-gas temperature, 2954°R ; total flow ratio, 0.0716.

Figure 8. - Typical circumferential profiles of wire-cloth temperature and cooling-air static pressure. Altitude, 35,000 feet; flight Mach number, 1.0.



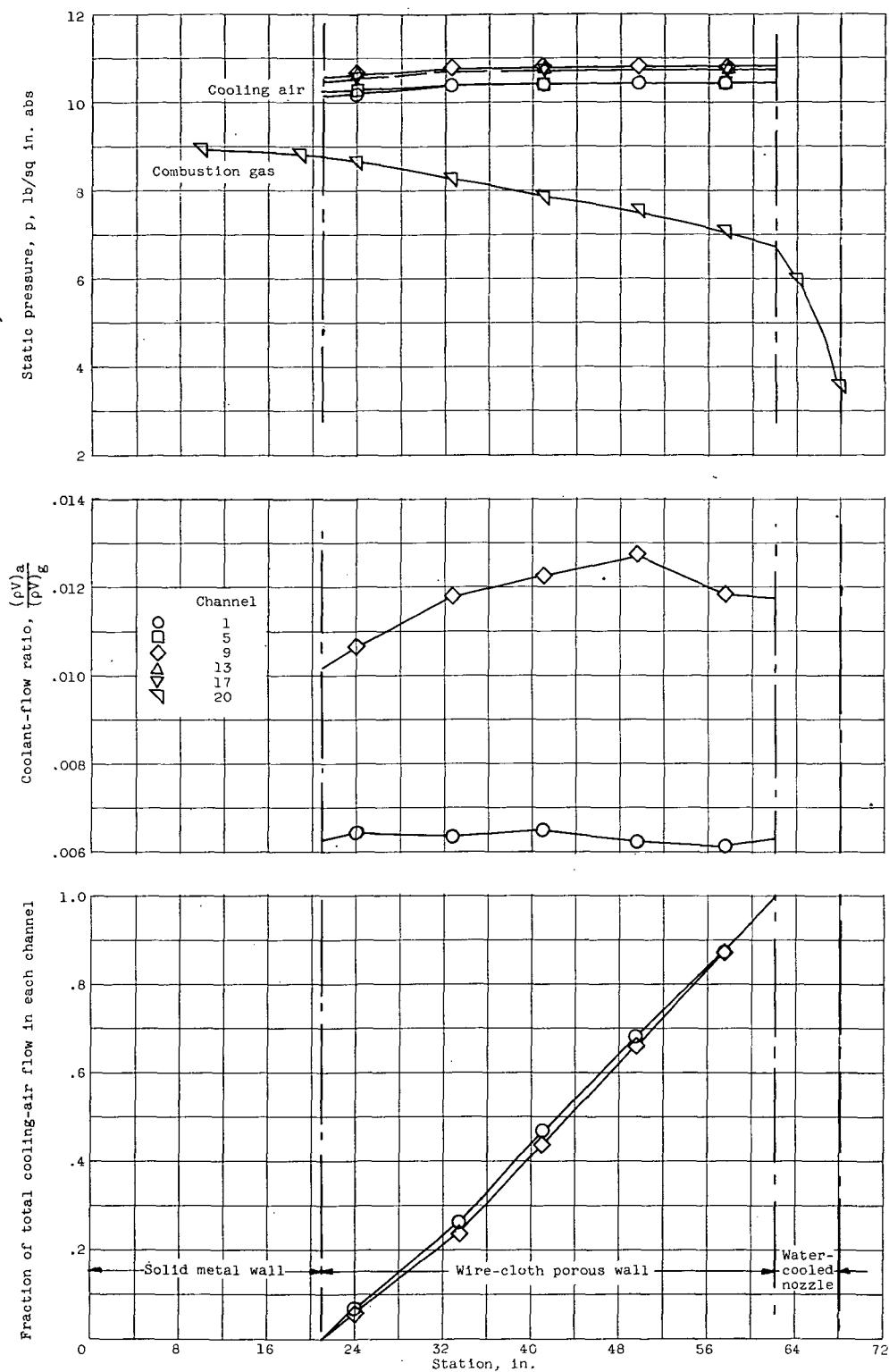
(b) Nonafterburning. Exhaust-gas temperature, 1249° R; total flow ratio, 0.0951.

Figure 8. - Concluded. Typical circumferential profiles of wire-cloth temperature and cooling-air static pressure. Altitude, 35,000 feet; flight Mach number, 1.0.



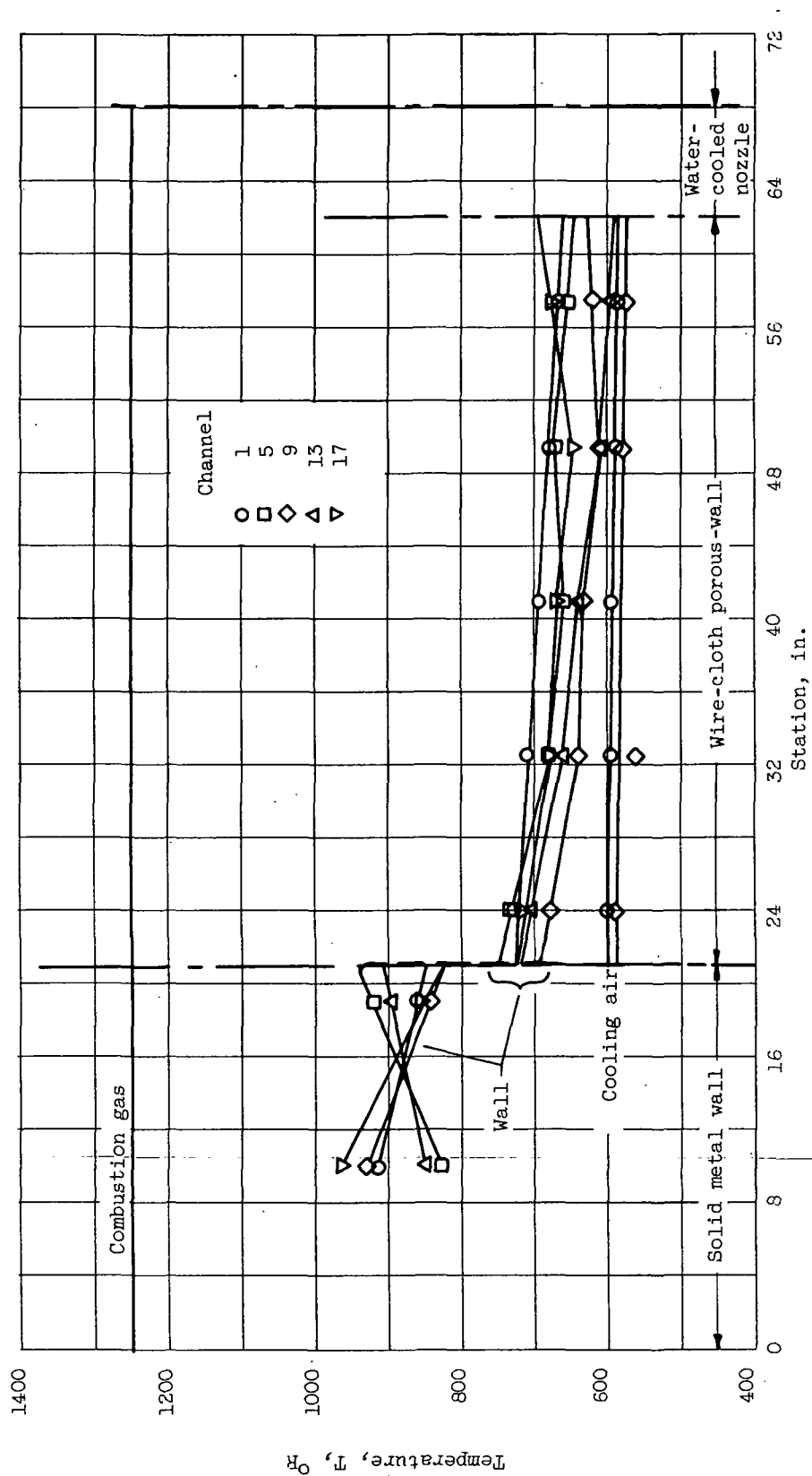
(a) Afterburning temperature profiles. Exhaust-gas temperature, 2954°R ; total flow ratio, 0.0716.

Figure 9. - Typical longitudinal profiles for wire-cloth afterburner. Altitude, 35,000 feet; flight Mach number, 1.0.



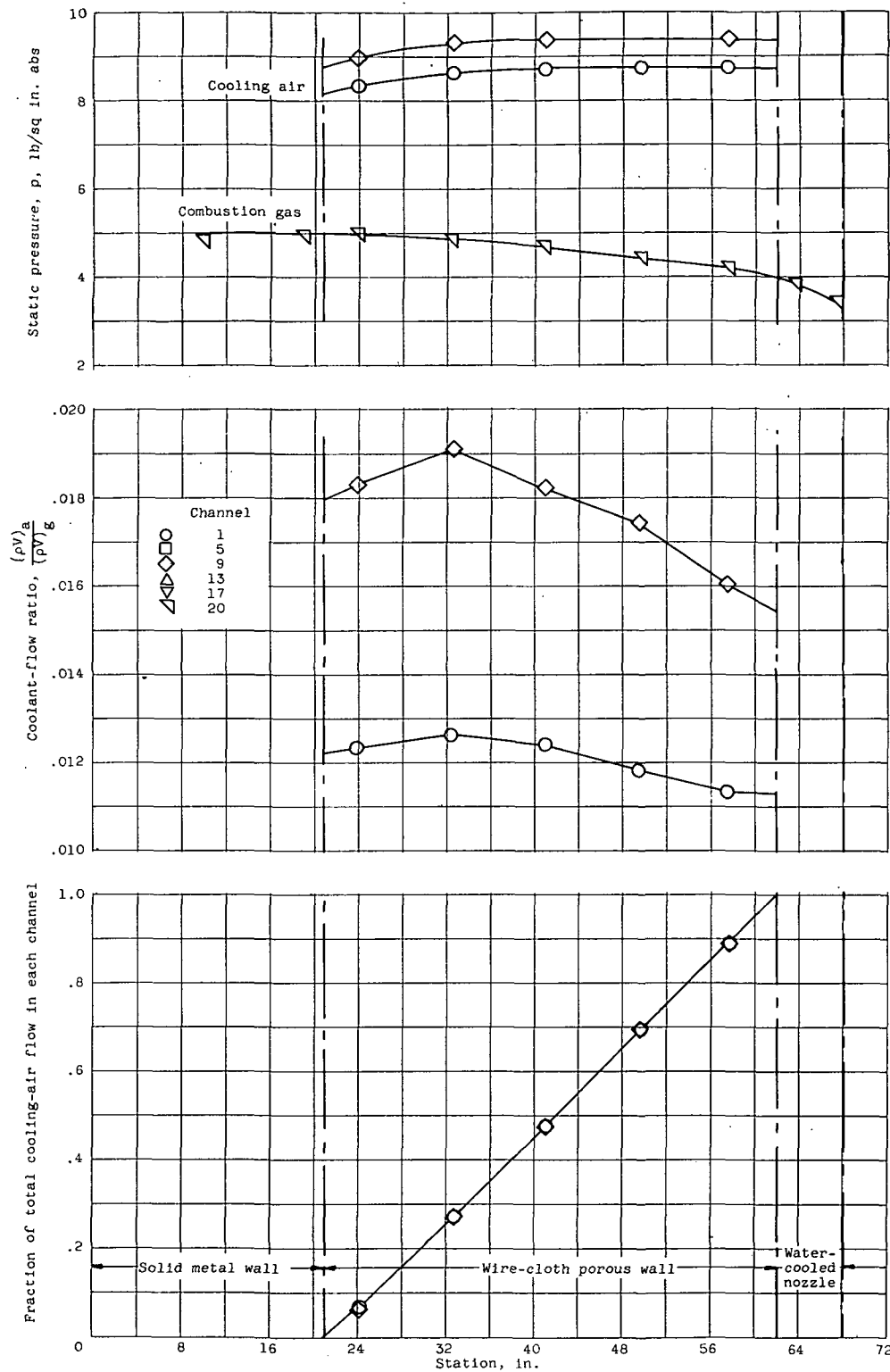
(b) Afterburning static-pressure and coolant-flow profiles. Exhaust-gas temperature, 2954° R; total flow ratio, 0.0716.

Figure 9. - Continued. Typical longitudinal profiles for wire-cloth afterburner. Altitude, 35,000 feet; flight Mach number, 1.0.



(c) Nonafterburning temperature profiles. Exhaust-gas temperature, $1249^{\circ}R$; total flow ratio, 0.0951.

Figure 9. - Continued. Typical longitudinal profiles for wire-cloth afterburner. Altitude, 35,000 feet; flight Mach number, 1.0.



(d) Nonafterburning static-pressure and coolant-flow profiles. Exhaust-gas temperature, 1249° R; total flow ratio, 0.0951.

Figure 9. - Concluded. Typical longitudinal profiles for wire-cloth afterburner. Altitude, 35,000 feet; flight Mach number, 1.0.

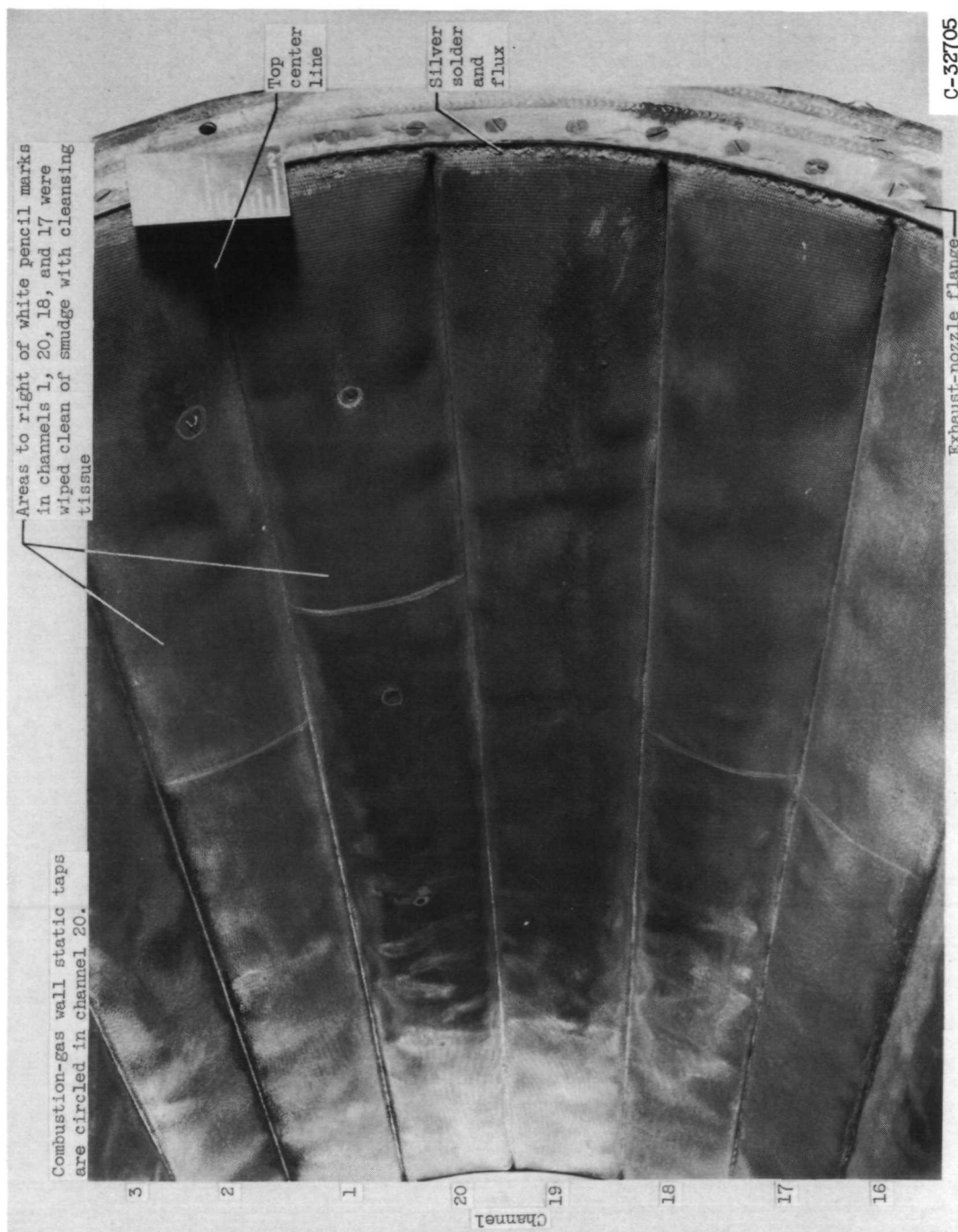
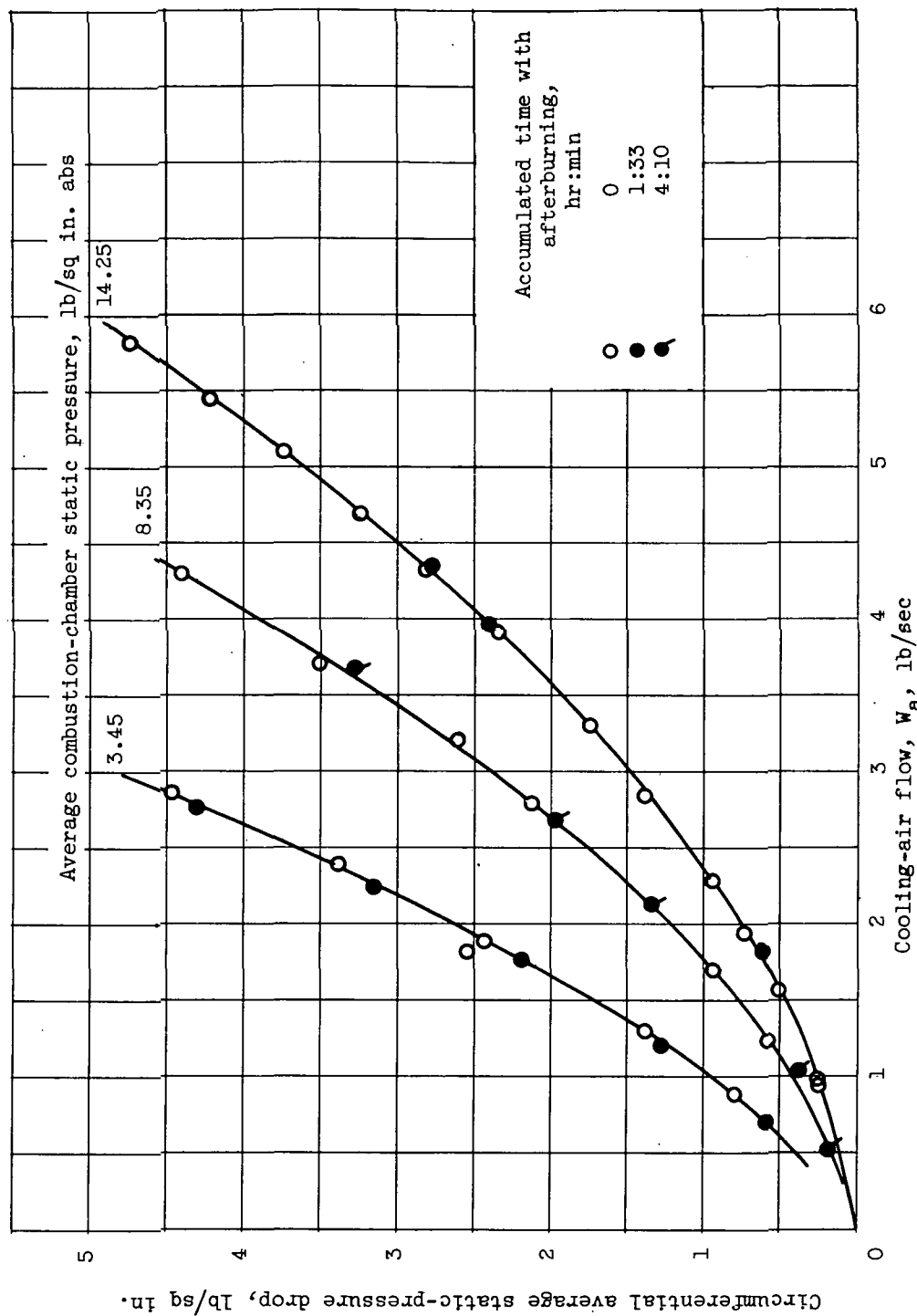
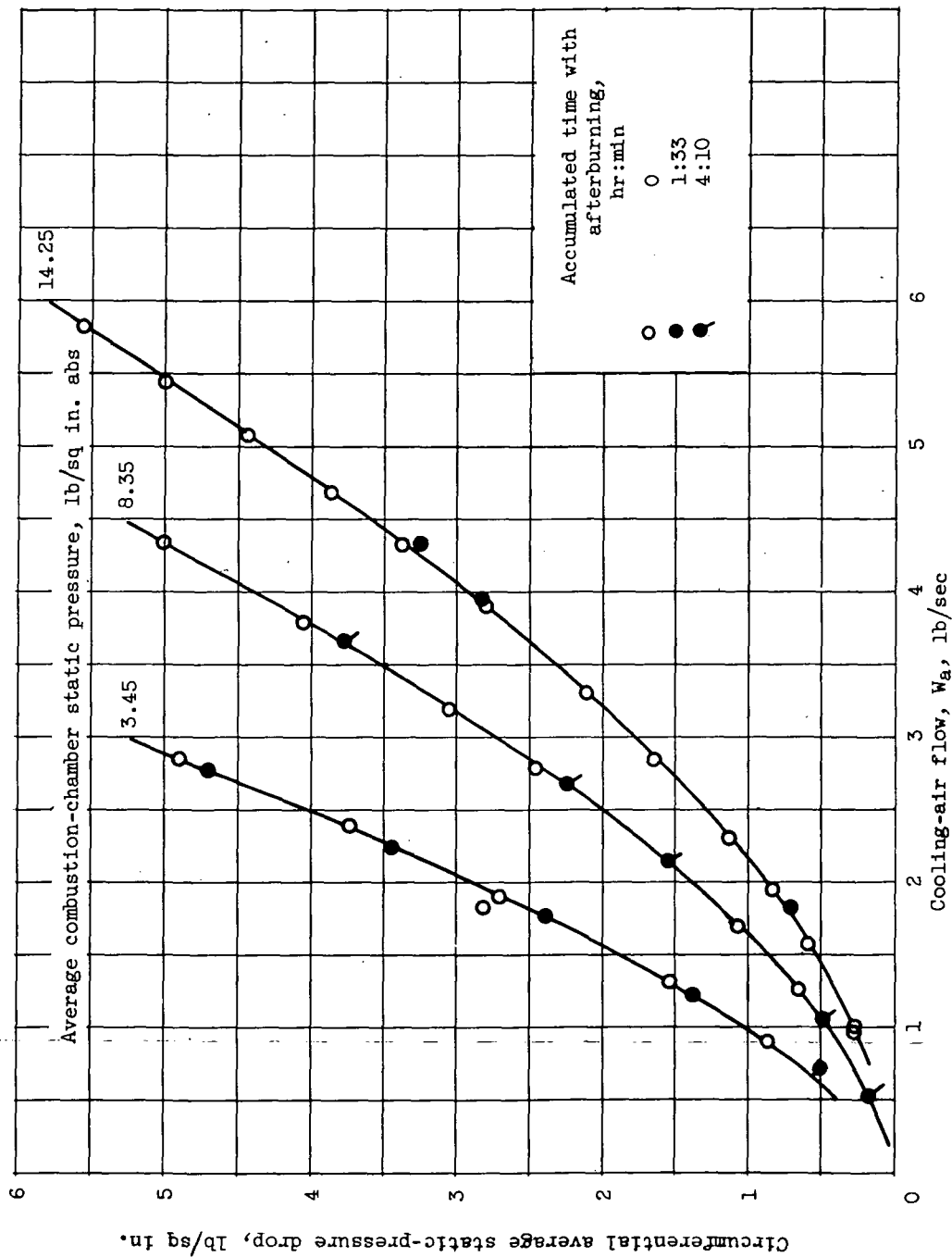


Figure 10. - Appearance of greasy smudge on wire cloth after 4 hours 10 minutes of afterburning.



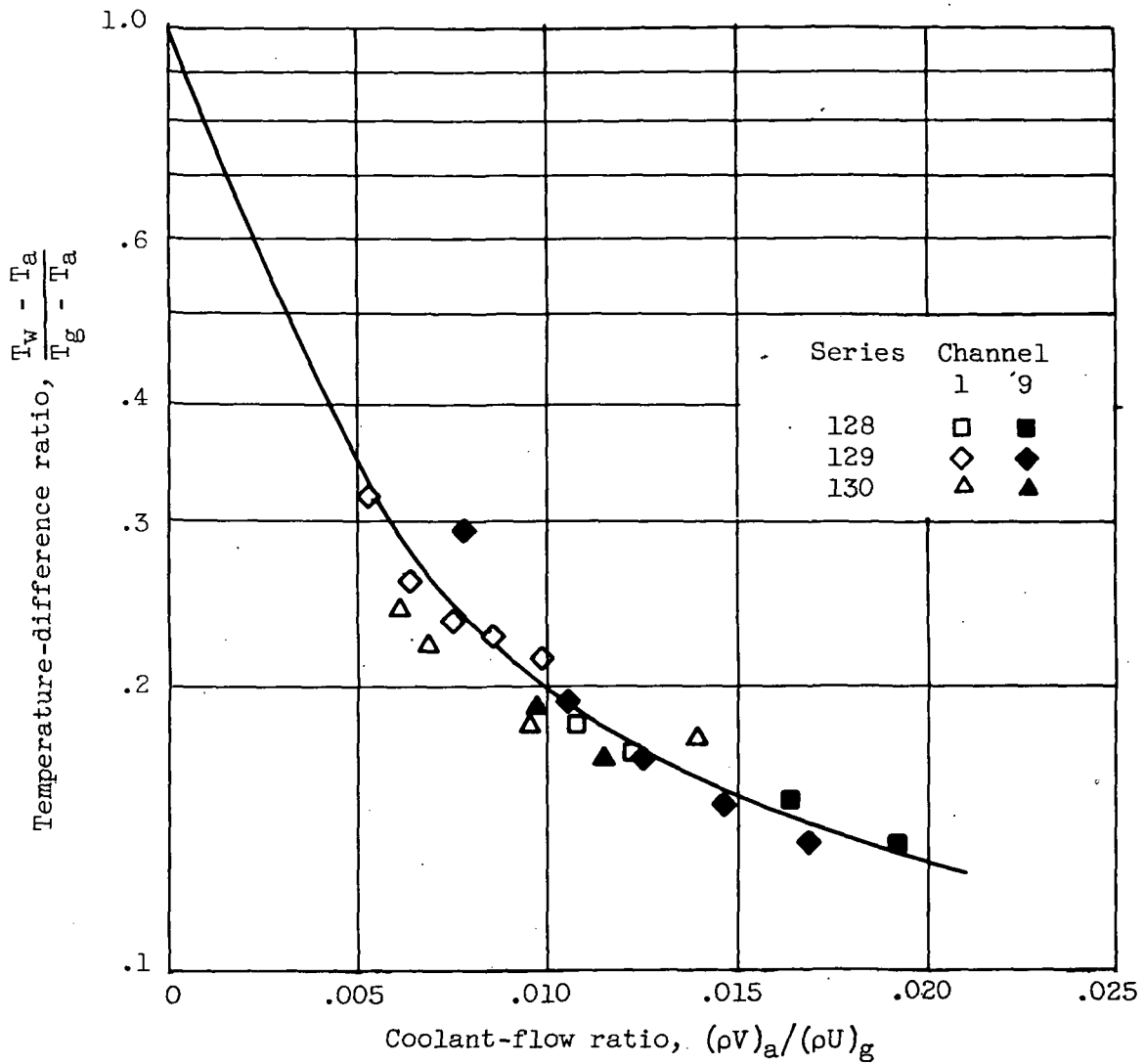
(a) Station 24.

Figure 11. - Variation of circumferential average pressure drop across wire cloth with total measured cooling-air flow.



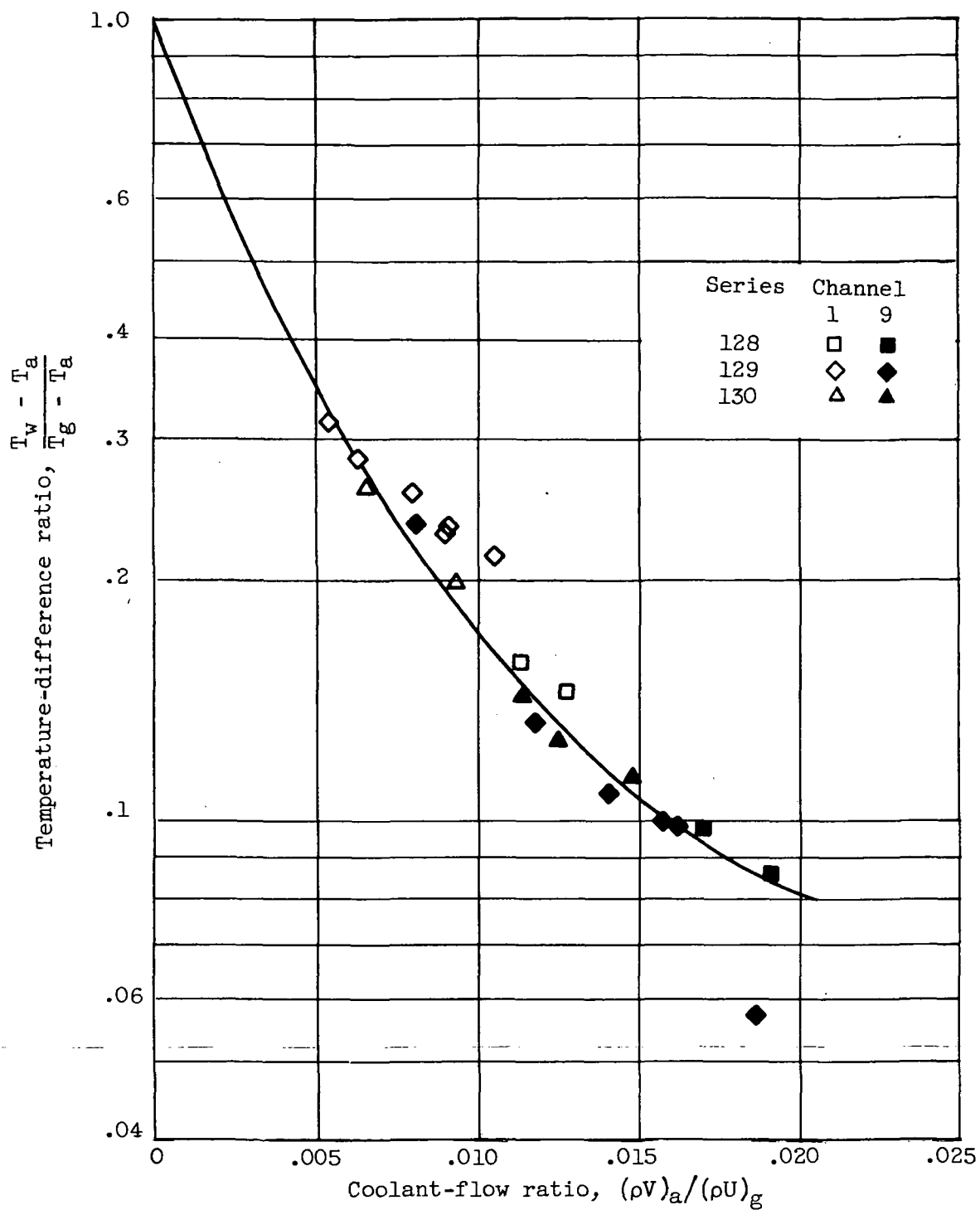
(b) Station 57.5.

Figure 11.1. - Concluded. Variation of circumferential average pressure drop across wire cloth with total measured cooling-air flow.



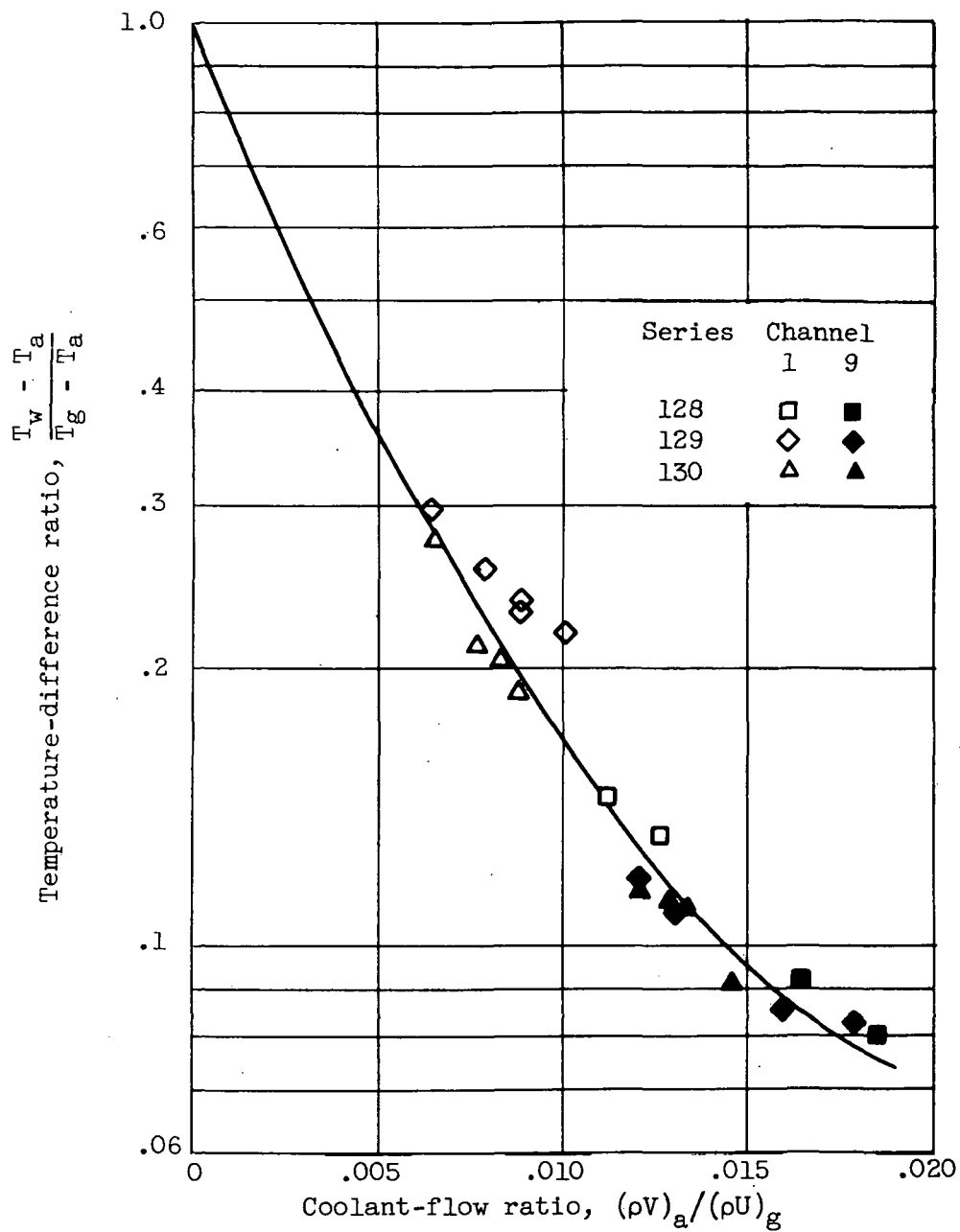
(a) Reynolds number, approximately 75,000.

Figure 12. - Correlation of afterburning cooling data for wire-cloth afterburner.



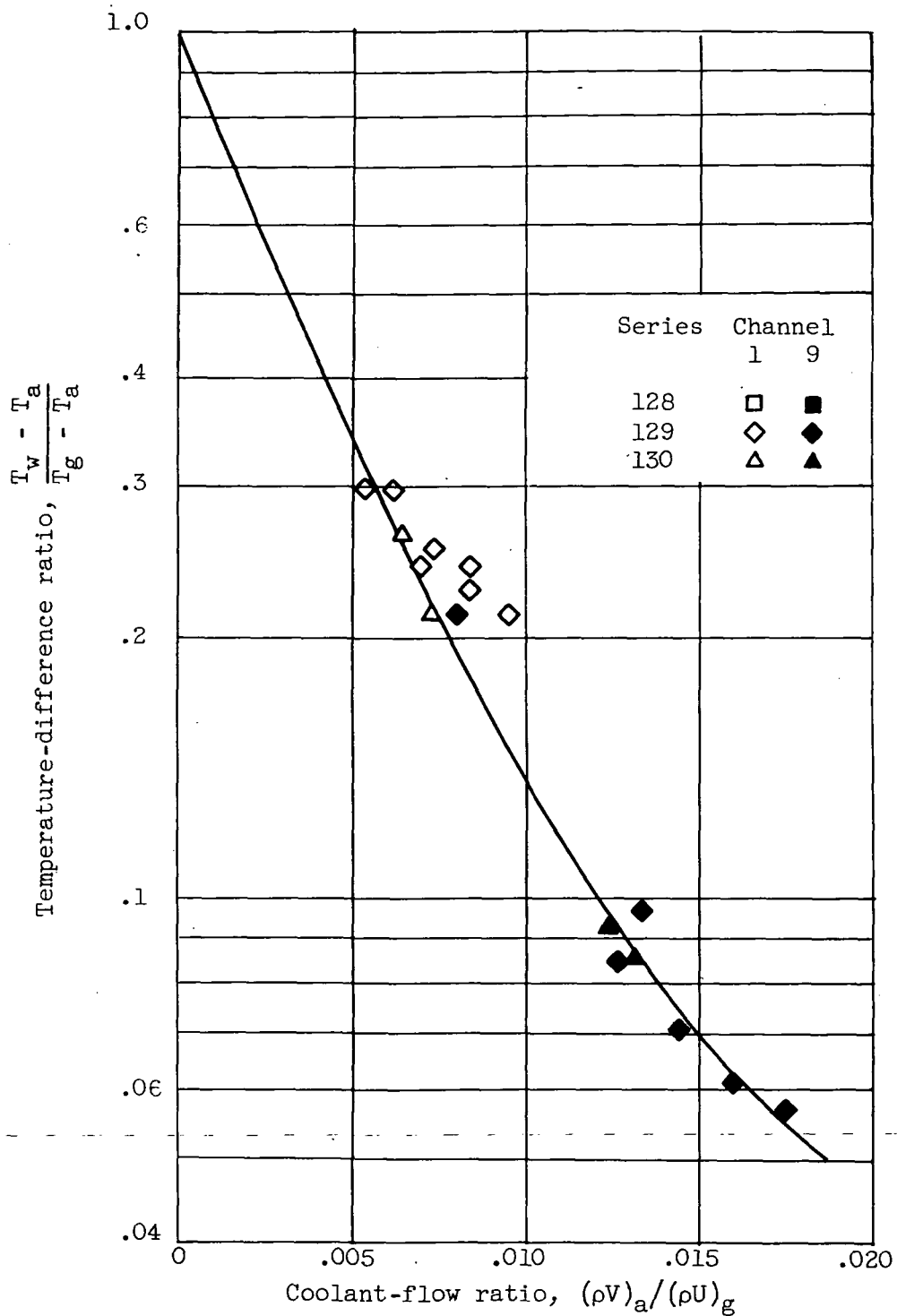
(b) Reynolds number, approximately 300,000.

Figure 12. - Continued. Correlation of afterburning cooling data for wire-cloth afterburner.



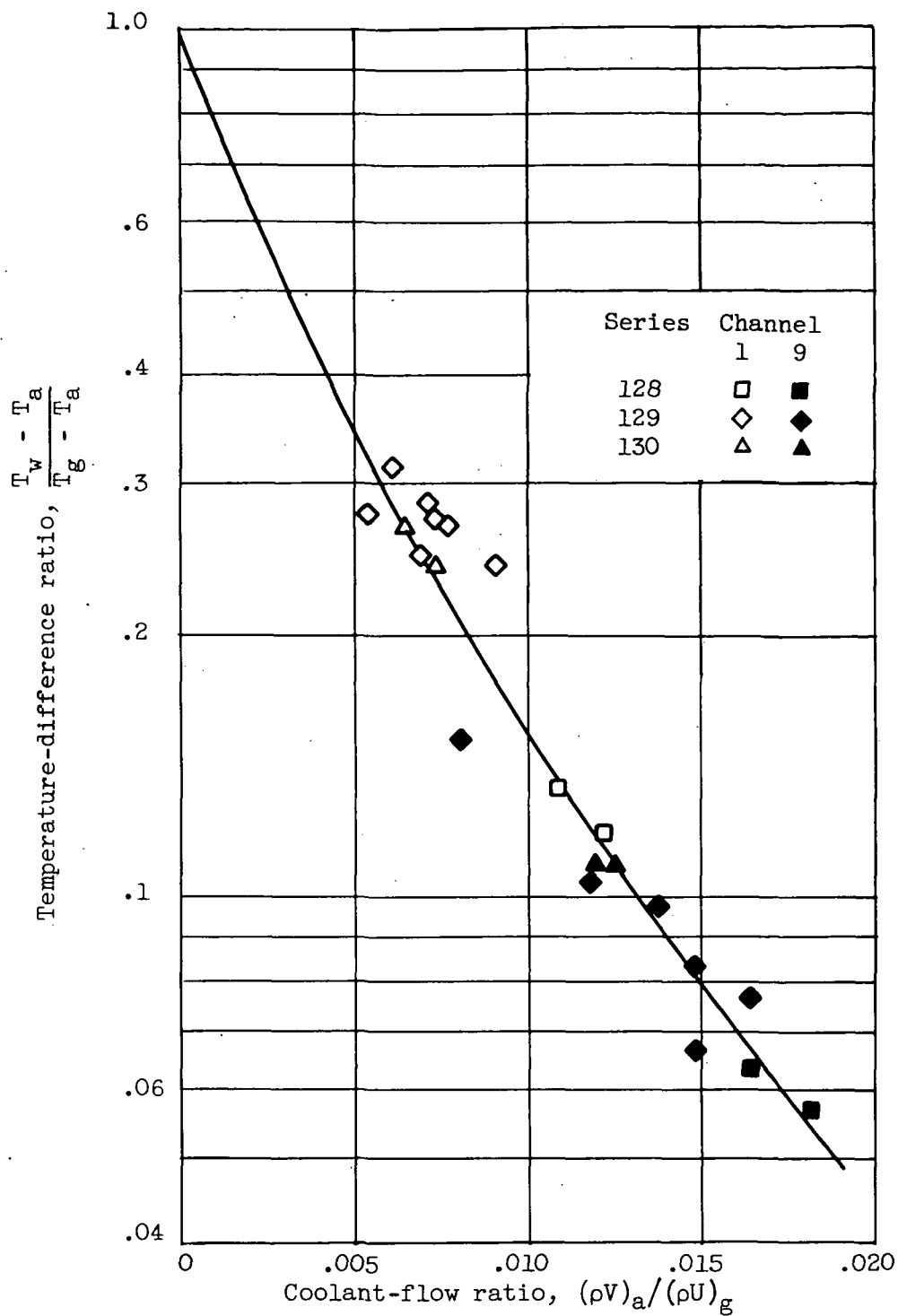
(c) Reynolds number, approximately 500,000.

Figure 12. - Continued. Correlation of after-burning cooling data for wire-cloth afterburner.



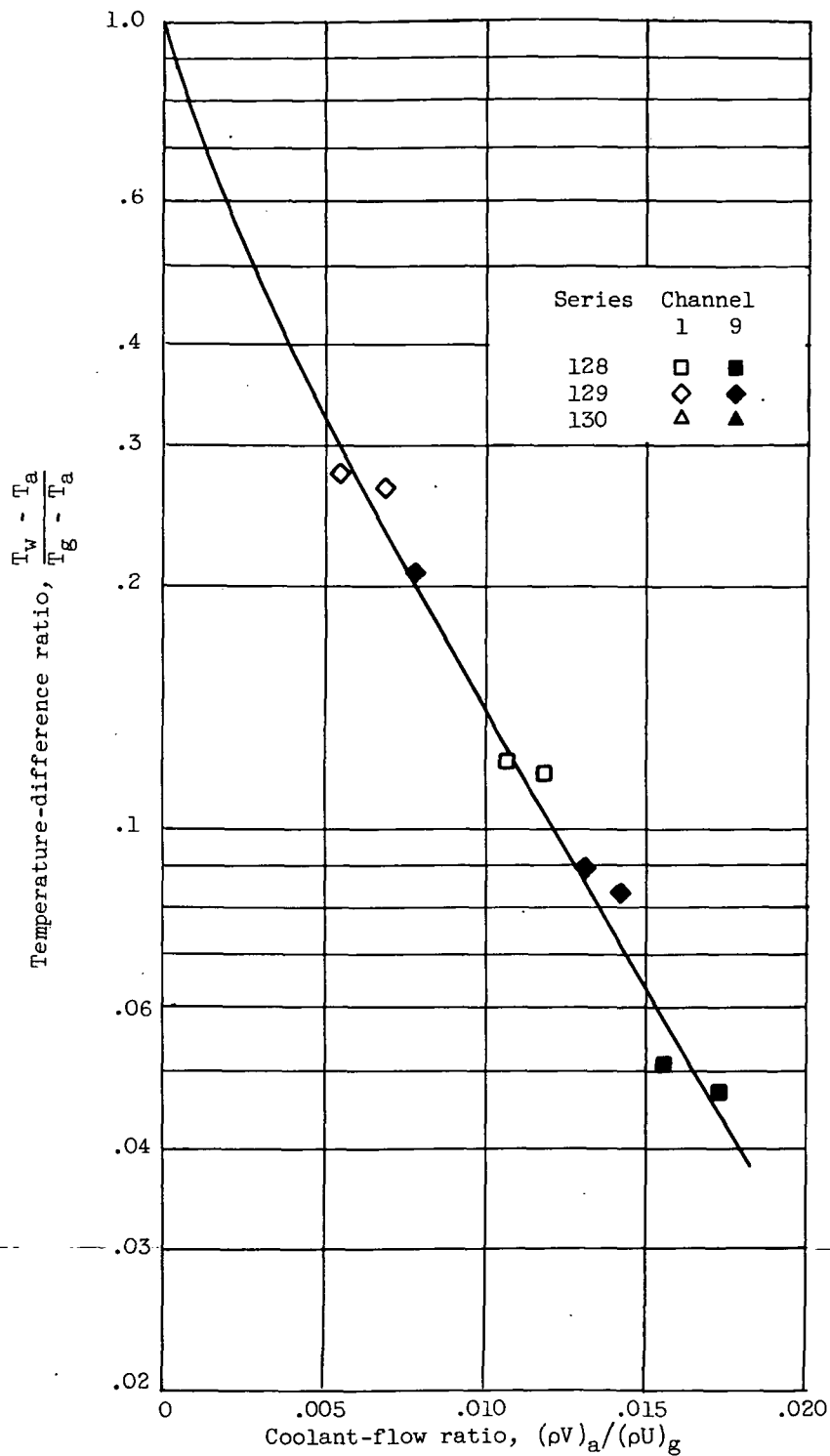
(d) Reynolds number, approximately 800,000.

Figure 12. - Continued. Correlation of after-burning cooling data for wire-cloth afterburner.



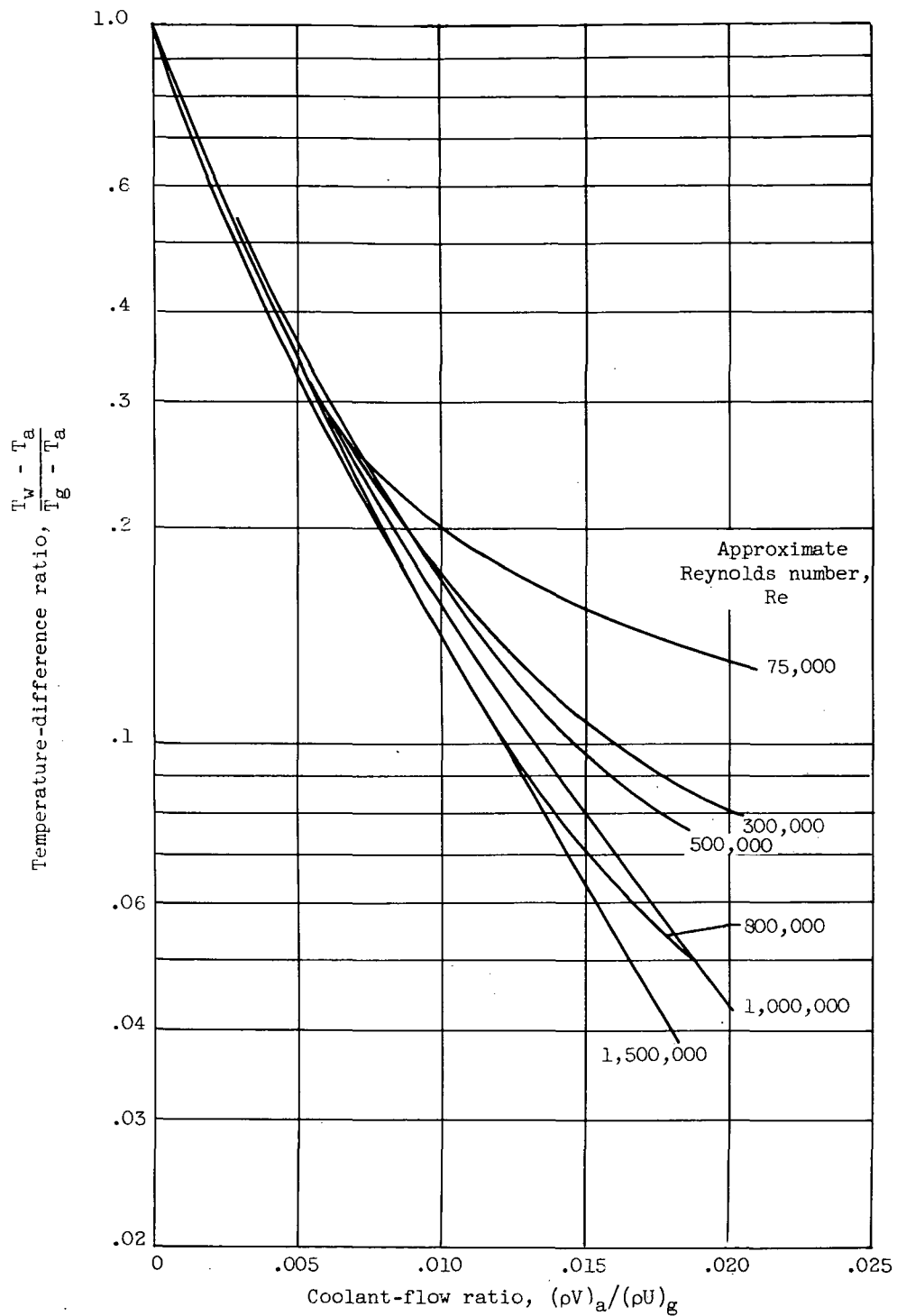
(e) Reynolds number, approximately 1,000,000.

Figure 12. - Continued. Correlation of after-burning cooling data for wire-cloth afterburner.



(f) Reynolds number, approximately 1,500,000.

Figure 12. - Continued. Correlation of after-burning cooling data for wire-cloth afterburner.



(g) Mean curves for approximate Reynolds numbers of 75,000 to 1,500,000.

Figure 12. - Concluded. Correlation of afterburning cooling data for wire-cloth afterburner.

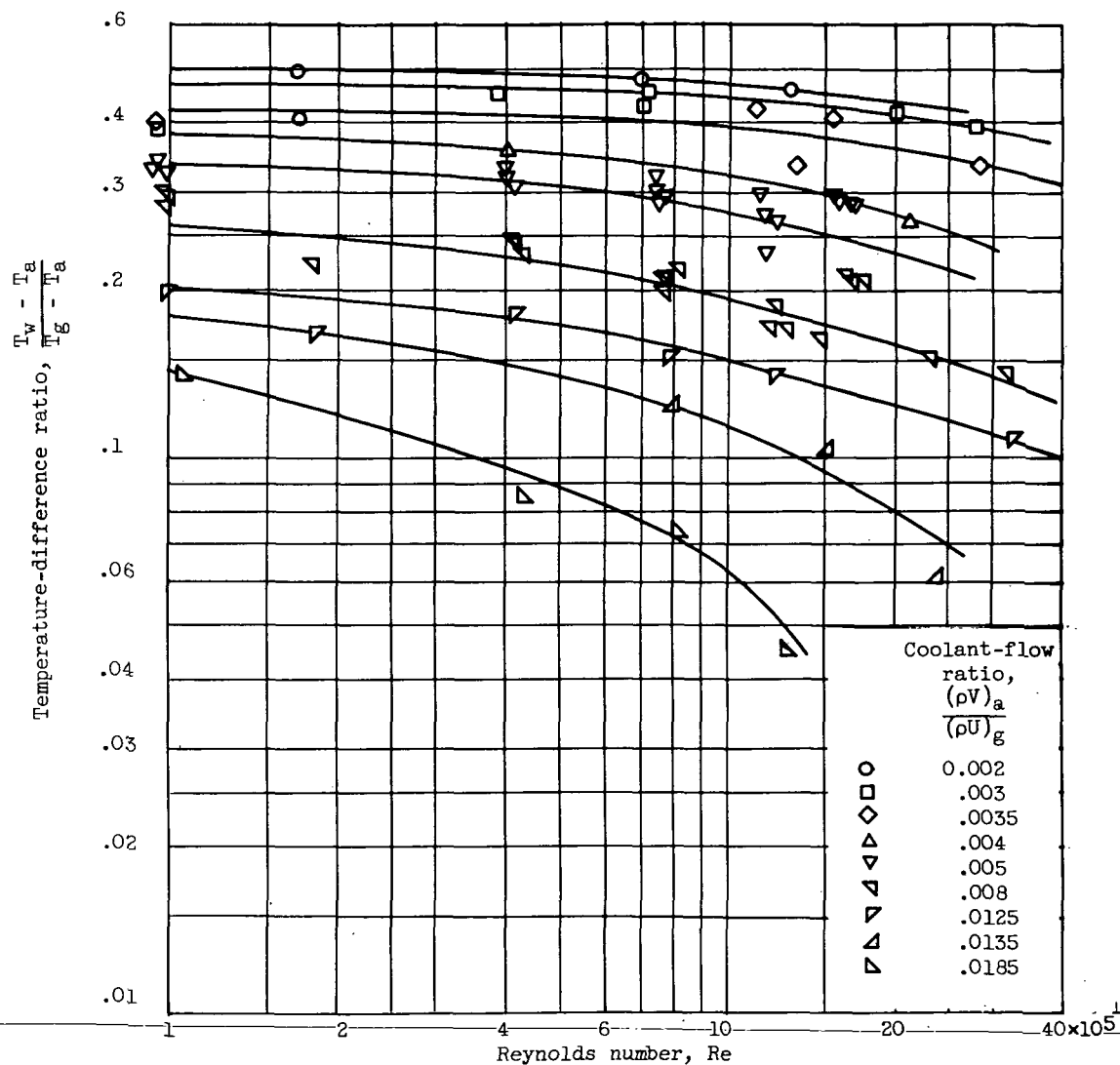


Figure 13. - Variation of temperature-difference ratio with Reynolds number for nonafterburning cooling data.

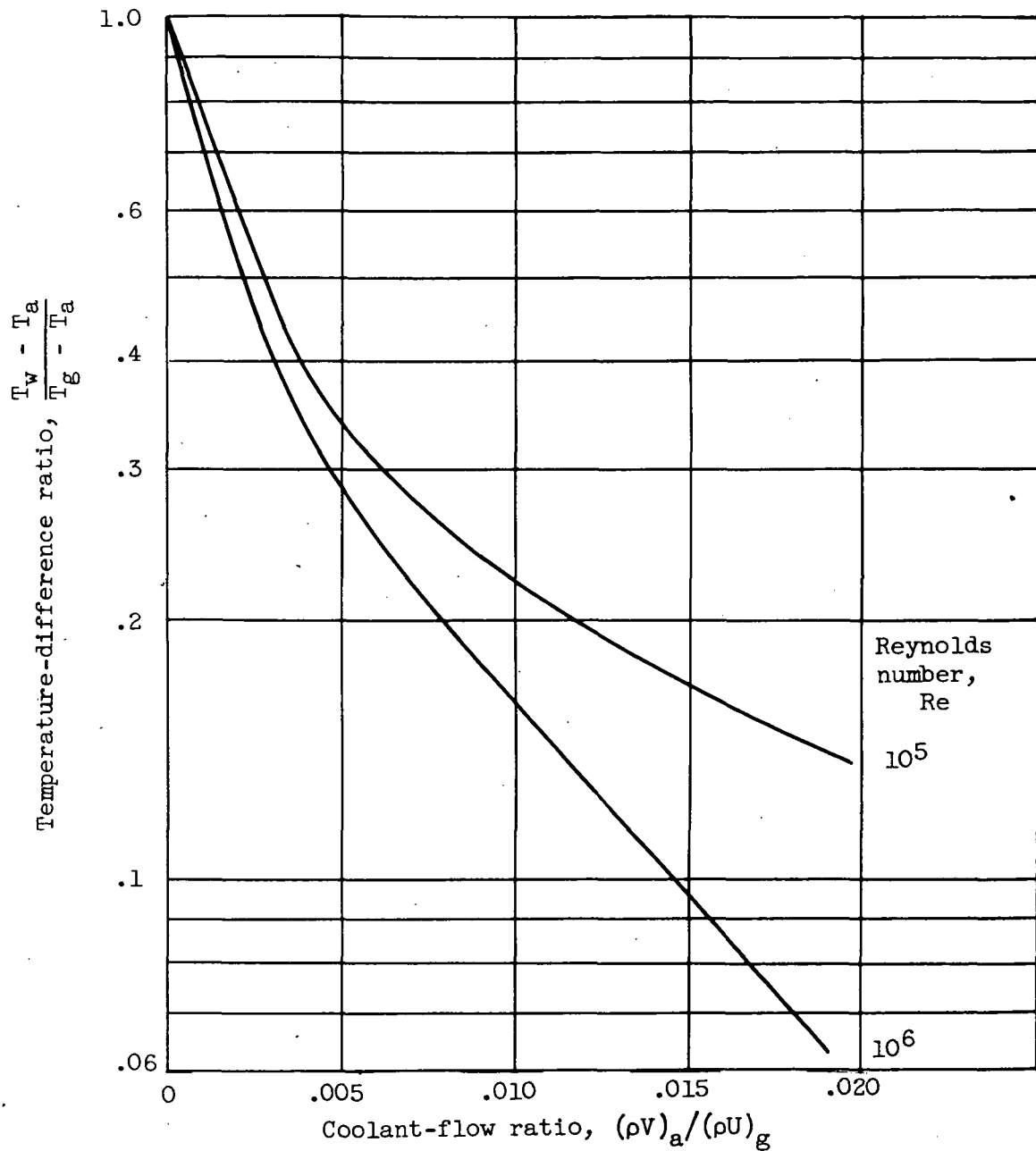


Figure 14. - Correlation of nonafterburning cooling data for wire-cloth afterburner.

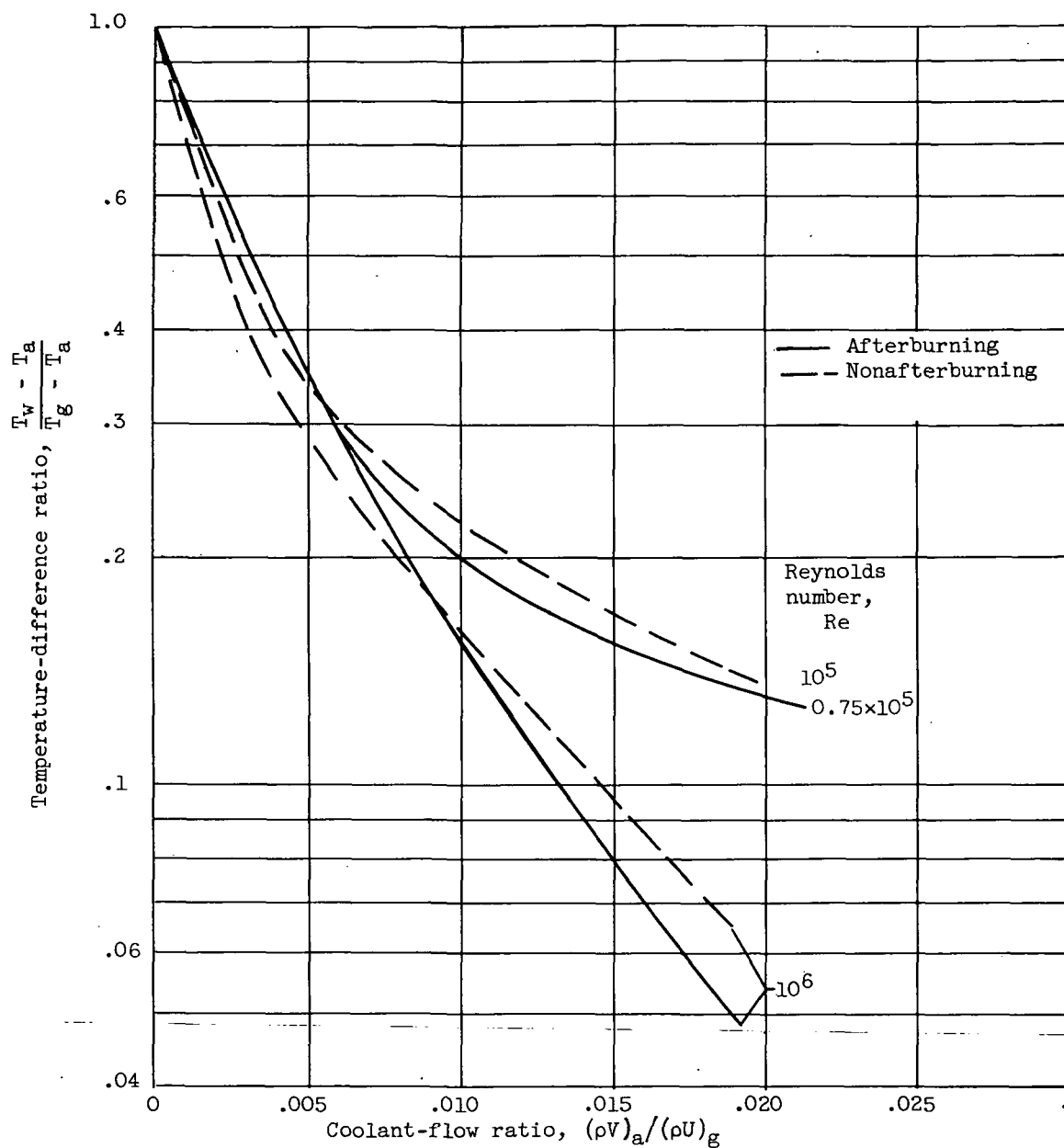


Figure 15. - Comparison of cooling correlations for afterburning and nonafterburning for wire-cloth afterburner.

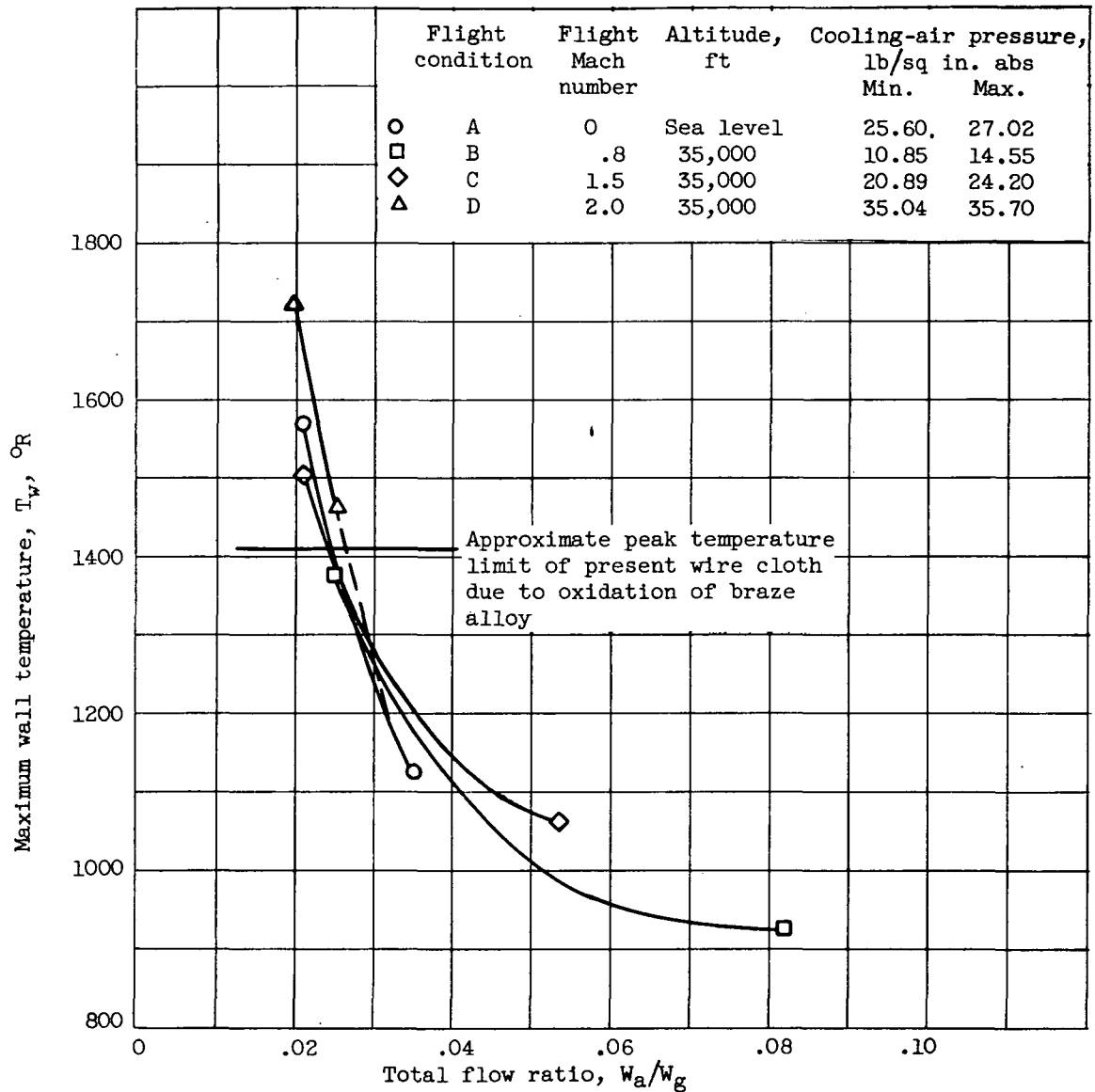


Figure 16. - Cooling characteristics of transpiration-cooled wire-cloth afterburner having uniform permeability distribution. Exhaust-gas temperature, 3700° R.

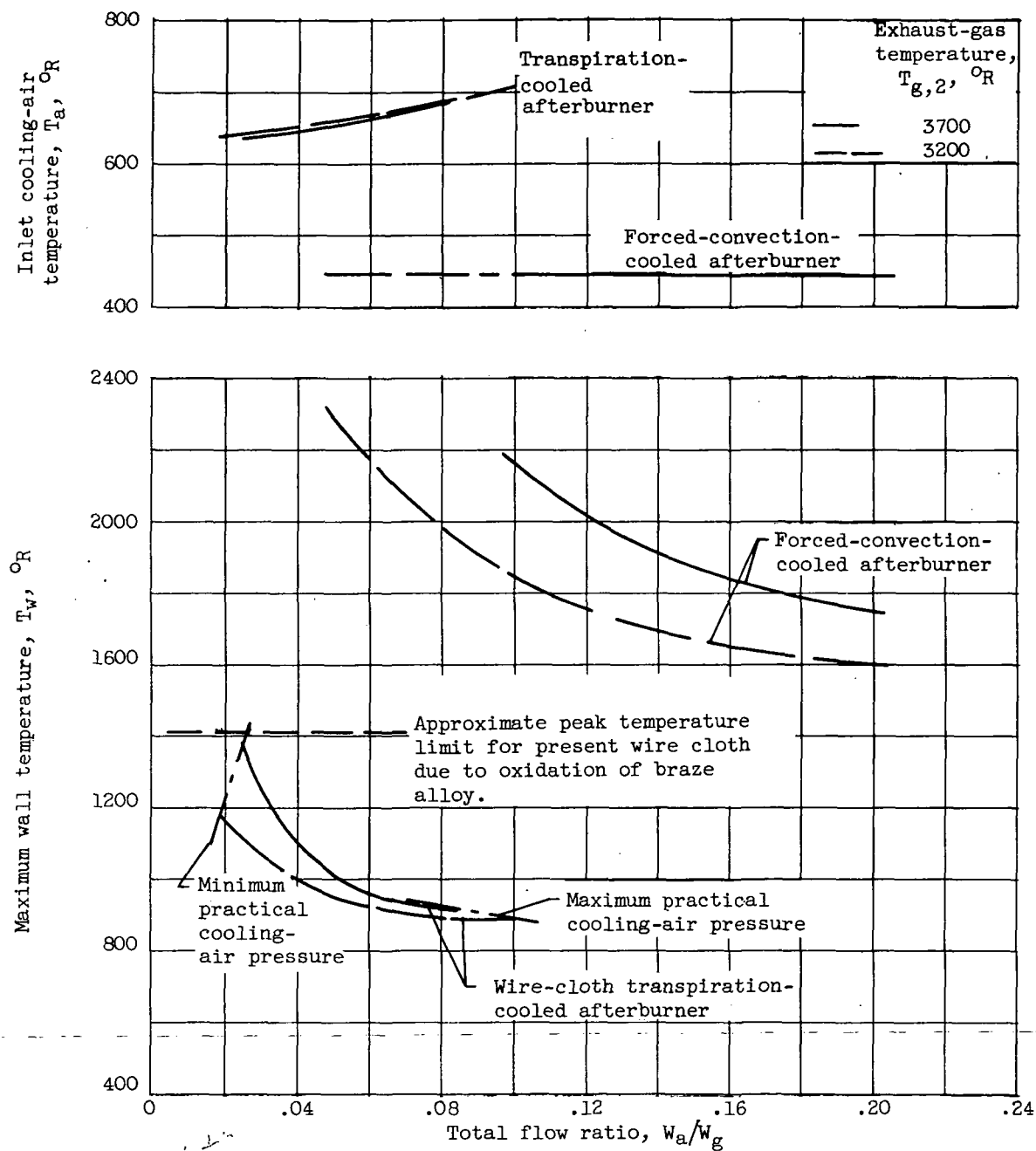


Figure 17. - Comparison of forced-convection and transpiration cooling applied to same afterburner. Uniform-permeability porous wall. Flight Mach number, 0.8; altitude 35,000 feet.

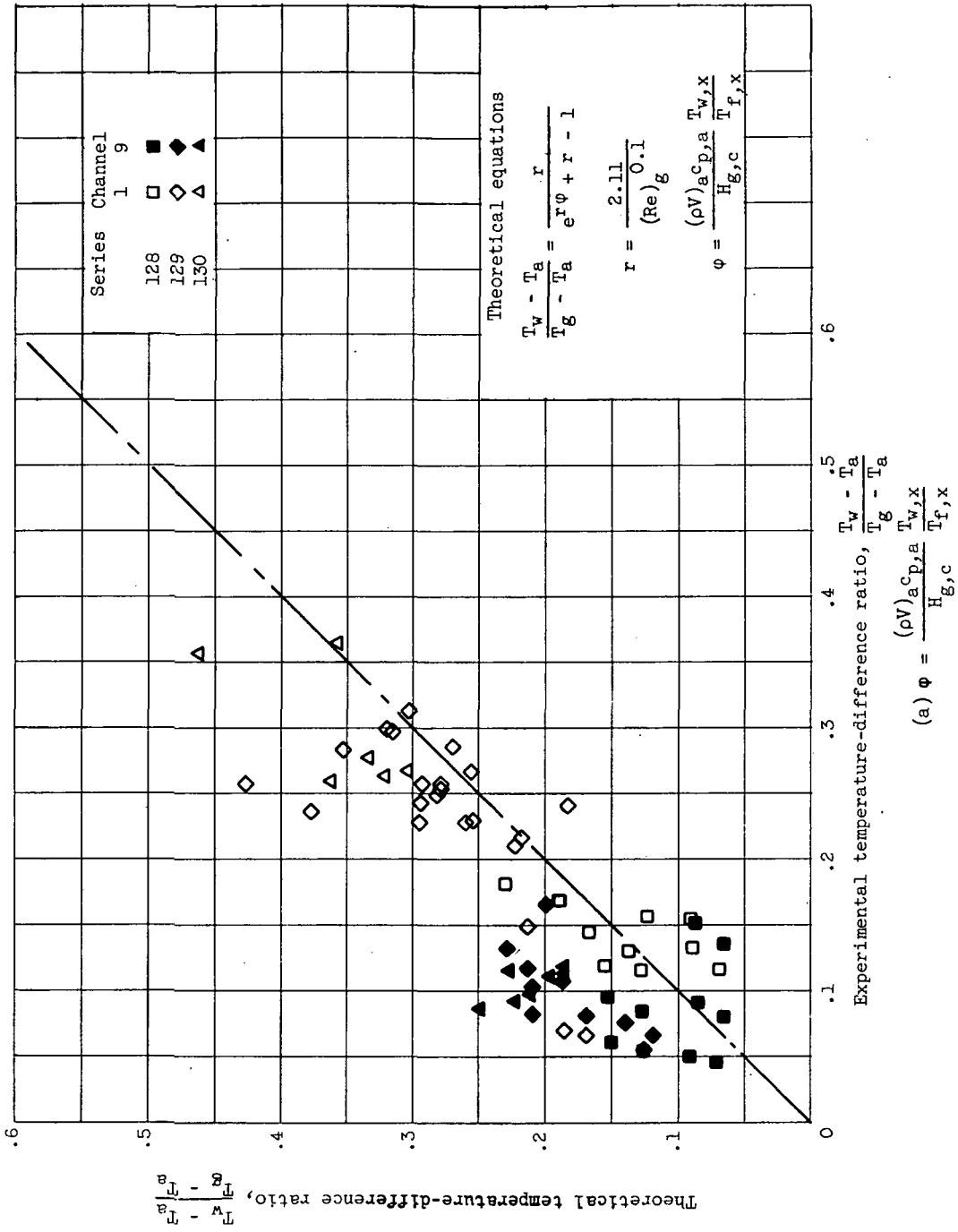


Figure 18. - Comparison of theoretical and experimental temperature-difference ratios for after-burning cooling data.

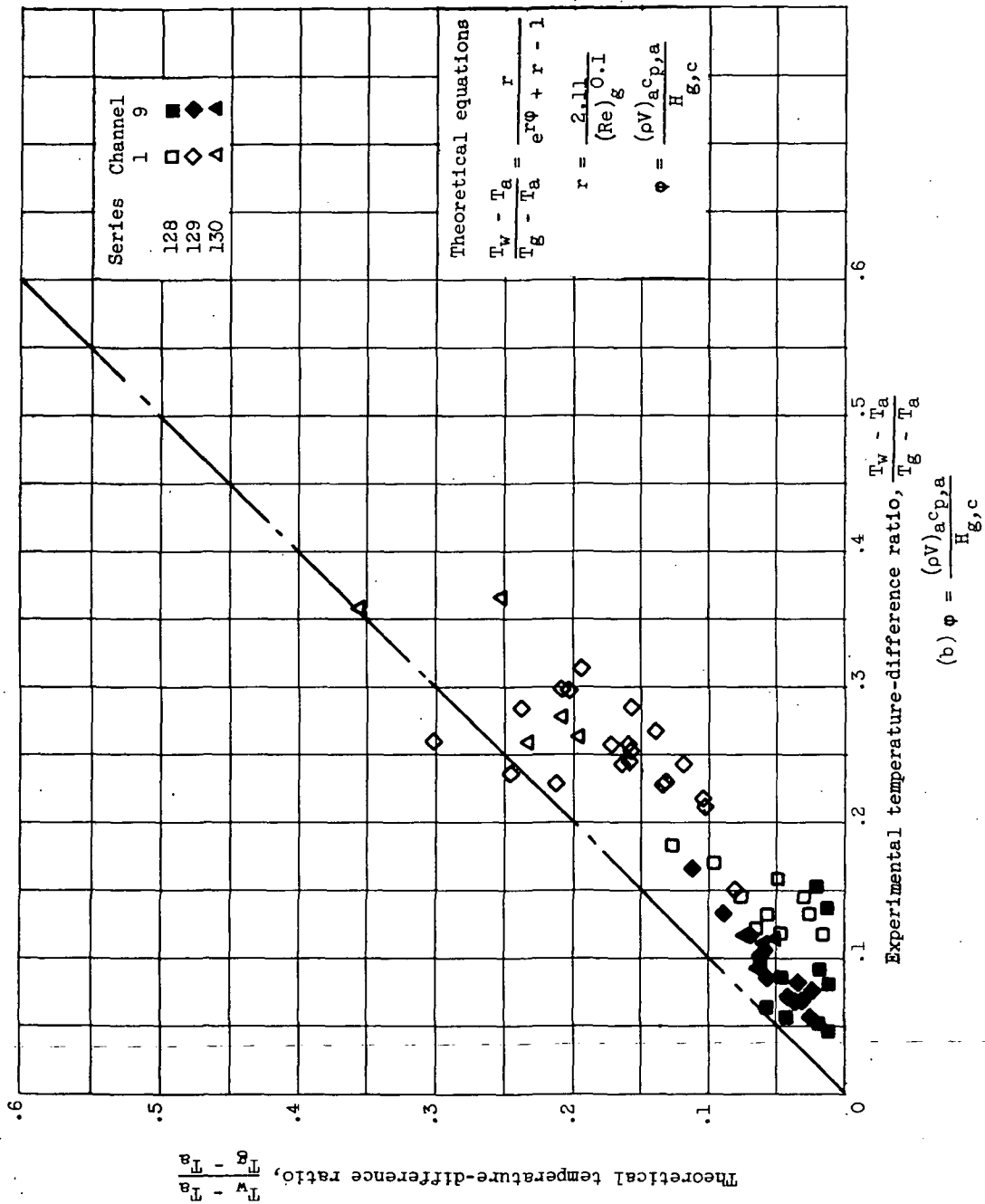


Figure 18. - Concluded. Comparison of theoretical and experimental temperature-difference ratios for afterburning cooling data.

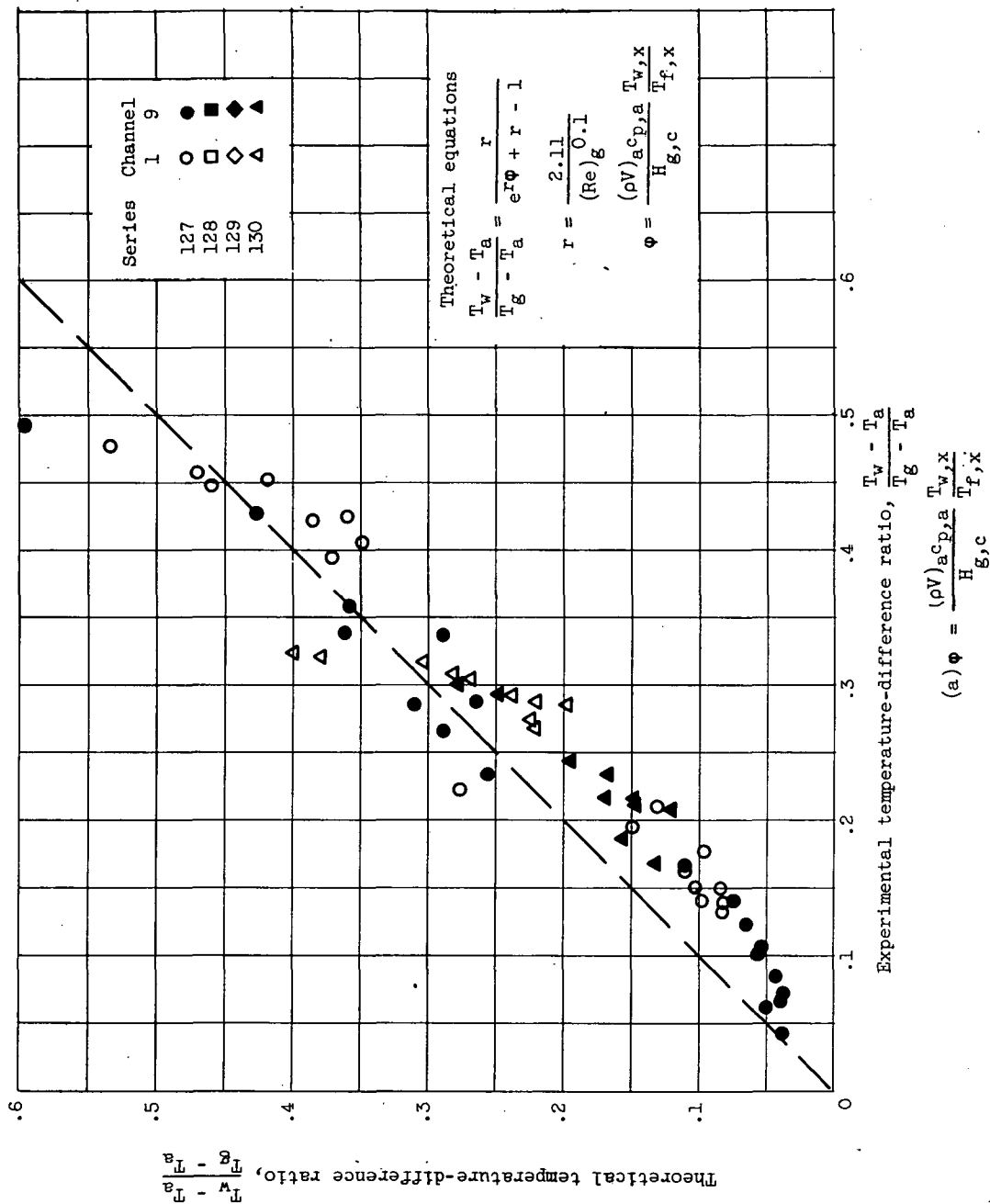


Figure 19. - Comparison of theoretical and experimental temperature-difference ratios for non-afterburning cooling data.

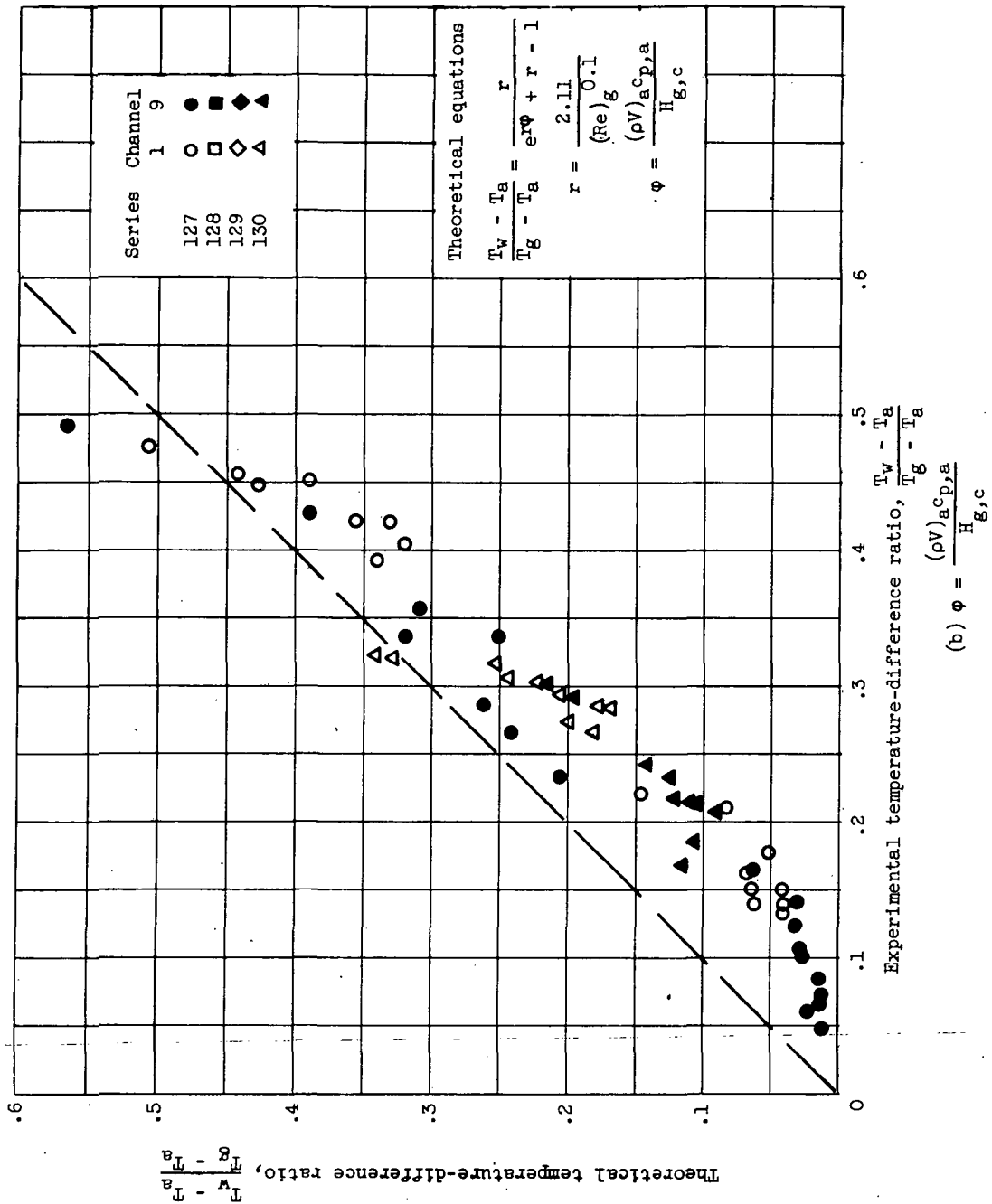


Figure 19. - Concluded. Comparison of theoretical and experimental temperature-difference ratios for nonafterburning cooling data.

CONFIDENTIAL

CLASSIFICATION CHANGED

To Unclassified

By authority of UACA Reclassification

Notice #127 Date 6/5/58 TCW

CONFIDENTIAL